CARBON MEMBRANES
PRECURSOR, PREPARATION AND FUNCTIONALIZATION

PROEFSCHRIFT

ter verkrijging van
de graad van doctor aan de Universiteit Twente,
op gezag van de rector magnificus,
prof. dr. F.A. van Vught,
volgens het besluit van het College van Promoties
in het openbaar te verdedigen
op vrijdag 16 januari om 15.00 uur

door

Jonathan Nathaniel Barsema

geboren op 20 juni 1972

te Groningen

Dit proefschrift is goedgekeurd door de promotor prof. dr.-ing. M.Wessling en de assistent promotor dr. ir. N.F.A. van der Vegt.

ISBN: 90-365-2007-X

Printed by PrintPartners Ipskamp, Enschede

Life is what happens to you
will you're busy making other plans
J.Lennon 1980

voor Marijke

Voorwoord

Toen ik in 1998 begon aan mijn afstudeeropdracht bij de vakgroep Membraan Technologie had ik niet kunnen vermoeden het nog tot 2004 zou duren voordat ik de groep weer zou verlaten. Het waren, met een korte tussenpauze, vijf hele mooie jaren van hard werken en veel plezier hebben.
Ik wil mijn promotor Matthias Wessling dan ook bedanken voor de kans die hij mij heeft geboden om in de Membraan Technologie Groep een promotieonderzoek te doen.
Veel van de inhoud van dit proefschrift was er niet geweest zonder de inbreng van mijn twee directe begeleiders. De eerste twee jaar in Enschede en later op afstand was dit ten eerste Nico van der Vegt. De laatste twee jaar was Geert Henk Koops mijn directe begeleider in Enschede. Een jonge onderzoeker moet zelf leren ideeën te vormen, nieuwe routes te verkennen en eigen verantwoordelijkheid te ontwikkelen. Dit is, mijns inziens, alleen mogelijk als je de vrijheid krijgt om zelfstandig te werken, maar er immer de tijd is voor vragen of een goede discussie. Ik wil jullie beiden dan ook bedanken voor het bieden van die mogelijkheid.
Zonder goede collega's kun je niet werken, dus wil ik iedereen met wie ik de laatste jaren heb gewerkt dan ook bedanken voor een mooie tijd. Een paar wil ik bij naam noemen. Ten eerste mijn kamergenoten: Bernd, Harmen, George, Laura en Sybrand. Ik ben nog steeds van mening dat dit het gezelligste kantoor is. George, without you there would be no chapter 2, thank you for sharing your knowledge and friendship.
Ten tweede de Geus groep: Ger, Antoine, Marcel, Bernd, Marcel, Warner, John, Peter en vele anderen. Natuurlijk ook de groene jasjes van 'Segregare Ducere Est': Ger, Bastiaan en Antoine.
Leon en Peter voor hun gezelschap tijdens de trip door Pennsylvania en naar de top van het WTC.
Twee hoofdstukken in dit proefschrift zijn gebaseerd op het werk van mijn afstudeerders: Sander Klijnstra en Jörg Balster. Jullie werk vormt een belangrijk deel van dit proefschrift, maar belangrijker vind ik de tijd die we er samen aan mochten werken.
Greet, John, Marcel, Betty, Herman, Ineke, Erik en Lydia, jullie hulp bij de dagelijkse gebeurtenisen op het lab en kantoor was onmisbaar.
Ik zal met veel plezier terugdenken aan de vele Batavierenraces, volleybal- en voetbalwedstrijden, badmintondagen, kartavonden, zeilweekenden in Friesland, en fietstochten, waaraan ik de laatste jaren heb mogen deelnemen.

Buiten de vakgroep wil ik Henk Veldhuis, Rob Beltman, Benny Hövels, Bert Kamp en Jan van Veen bedanken voor het vervaardigen (en repareren) van vele onderdelen van mijn meetopstellingen.

Tijdens mijn verdediging zullen mijn paranimfen Tiemen Postma en Antoine Kemperman mij ondersteunen. Naast het feit dat ik jullie hiervoor erg dankbaar ben, wil ik jullie bedanken voor de periodes, dagen en avonden waarin jullie huisgenoot, collega, klaverjasmaat, Geus (of andere kroeg) bezoeker, voetbalfan (Feyenoord en Oranje) of bioscoop- en concert bezoeker waren (ik ben er ongetwijfeld een paar vergeten).

Tenslotte wil ik mijn ouders en zus bedanken voor alle steun die zij mij in de afgelopen jaren hebben gegeven. Marijke, ik kom woorden tekort om te beschrijven hoeveel je voor mij betekent, zonder jou was dit proefschrift er nooit gekomen. En natuurlijk Susan, de zonnestraal die er elke ochtend voor zorgt dat ik op tijd wakker word.

go raibh maith agat

Jonathan

Contents

Summary

In this thesis we study the preparation of Carbon Molecular Sieve (CMS) membranes for the separation of gases. The gases are separated based on their size difference and affinity for the membrane material.
This study can be roughly divided into three parts treating separate issues.

- Chapter 2 and 3: preparation and characterization of polymeric precursor structures;
- Chapter 4 and 5: pyrolysis of polymers for the preparation of CMS membranes;
- Chapter 6 and 7: functionalization of CMS membranes for improved O_2 over N_2 separation.

Before one can start preparing CMS membranes a thorough investigation into the properties of the precursor material is necessary. Therefore, in chapter 2 the properties of the intended precursor material, the co-polyimide P84, are studied. Besides showing the high ideal selectivity of this polymer for the separation of gases, the distinctly different behavior of thin separating layers as compared to their thick counterparts is shown, particularly when plasticization is considered.

As the transition from polymer to carbon during pyrolysis is not instantaneous, it is interesting to investigate the effects of a heat treatment on the membrane performance. The effects of heat treatments, with temperatures between 300 and 600 °C, on the properties of membranes prepared from Matrimid 5218 polyimide are reported in chapter 3. This highly permeable and selective polymer is sensitive to plasticization by propylene at low feed pressures, enabling close screening of the effects of heat treatment on permeability, selectivity, and plasticization behavior. The polymer to carbon intermediate membranes show a slight loss of permeability with increased heat treatment temperature, however, the plasticization resistance increased significantly. When the heat treatment temperature is raised over 475 °C, substantial thermal degradation of the polymer chains was identified and as the carbonization process progressed the membranes show increased values for the permeability and a lower selectivity.

Raising the temperature of heat treatment further, up to 900 °C, the precursor membranes are pyrolysed and CMS membranes are formed. In chapter 4, homogeneous dense flat sheet CMS membranes prepared from P84 are studied to obtain information on the intrinsic material properties. By following the effect of pyrolysis end temperature on for instance the weight loss, gas permeability, and separation properties, the process of CMS formation is elucidated.

In chapter 5 the translation is made from relatively thick (>20 μm), homogeneous dense flat sheet membranes to integrally skinned asymmetric hollow fiber membranes with thin (< 3μm) selective top layers. These thin top layers allow for high permeance rates while maintaining selectivity. Using Ultra Filtration membrane fibers to prepare gas selective CMS membranes shows that it is not necessary to prepare pinhole free precursors. By measuring the permeation of 11 different gases through membranes prepared at different temperatures of pyrolysis, the evolution of the pore size and overall porosity was followed.

To increase the intrinsic selectivity of the separation of O_2 and N_2, Ag-nanoclusters are added to the carbon matrix to obtain Ag functionalized CMS membranes, as described in chapter 6. The interaction between O_2 and Ag provides the means to significantly enhance the separation performance of the prepared CMS membranes. Where the addition of Ag-nanoclusters leads to a substantial increase of the general permeability at low pyrolysis end temperatures (< 600 °C), at higher pyrolysis end temperatures the selectivity is increased by as much as 55 % (750 °C). The observed increase in both permeability and selectivity can be explained by the formation of selective bypasses around the Ag-nanoclusters.

In chapter 7 a new concept is introduced for the preparation of Ag functionalized CMS membranes. In contrast to chapter 6, where the Ag^+ source was water soluble $AgNO_3$, in chapter 7 the precursor is blended with an Ag^+ loaded ionomer. Again an enhancement of the O_2 over N_2 selectivity is observed. This new preparation method opens the road to incorporating the concept of Ag functionalization of CMS, introduced in chapter 6, into precursor structures prepared by aqueous phase inversion techniques like those presented in chapter 5.

Samenvatting (voor leken)

In dit proefschrift bestuderen we de vervaardiging van Koolstof Moleculaire Zeef (KMZ) membranen voor het scheiden van gassen. Deze gassen bestaan uit kleine deeltjes met een diameter van ongeveer 3 tot 4 duizendste van een duizendste van een tiende millimeter, die worden gescheiden op basis van hun verschil in grootte en affiniteit met het membraan.
Dit proefschrift kan grofweg worden verdeeld in drie stukken, welke elk een apart onderwerp behandelen.

- Hoofdstuk 2 en 3: vervaardiging en karakterisering van de polymere, een plastic, grondstof strukturen;
- hoofdstuk 4 en 5: pyrolyse van polymeren voor het vervaardigen van KMZ membranen;
- hoofdstuk 6 en 7: modificering van KMZ membranen voor een verbeterde O_2 (zuurstof) over N_2 (stikstof) scheiding.

Pyrolyse, in het tweede punt, is een term afkomstig uit het grieks (pyro staat voor vuur) en wordt gebruikt voor het proces waarbij materialen worden verhit tot ze ontleden (= lyse) bij afwezigheid van zuurstof.

Voor men kan beginnen met het vervaardigen van KMZ membranen, is het noodzakelijk eerst de eigenschappen van de gebruikte grondstoffen nauwkeurig te onderzoeken. Daarom worden in hoofdstuk 2 de eigenschappen van de beoogde grondstof, het polymeer P84 (een co-polyimide) onderzocht. Naast het feit dat dit polymeer een hoge ideale selectiviteit, maat voor hoe goed het kan scheiden, heeft voor gassen, laten we ook zien dat het gedrag van dunne scheidende lagen sterk afwijkt van dat van dikke films. Dit is vooral goed zichbaar wanneer men het plastificeringsgedrag (het polymeer wordt week als er erg veel gas in oplost) in ogenschouw neemt.

Gezien de transformatie van polymeer naar koolstof niet instantaan verloopt, is het interessant om te kijken naar de effecten van een warmtebehandeling op de membraan prestaties. De effecten van warmte behandelingen bij temperaturen tussen de 300 en 600 °C op de eigenschappen van membranen van het polyimide Matrimid 5218 worden beschreven in hoofdstuk 3. Dit hoog permeabel (er gaat veel gas doorheen) en selectief polymeer is erg gevoelig voor plastificering door propyleen bij lage voedingsdrukken. Dit maakt het

mogelijk de effecten van een warmtebehandeling op de permeabiliteit, selectiviteit en plastificeringsgedrag nauwgezet te volgen. De polymeer-koolstof intermediate membranen (denk aan de intermediates in de Formule 1, geen regen of droog weer banden maar er net tussenin) laten een kleine vermindering van de permeabiliteit zien, echter de weerstand tegen plastificering neemt significant toe. Wanneer de temperatuur, waarop de behandeling plaats vindt, verhoogd wordt boven de 475 °C, ziet men een duidelijke thermische degradatie van de polymeer ketens. Als het carboniseringsproces (het vormen van koolstof) voortschrijdt, laten de membranen verhoogde permeabilitieten en verminderde selectiviteiten zien.

Verdere verhoging van de behandelingstemperatuur, tot 900 °C, leidt tot pyrolyse van de op de grondstof gebaseerde membranen en het ontstaan van KMZ membranen. In hoofstuk 4 worden homogene dicht vlakke film KMZ membranen, gemaakt van P84, bestudeerd om de intrinsieke (materiaal eigen) materiaal eigenschappen te bepalen. Door het volgen van de effecten van de pyrolyse eindtemperatuur op bijvoorbeeld het gewichtsverlies, gaspermeabiliteit en selectiviteit eigenschappen kan het vormingsproces van KMZ membranen worden blootgelegd.

In hoofdstuk 5 wordt de stap gezet van relatief dikke (dikker dan 20 μm, 20 duizendste millimeter) homogene dichte vlakke film membranen naar asymmetrische holle vezel membranen met op het oppervlak een dunne (dunner dan 3 μm) scheidende laag. Vanwege de beperkte dikte van de scheidende laag, kunnen nu hoge permeabilitieten worden gehaald, terwijl de selectiviteit behouden blijft. Door ultrafiltratie vezel membranen (deze hebben te grote gaten om gassen te scheiden) te gebruiken voor de vervaardiging van gasselectieve KMZ membranen wordt aangetoond dat het niet nodig is om perfecte defectvrije polymere gasscheidingsmembranen te gebruiken als grondstof. Door de permeatie te meten van 11 verschillende gassen door op verschillende temperaturen vervaardigde KMZ membranen, kon het onstaan en verloop van de poriegrootte en de totale porositeit worden gevolgd.

Om de intrinsieke selectviteit van de scheiding van O_2 en N_2 te verhogen, worden Ag-nanoclusters (zilverdeeltjes met een diameter van 50 duizendste van een duizendste millimeter) aan de koolstofstructuur toegevoegd en ontstaan zilver-gemodificeerde KMZ membranen, beschreven in hoofdstuk 6. De interactie van zilver met zuurstof maakt het mogelijk de scheidingscapaciteiten van de vervaardigde KMZ membranen sterk te

verbeteren. Waar het toevoegen van deze deeltjes bij relatief lage pyrolyse-temperaturen (tot 600 °C) alleen leidt tot het verhogen van de permeabiliteit, bij hogere pyrolyse-temperaturen leidt dit tot een verhoging van de selectiviteit tot 55 % (gemaakt bij 750 °C). Deze verhoging van de selectiviteit wordt toegeschreven aan het ontstaan van selectieve paden tussen het zilverdeeltje en de koolstofstructuur

In hoofdstuk 7 wordt een nieuw concept geïntroduceerd voor het vervaardigen van zilver-gemodificeerde KMZ membranen. In tegenstelling tot hoofdstuk 6, waarin het wateroplosbare zout zilvernitraat werd gebruikt als zilverbron, gebruiken we een mengsel van de grondstof met een ionomeer (een polymeer met een ion eraan) met een gekoppeld zilverion. Ook nu wordt een verbetering van de scheiding van zuurstof en stikstof gemeten. Deze nieuwe methode maakt het mogelijk om de ontwikkelingen beschreven in hoofdstuk 6 te gebruiken tijdens het vervaardigen van polymere grondstofstructuren via een op water gebaseerde fase-inversie methode (door het in contact brengen van een polymeeroplossing met water wordt het polymeer vast en lost het niet meer op), zoals gebruikt voor het maken van de structuren beschreven in hoofdstuk 5.

Chapter 1

Introduction.

1.1 Gas separation.

Gas separation presently provides raw components for a wide range of industrial chemical processes. O_2 and N_2 are momentarily the third and fifth largest bulk chemicals produced worldwide [1]. Other important separations are the recovery of hydrogen e.g. in the production of syn gas [1], and the dehydration and de-acidification of natural gas [1]. Most of these separations are preformed using cryogenic destillation and various methods based on the pressure swing adsorption principle [2]. Membrane gas separation competes with these technologies and each apart are preferred for a certain operational window. The latter is often quantified by plotting the purity of the desired gas versus the productivity. Although membranes have gone through a tremendous development increasing performance, chemical and mechanical stability, and reduction of production cost, the present state of the art gas separation membrane processes cover only a small section in the entire range of purity versus productivity, see Figure 1.

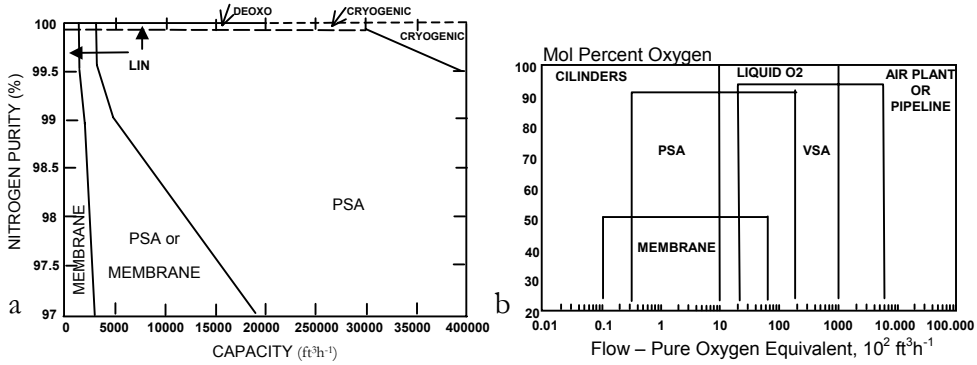

Fig. 1: Cost effectiveness comparison for a-N_2 and b-O_2 production by membrane, PSA, and cryogenic processes [3, 4].

The use of membranes is restricted to processes demanding either relatively low productivity or low selectivity. These restrictions are related, as shown by Robeson [5] for O_2/N_2 separation for a large number of polymeric membranes reported in literature (see Figure 2). With increasing selectivity the productivity generally decreases and vice versa with increasing productivity we find a relatively low selectivity. This is visualized by the apparent upper-bound, as depicted in Figure 2, suggested by Robeson. To expand the operational

window of membranes we must find membranes that will break the upper-bound and achieve high selectivity while sustaining the permeability.

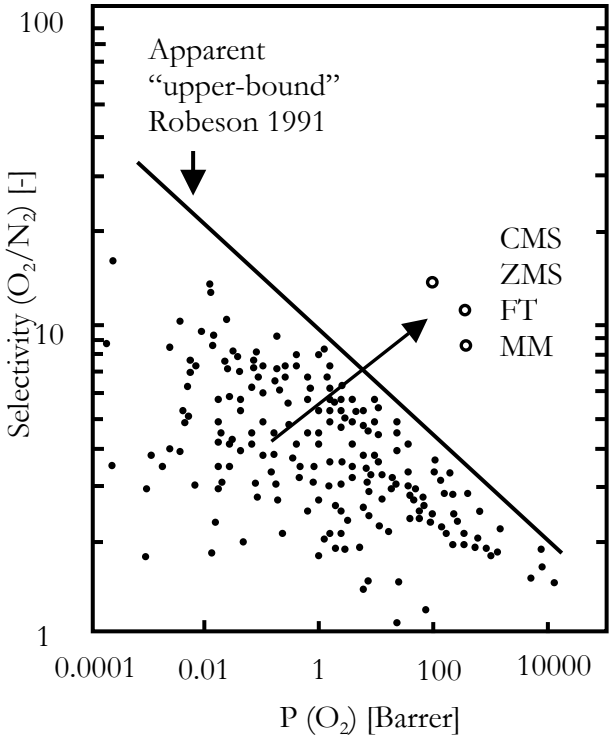

Fig. 2: Robeson plot for O_2 and N_2 separation. Solid symbols represent the performance of membranes reported in literature, open symbols represent predicted performances. (CMS: Carbon Molecular Sieve membranes, ZMS: Zeolite Molecular Sieve membranes, FT: Facilitated Transport membranes, and MM: Mixed Matrix membranes).

In the last decades, several promising new membrane concepts have been developed, which have shown performances exceeding the Robeson 1991 upper-bound. Examples of these membranes are: Carbon Molecular Sieve membranes [6], Zeolite Molecular Sieve membranes [7], Facilitated Transport membranes, where O_2 selective carriers in aqueous solutions are restrained in polymer matrices [8], and Mixed Matrix membranes based on a polymer matrix either containing zeolite or carbon molecular sieves. [9, 10]. The latter type of membranes hopes to combine the good selectivity and permeability of molecular sieves with the processability and mechanical strength of the polymer.

In this thesis we will concentrate on Carbon Molecular Sieve membranes prepared from polymeric precursor membranes. Pyrolysis of these polymeric precursors in inert atmospheres, results in carbon structures able to separate gases.

1.2 Carbon.

Carbon is found in abundance as well on earth as in the rest of the universe. It is the basis of all hydrocarbon-based life. Most of earth's carbon is found as carbon compounds, although its pure form exists as natural graphite and diamond. Well-known natural carbon compounds such as coal, natural gas, oil, and wood are widely used to prepare synthetic carbon compounds like polymers, bitumen, carbon fibers, paper, and fuels.

1.2.1 The element.

The carbon atom can be found on position 6 in Mendeleev's periodic system of elements and three isotopes exist naturally i.e. C^{12} (98.89 %), C^{13} (1.11%), and C^{14} (< 0.01 %). The complete C^{12} atom has a radius of 0.77 Å and in the ground state the atom configuration is given below:

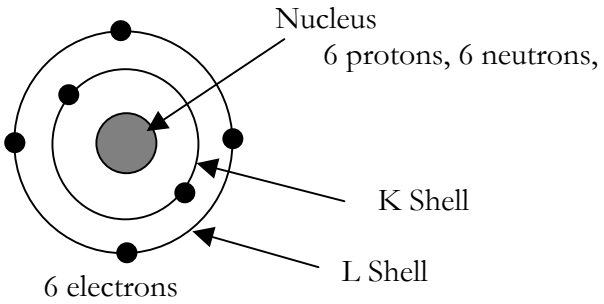

Fig. 3: The ground state configuration of the C^{12} atom.

1.2.2 Structure and properties of carbon materials.

When more than one atom is considered, carbon can form a wide range of structures with substantially different properties. The main reason for this diversity is the ability of the carbon atom to form several hybrid electron orbitals, available for bonding.

A well-known example, portraying this hybridization ability, is the structure of methane. This spherical molecule consists of one carbon atom surrounded by four hydrogen atoms. As the molecule is spherical, all bond lengths must be equal. However, if one takes a close look at the electron distribution of the carbon atoms it is clear that only three 2p orbitals are available for bonding supplemented with a 2s orbital to form 4 bonds. The 2p and 2s orbitals differ in shape and bond length (Figure 4), hence resulting in a non-spherical molecule.

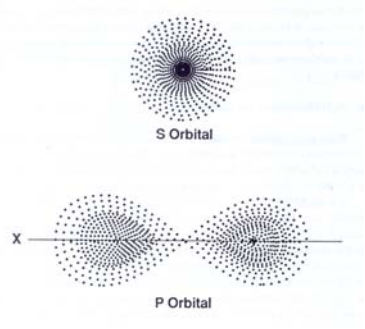

Fig. 4: Schematic representation of the 2s and 2p orbitals of the carbon atom [11].

To be able to form an energetically favorable structure with four bonds of equal length one 2s and three 2p orbitals combine to form four sp^3 hybrid orbitals, resulting in the spherical methane molecule (Figure 5).

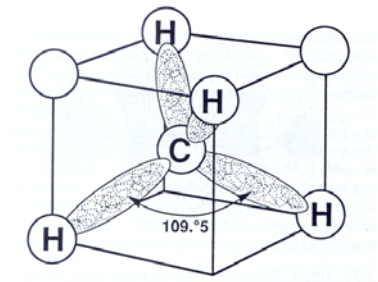

Fig. 5: Schematic representation of methane [11].

The carbon orbitals can form two other hybrid orbitals, i.e. the sp and sp^2. The different hybrid orbitals are schematically shown in Figure 6. Each of these orbital configurations enables the formation of different carbon structures.

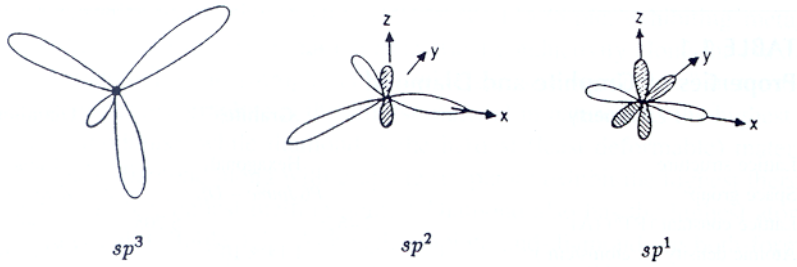

Fig. 6: Schematical representation of sp, sp^2, and sp^3 orbital configuration [12].

sp^3: The sp^3 bonds are found in all aliphatic compounds, including paraffins, olefins, and their derivatives, but are most famous for forming diamond.

sp^2: The two dimensional sp^2 bond is mainly found in graphite or graphite like structures, e.g. glassy carbon and amorphous or turbostratic carbon, Figure 7 .

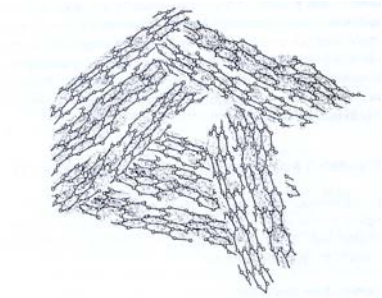

Fig. 7: Structure of turbostratic graphite [11].

Both glassy and amorphous carbons consist of small graphene plates or graphite crystals packed in a highly disordered structure. A perfect graphite structure, i.e. defect free stacked graphene crystals with an infinite length, has a theoretical density of 2.26 gcm^{-3}. Glassy and amorphous carbons have densities between 1.4 and 1.9 gcm^{-3}, indicating a large porosity, although sometimes inaccessible.

sp: The sp orbital is found in, for instance, acetylene and in the unstable carbines, which are cross-linked linear chain carbon polytypes.

Only recently, a new configuration was found with the discovery of fullerenes. These large sphere-like structures must have bonds originating from modifications of the sp^3 and sp^2 hybrid bonds.

1.3 Carbon Molecular Sieve membranes.

Carbon Molecular Sieves (CMS) have been well known for their separation properties when used in PSA systems [2] and have been researched to great extent as shown by Koresh and Soffer [13, 14]. Barrer, in cooperation with several other authors, first introduced the term carbon membrane for carbon plugs prepared from compressed carbon powders [15, 16]. However, their materials were too porous to obtain a high selectivity. Koresh and Soffer [17] and others [18] published in 1983 the concept of using pre-shaped polymeric precursor materials for the direct formation of carbon membranes, without the need for a post treatment like compression. The basic principle of preparing CMS membranes is simple: one heats a polymeric precursor to temperatures between 500 and 1000 °C in an inert atmosphere, thereby removing all non-carbon compounds, through thermal decomposition, to obtain a carbon structure. This carbon structure is primarily highly porous turbostratic (seen in Figure 7), allowing for the permeation of gases through slit-like pores [13].

Geiszler [19] systematically researched the effect of pyrolysis atmosphere (vacuum, He, Ar, or CO_2), purge gas flow rate, and pyrolysis temperature on the properties of CMS membranes prepared from the same polyimide (TPDA/BPDA-6FDA).
Many authors have produced CMS membranes from a wide range of polymeric precursors. To obtain good CMS membranes the precursor polymer should satisfy a number of criteria e.g. high aromatic carbon content and a high T_g . Frequently used polymers are polyimides [20-26], polyacrylonitrile [27, 28], and polyetherimide [29]. Although other polymers such as for instance polyfurfuryl alcohol [30], polyvinylidene chloride [31, 32], and phenolic resin [33, 34] have also been used quite successfully for preparing CMS membranes.
The research on CMS membranes has taken several directions, i.e. separation of gases based on size, affinity or condensability as well as unsupported homogeneous, unsupported asymmetric, or supported composite CMS membranes.

CMS membranes can be produced in three configurations. Homogeneous unsupported membranes with known thickness, density, and structure, providing the means to determine the intrinsic properties of the carbon material, like permeability and ideal selectivity [35, 36]. Asymmetric porous structures, like integrally skinned asymmetric hollow fiber membranes, result in high permeance rates obtained by reducing the effective membrane thickness and thus resistance [28, 37-39]. If the polymer is not thermosetting or if enhancement of the mechanical stability is desired, the CMS membrane can be prepared on a porous support. As support can be used, e.g. sintered metals, alumina, or graphite like, either in flat disk or tubular configurations. Reported deposition methods are, among others, spin coating [34], spray coating [40], ultrasonic deposition.

1.4 Separation mechanisms in CMS membranes.

Molecular sieve membranes differ significantly from their polymeric counterparts when the mechanism of separation is considered.
Polymeric membranes separate gases on a solution-diffusion mechanism [41]. The gas molecules dissolve into the membrane, then subsequently diffuse across the membrane thickness, and desorb on the other side. The gas molecules jump from free volume to free volume, whilst interacting with the polymer chains. The permeability of a gas is now ideally given by the product of the solubility and the diffusion coefficient:

$$P = D \cdot S . \qquad (1)$$

Where P is the permeability [Barrer, 10^{-10}cm^3(STP)cm cm^{-2}s^{-1}cmHg^{-1}], D is the diffusion coefficient [cm^{2}s^{-1}], and S the solubility coefficient [cm^3(STP)cm^{-3}cmHg^{-1}].

In the case of molecular sieve membranes, the pore walls are rigid and the space available for permeation is fixed. Depending on the pore size, different mechanisms resulting in separation can be distinguished: Knudsen diffusion, molecular sieving, and surface diffusion.

1.4.1 Knudsen diffusion.

When the pore size is reduced to sizes below 0.1 μm the main transport mechanism is Knudsen diffusion. This pore diameter is small enough to allow

the molecules to interact primarily with the pore wall, rather than with each other.
The Knudsen flux [41] is given by equation 2:

$$J = \frac{\pi n r^2 D_k \Delta p}{RT\tau\ell} \tag{2}$$

where D_k, the Knudsen diffusion coefficient, is given by $D_k = 0.66r\sqrt{\frac{8RT}{\pi M_w}}$.
When the separation of two gases is considered, the separation factor will be based on the differences in molecular weight. The selectivity now equals the square root of the reciprocal molecular weight ratio:

$$\alpha_{a/b} = \sqrt{\frac{M_b}{M_a}} \tag{3}$$

Industrially, this separation mechanism has gained significance for the separation to UF_6 isotope enrichment.

1.4.2 Molecular sieving.

As the pore size is reduced below the kinetic diameter of one of the feed components, molecular sieving can take place. Now some molecules can enter the pore, whereas others are denied entrance solely based on their size. This allows for the separation of gases similar in size, membrane affinity, and molecular weight with high selectivity factors.
Shiflett and Foley [30, 42] used ultrasonic deposition of polyfurfuryl alcohol on a sintered stainless steel support to produce highly selective size discriminating CMS membranes. By exact tailoring of the pore size distribution, the prepared membranes could discriminate between He/H_2 (Δd_{kin}: 0.29 Å) and O_2/N_2 (Δd_{kin}: 0.18 Å) with a selectivity of 178 and 30.4, respectively. Suda and Haraya [36] even obtained, based of a Kapton polyimide precursor, an O_2/N_2 selectivity of 36. However, the increase of selectivity is, as predicted by the Robeson plot, combined with a reduced permeability. An interesting separation, from an industrial point of view, is that of H_2 and CH_4. Jones and Koros [37] obtained a selectivity for H_2/CH_4 of approximately 500 with a permeance of 225 GPU (10^{-6} $cm^3(STP)cm^{-2}s^{-1}cmHg^{-1}$) using a tailor made polyimide. Ogawa and Nakano [38] used Kapton as precursor to find a

significantly higher permeance, approximately $1.2x10^5$ GPU, however not reaching a selectivity higher than 180.

1.4.3 Surface diffusion.

Surface diffusion can have a significant effect on the obtained separation, if one or more components in the feed have an affinity to the membrane material. A molecule can adsorb on the pore wall and subsequently pass through the pore whilst diffusing over the surface of the pore wall. Surface diffusion occurs independent of the pore size. However, the effect can be neglected if the transport through the bulk of the pore is prevalent [43]. Examples of these affinity gases are CO_2 and olefins like C_2H_4 and C_3H_6. Ogawa and Nakano [44] achieved selectivity values up to 267 for CO_2 over CH_4 with a permeance of $4.1x10^4$ GPU, using CMS membranes based of Kapton polyimide. The obtained permeance was even higher for the membranes prepared by Hayashi [45], reaching $1.5x10^6$ GPU with a selectivity of 166. An important but difficult separation is that of olefins from parafins. Kita [33] prepared CMS membranes from vacuum impregnated phenolic resin in silica coated alumina substrates; achieving high selectivity values for both the separation of C_2H_4/C_2H_8 (P: 16.8 GPU, α: 16.6) and C_3H_6/C_3H_8 (P: 17.8 GPU, α: 130).

Figure 8 relates the different mechanisms to the pore sizes present in the membrane.

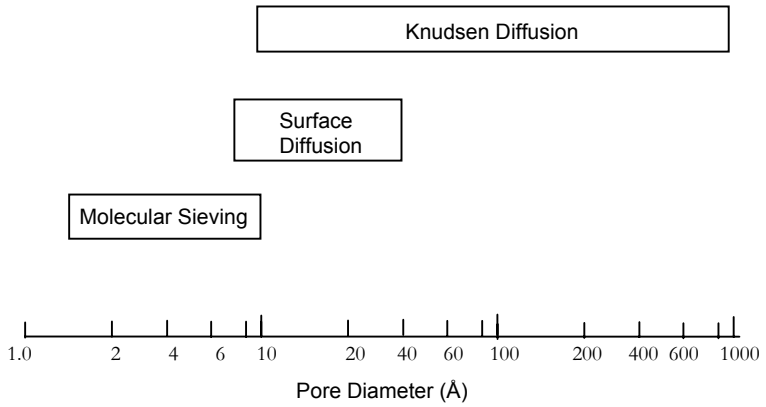

Fig. 8: Approximate operative pore size ranges for various mechanisms [43].

1.4.4 Pore blocking by condensation.

In the case of very high affinity or high condensability of the gas, a fourth separation mechanism can occur, referred to as **selective pore condensation**.

As one gas species condenses the pore is filled with a liquid, effectively blocking the pore for all other molecules than the condensed one. This allows for the preferential permeation of large (condensable) molecules over smaller molecules.
Fuertes [46] separated a mixture of 16.3% CH_4, 16.1% C_2H_6, 16.2% C_3H_8, 20% *n*-C_4H_{10}, and 31.4% N_2 and found selectivity values for the different components over N_2 of CH_4 3 (P: 52 GPU); C_2H_6 12 (P: 210 GPU); C_3H_6 30 (P: 520 GPU); and *n*-C_4H_{10} 74 (P: 1280). The CMS membrane used, was based on a phenolic resin precursor and was activated by an air oxidation treatment. Rao and Sircar [32, 47] found comparable results for the separation of hydrocarbons over H_2.

1.5 Motivation.

Section 1.4 makes a distinct division between polymer and CMS membranes, both of which provide quite different mechanisms for separating gases. In reality the transition from polymer to carbon is not instantaneous and the materials formed during the transition from polymer to carbon may posses properties of both polymer and CMS materials. Therefore, it is interesting to study the properties of the transition materials as the temperature of heat treatment increases.
In the previous paragraph, four different separation mechanisms for CMS membranes were described. When CO_2 is separated from a gas with a larger diameter two of these mechanisms will contribute to the separation, i.e. molecular sieving and surface diffusion, resulting in high separation factors. However, this synergetic effect is restricted to separations of mixtures containing a gas species with a high affinity to the carbon matrix. By introducing other materials in the carbon matrix, thereby functionalizing it to interact with other gas species, this synergetic effect may be extended to more gas mixtures.

1.6 Structure of this thesis.

In chapter 2 '***Preparation and characterization of highly selective dense and hollow fiber asymmetric membranes based on P84 co-polyimide***', the properties of the intended precursor material, the co-polyimide P84 (BTDA-TDI/MDI) are studied. We have looked at its properties for gas separation like permeability, ideal selectivity, mixed gas selectivity, and sensitivity toward plasticization. Furthermore, we investigated the possibility to

prepare asymmetric hollow fiber structures and their separation performance and plasticization behavior.

In **chapter 3 '*Intermediate polymer to carbon gas separation membranes based on Matrimid PI*'**, we tried to elucidate the changes taking place in the polymer membrane during the early stages of heat treatments, i.e. the temperature range between the T_g of the polymer and the thermal decomposition temperature. Again the permeability and selectivity of membranes is monitored closely. By choosing the highly plasticizible polyimide polymer Matrimid 5218 (BTDA-AAPTMI), we could investigate the effect of the applied heat treatments on the plasticization behavior of the membranes.

Chapter 4 '*Preparation of Carbon Molecular Sieve membranes from P84 co-polyimide precursor*' describes the preparation and properties of CMS membranes prepared from P84 co-polyimide. By following the permeation behavior of four gases through CMS membranes prepared at different pyrolysis end temperatures, we study the structural evolution of the CMS membranes with the temperature of pyrolysis. By preparing flat dense CMS membranes we obtained valuable information on the intrinsic properties of P84 based carbon molecular sieves.

The applicability of the findings to prepare asymmetric hollow fiber CMS membranes with thin selective top layers is researched in **chapter 5 '*Carbon Molecular Sieve membranes prepared from porous fiber precursors*'.** Here, the results are reported for the preparation and gas permeation properties of CMS asymmetric hollow fiber membranes. These membranes were prepared using porous ultra filtration hollow fibers as precursor, showing that highly selective CMS membranes can be prepared from non-selective porous precursors. By following the permeation of 11 different gases through membranes prepared at different temperatures of pyrolysis the evolution of the pore size and overall porosity was followed.

To enhance the separation of O_2 and N_2, we functionalized the CMS membranes with Ag in **chapter 6 '*Functionalized Carbon Molecular Sieve membranes containing Ag-nanoclusters*'**. By adding small amounts of Ag^+ containing salts to the precursor solution we could form Ag-nanoclusters in the resulting CMS, using the mechanism of Ostwald ripening [48]. Monitoring the properties of dense flat sheet membranes allows elucidating the intrinsic properties of the functionalized carbon molecular sieve.

The gas specific enhancement factor quantifies the effect of the functionalization on the permeability of a specific gas molecule.

Finally, **chapter 7** ***'Ion exchange blend polymeric precursors for Ag containing Carbon Molecular Sieve membranes'***, describes a new concept to overcome the disadvantages of using water soluble Ag salts as Ag source for the nanoclusters. Blending the precursor polymer with the ionomer sulphonated poly(ether ether ketone) allows to electro chemically bind Ag^+ ions This opens the way to improved precursor configurations, like those prepared by phase inversion in aqueous non-solvents. Special attention was given to the quality of the prepared blend and the effect of changing blend composition.

Appendix I '*Optimizing pyrolysis procedure and set-up for the preparation of CMS membranes*' explains the details and constraints of the pyrolysis procedures used to obtain the CMS membranes reported in this thesis.

A second appendix ***'Formation of carbon fibers by metal particle catalysis'*** describes the formation of thin carbon fibers on the surface of metal functionalized CMS membranes.

1.7 References.

[1] R. W. Baker, Future directions of membrane gas separation technology, Ind. Eng. Chem. Res. 41 (2002) p1393-1411.

[2] D. M. Ruthven, S. Farooq, K. S. Knaebel, Pressure swing adsorption, 1st Edition, VCH Publishers, Inc., New York, 1994.

[3] R. M. Thorogood, Developments in air separation, Gas Sep. Purif. 5 (1991) p83-94.

[4] R. W. Spillman, Economics of Gas Separation Membranes, Chem. Eng. Prog. 85 (1989) p41-62.

[5] L. M. Robeson, Correlation of separation factor versus permeability for polymeric membranes, J. Membr. Sci. 62 (1991) p165-185.

[6] A. F. Ismail, L. I. B. David, Future direction of R&D in carbon membranes for gas separation, Membrane Technology 2003 (2003) p4-8.

[7] R. M. de Vos, H. Verweij, High-selectivity, high-flux silica membranes for gas separation, Science 279 (1998) p1710-1711.

[8] A. Figoli, W. F. C. Sager, M. H. V. Mulder, Facilitated oxygen transport in liquid membranes: review and new concepts, J. Membr. Sci. 181 (2001) p97-110.

[9] J.-M. Duval, B. Folkers, M. H. V. Mulder, G. Desgrandchamps, C. A. Smolders, Adsorbent filled membranes for gas separation. Part 1. Improvement of the gas separation properties of polymeric membranes by incorporation of microporous adsorbents, J. Membr. Sci. 80 (1993) p189-198.

[10] D. Q. Vu, W. J. Koros, S. J. Miller, Mixed matrix membranes using carbon molecular sieves: I. Preparation and experimental results, J. Membr. Sci. 211 (2003) p311-334.

[11] H. O. Pierson, Handbook of carbon, graphite, diamond, and fullerenes. Properties, processing and applications., 1st Edition, Noyes Publications, Park Ridge, 1993.

[12] M. S. Dresselhaus, D. Dresselhaus, P. C. Eklund, R. Saito, M. Endo, in Carbon nano tubes - Preparation and properties, T. W. Ebbesen ed., CRC Press Inc., New York, 1997, p6.

[13] J. E. Koresh, A. Soffer, Study of Molecular Sieve Carbons. Part 1.: Pore Structure, Gradual Pore Opening and Mechanism of Molecular Sieving, Journal of the Chemical Society. Faraday I 76 (1980) p2457-2471.

[14] J. E. Koresh, A. Soffer, Study of Molecular Sieve Carbons. Part 2.: Estimation of Cross-sectional Diameters of Non-spherical Molecules, Journal of the Chemical Society. Faraday I 76 (1980) p2472-2485.

[15] L. A. G. Aylmore, R. M. Barrer, Surface and volume flow of single gases and of binary gas mixtures in a microporous carbon membrane, Proc.Royal Soc. A 290 (1966) p477-489.

[16] R. Ash, R. W. Baker, R. M. Barrer, Sorption and surface flow in graphitized carbon membranes. I. The steady state, Proc.Royal Soc. A 299 (1967) p434-454.

[17] J. E. Koresh, A. Soffer, Molecular Sieve Carbon permselective membrane. Part I. Presentation of a new device for gas mixture separation., Sep. Sci. Technol. 18 (1983) p723-734.

[18] A. J. Bird, D. L. Trimm, Carbon molecular sieves used in gas separation membranes, Carbon 21 (1983) p177-180.

[19] V. C. Geiszler, W. J. Koros, Effects of polyimide pyrolysis conditions on carbon molecular sieve membrane properties, Ind. Eng. Chem. Res. 35 (1996) p2999-3003.

[20] D. T. Clausi, W. J. Koros, Formation of defect-free polyimide hollow fiber membranes for gas separations, J. Membr. Sci. 167 (2000) p79-89.
[21] A. B. Fuertes, T. A. Centeno, Preparation of supported asymmetric carbon molecular sieve membranes, J. Membr. Sci. 144 (1998) p105-111.
[22] A. B. Fuertes, D. M. Nevskaia, T. A. Centeno, Carbon composite membranes from Matrimid (R) and Kapton (R) polyimides for gas separation, Microporous Mesoporous Mat. 33 (1999) p115-125.
[23] J. Hayashi, H. Mizuta, M. Yamamoto, K. Kusakabe, S. Morooka, Pore size control of carbonized BPDA-pp'ODA polyimide membrane by chemical vapor deposition of carbon, J. Membr. Sci. 124 (1997) p243-251.
[24] Y. Kusuki, H. Shimazaki, N. Tanihara, S. Nakanishi, T. Yoshinaga, Gas permeation properties and characterization of asymmetric carbon membranes prepared by pyrolyzing asymmetric polyimide hollow fiber membrane, J. Membr. Sci. 134 (1997) p245-253.
[25] H. Suda, K. Haraya, Molecular-Sieving Effect of Carbonized Kapton Polyimide Membrane, J. Chem. Soc.-Chem. Commun. (1995) p1179-1180.
[26] H. B. Park, S. Y. Nam, J. G. Jang, Y. M. Lee, Preperation, characterization, and gas permeation properties of carbon molecular sieve membranes derived from dense P84-polyimide film, Korean Membr. J. 4 (2002) p25-35.
[27] A. S. Damle, S. K. Gangwal, V. K. Venkataraman, Carbon Membranes for Gas Separation - Developmental Studies, Gas Sep. Purif. 8 (1994) p137-147.
[28] V. M. Linkov, R. D. Sanderson, E. P. Jacobs, Highly Asymmetrical Carbon Membranes, J. Membr. Sci. 95 (1994) p93-99.
[29] A. B. Fuertes, T. A. Centeno, Carbon molecular sieve membranes from polyetherimide, Microporous Mesoporous Mat. 26 (1998) p23-26.
[30] M. B. Shiflett, H. C. Foley, Ultrasonic deposition of high-selectivity nanoporous carbon membranes, Science 285 (1999) p1902-1905.
[31] T. A. Centeno, A. B. Fuertes, Carbon molecular sieve gas separation membranes based on poly(vinylidene chloride-co-vinyl chloride), Carbon 38 (2000) p1067-1073.
[32] M. B. Rao, S. Sircar, Nanoporous Carbon Membranes for Separation of Gas-Mixtures by Selective Surface Flow, J. Membr. Sci. 85 (1993) p253-264.

[33] H. Kita, H. Maeda, K. Tanaka, K. Okamoto, Carbon molecular sieve membrane prepared from phenolic resin, Chem. Lett. (1997) p179-180.
[34] T. A. Centeno, A. B. Fuertes, Supported carbon molecular sieve membranes based on a phenolic resin, J. Membr. Sci. 160 (1999) p201-211.
[35] A. Singh-Ghosal, W. J. Koros, Air separation properties of flat sheet homogeneous pyrolytic carbon membranes, J. Membr. Sci. 174 (2000) p177-188.
[36] H. Suda, K. Haraya, Gas permeation through micropores of carbon molecular sieve membranes derived from Kapton polyimide, J. Phys. Chem. B 101 (1997) p3988-3994.
[37] C. W. Jones, W. J. Koros, Carbon Molecular-Sieve Gas Separation Membranes .1. Preparation and Characterization Based on Polyimide Precursors, Carbon 32 (1994) p1419-1425.
[38] M. Ogawa, Y. Nakano, Gas permeation through carbonized hollow fiber membranes prepared by gel modification of polyamic acid, J. Membr. Sci. 162 (1999) p189-198.
[39] J. Petersen, M. Matsuda, K. Haraya, Capillary carbon molecular sieve membranes derived from Kapton for high temperature gas separation, J. Membr. Sci. 131 (1997) p85-94.
[40] M. Acharya, H. C. Foley, Spray-coating of nanoporous carbon membranes for air separation, J. Membr. Sci. 161 (1999) p1-5.
[41] M. H. V. Mulder, Basic principles of membrane technology, 2nd Edition, Kluwer Academic Publishers, Dordrecht, 1996, p232.
[42] M. B. Shiflett, J. F. Pedrick, S. R. McLean, S. Subramoney, H. C. Foley, Characterization of supported nanoporous carbon membranes, Adv. Mater. 12 (2000) p21-25.
[43] J. D. Way, D. L. Roberts, Hollow Fiber Inorganic Membranes for Gas Separations, Sep. Sci. Technol. 27 (1992) p29-41.
[44] M. Ogawa, Y. Nakano, Separation of CO2/CH4 mixture through carbonized membrane prepared by gel modification, J. Membr. Sci. 173 (2000) p123-132.
[45] J. Hayashi, M. Yamamoto, K. Kusakabe, S. Morooka, Simultaneous Improvement of Permeance and Permselectivity of 3,3',4,4'-Biphenyltetracarboxylic Dianhydride-4,4'-Oxydianiline Polyimide Membrane by Carbonization, Ind. Eng. Chem. Res. 34 (1995) p4364-4370.
[46] A. B. Fuertes, Effect of air oxidation on gas separation properties of adsorption-selective carbon membranes, Carbon 39 (2001) p697-706.

[47] M. B. Rao, S. Sircar, Performance and pore characterization of nanoporous carbon membranes for gas separation, J. Membr. Sci. 110 (1996) p109-118.
[48] A. Heilmann, Polymer films with embedded metal nanoparticles, 1st Edition, Springer-Verlag, Berlin, 2003, p79.

Chapter 2

Preparation and characterization of highly selective dense and hollow fiber asymmetric membranes based on P84 co-polyimide*.

J.N. Barsema, G.C. Kapantaidakis, N.F.A. van der Vegt, G.H. Koops,and M. Wessling

Abstract

In this work, the preparation, the characterization, and the permeation properties of dense flat sheet and asymmetric hollow fiber membranes, based on BTDA-TDI/MDI co-polyimide (P84), are reported. Results are shown for pure gases and for the separation of a CO_2/N_2 80/20% mixture. Dope viscosity measurements were performed to locate the polymer concentrations where significant chain entanglement occurs. Asymmetric hollow fibers were spun, using the dry/wet phase inversion process. Scanning Electron Microscopy (SEM) was used to investigate the morphological characteristics and the structure of the developed fibers. The permeation rates of He, CO_2, O_2, and N_2 were measured by the variable pressure method at different feed pressures and temperatures. P84 co-polyimide proved to be one of the most selective glassy polymers. The achieved ideal selectivity coefficients are: 285-300 for He/N_2, 45-50 for CO_2/N_2, and 8.3-10 for O_2/N_2, which are in the range of the highest values ever reported for polymeric membranes. The permeability of CO_2 is relatively low (~1 Barrer, 25 °C), however, it is independent of feed pressure, indicating that the P84 dense membranes are not plasticized at CO_2 feed pressures up to 30 bar. On the contrary, the permeance of CO_2 through the asymmetric hollow fiber membranes increases with pressure, indicating that the plasticization behavior of asymmetric membranes differs from the respective dense ones. However, no evidence of plasticization was observed when a CO_2/N_2, 80/20% mixture was fed to the hollow fiber membranes for pressures up to 30 bar. In all cases, CO_2 permeance decreased with pressure while that of N_2 remained constant.

* Published as 'J.N. Barsema *et.al.*, J. Membr. Sci 216 (2003) p195-205'.

2.1 Introduction.

In the last two decades, various engineering glassy polymers have been developed on both experimental and commercial level [1]. These materials combine high selectivities with acceptable permeability coefficients, and therefore, are suitable for the preparation of gas separation membranes, especially asymmetric hollow fibers with thin top layers (< 0.1 μm). Glassy polymer membranes perform well in separations of mixtures of non-condensable permanent gases (e.g. O_2/N_2, H_2/CO, etc), however their separation properties deteriorate in the presence of condensable gases and organic vapors. For example, the commercial polyimide Matrimid 5218 exhibits high selectivity coefficients at low CO_2 feed pressures, but with increased partial CO_2 feed pressure the selectivity drops. In particular, the permeability of the slower gas is facilitated by the, highly soluble, faster gas. This phenomenon is attributed to plasticization effects, caused by the high CO_2 solubility or interactions between CO_2 and the polyimide [2]. As the membrane is plasticized the permeability increases significantly, but the selectivity for gaseous mixtures decreases. Well know examples of separations where these plasticization effects occur are CO_2 over CH_4 [2], C_2H_4 over C_2H_6, and C_3H_6 over C_3H_8 [3]. Plasticization problems, ageing phenomena, low processability and high cost are the main reasons that today only eight to nine different polymers are used in 90% of the commercial applications [4].
In literature many articles can be found reporting different procedures to reduce the extent of plasticization phenomena in glassy polymer membranes. Methods used are: 1) annealing, 2) thermally induced cross-linking, 3) chemical cross-linking, 4) inter-penetrating networks and 5) polymer blending [3, 5-9]. In most of these methods, where flat sheet membranes were tested, the suppression of CO_2 plasticization caused also a considerable reduction of gas permeability. However, it is known that ultra thin dense or asymmetric hollow fiber membranes exhibit differences in physicochemical properties, like ageing phenomena and plasticization behavior when compared with thicker membranes prepared from the same polymeric material [10-12]. In the field of CO_2 plasticization Wessling et. al. found that the plasticization behavior of polyimide/polydimethylsiloxane composite membranes is thickness dependent [12]. The same material (Matrimid 5218) in the form of relatively thick (50 μm) flat sheet dense membranes was plasticized at a partial feed pressure of 12 bar, while in the form of thin (PI~1 μm)/ PDMS composite membrane the CO_2 plasticization was accelerated. Slightly thicker membranes (~3 μm) showed a higher resistance to CO_2 swelling. In another work, Wang et. al. reported an

immediate increase of CO_2 permeance with feed pressure in pure polyimide asymmetric hollow fiber membranes [13]. Kapantaidakis et. al. showed the same with ultra thin asymmetric hollow fibers based on Matrimid 5218 and Polyethersulfone blends [14].
If asymmetric hollow fiber membranes show such different behavior as compared to thick films it would be interesting to investigate the properties of a material known until now to be non-plasticizible. For this reason, we have chosen the co-polyimide BTDA-TDI/MDI for further investigation. It has already been reported that BTDA-TDI/MDI dense membranes exhibit low CO_2 permeability coefficients but can withstand high CO_2 partial feed pressures without showing any evidences of plasticization [8]. Therefore, the scope of this work is to determine in detail the permeation properties and the plasticization behavior of both pure gases and gaseous mixtures for dense flat sheet and asymmetric hollow fiber BTDA-TDI/MDI membranes.

2.2 Experimental.

2.2.1 Materials.

The selected co-polyimide BTDA-TDI/MDI is a commercial polymer produced by Lenzing with the trade name P84. The chemical structure of this polymer is shown in Figure 1.

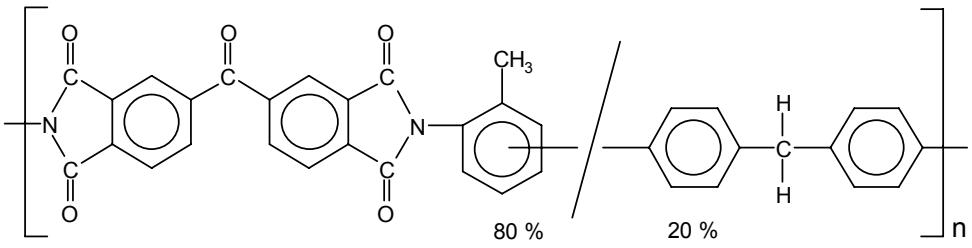

Fig. 1: Chemical structure of BTDA-TDI/MDI (P84) co-polyimide.

Its glass transition temperature is 315 °C. N-methyl-pyrrolidone (NMP), Merck 99 %, was used as the solvent and tap water as the external coagulant in the spinning of hollow fibers. Polydimethylsiloxane (Sylgard-184), commercialized by DOW Corning Corp., was used as the rubber coating material to plug undesired surface porosity, i.e. defects, of the produced hollow fibers. n-Hexane was the solvent for the Sylgard-184. Pure (99.5+%) CO_2 and N_2 gases

and a mixture of CO_2/N_2 80/20% used for gas permeation experiments were delivered from Praxair N.V. Belgium.

2.2.2 Dense flat sheet membranes.

P84 dense membranes were prepared by a casting method using a 13 wt% solution of P84 in NMP. After allowing the polymer to dissolve in the NMP overnight, the solution was filtered over a 25 μm metal filter to remove any impurities existing in the raw polymer material. The solution was subsequently cast on glass plates using a 200 μm casting knife. The produced specimen were first placed in a dry N_2 box for three days and then dried in a N_2 oven for two days at 150 °C to remove the solvent. The thickness of the obtained membrane was determined by using a micro screw gauge and was found to be approximately 20 μm.

2.2.3 Viscosity measurements.

The viscosities of P84/NMP solutions were measured by using a Brabender® cone and plate viscometer (Viscotron) at three different temperatures, 30, 50 and 70°C and at a shear rate of 32/min. Various concentrations (20-32 wt%) of P84 in NMP were tested. The viscosity value of each polymer concentration was determined by the magnitude of torque needed to overcome the viscous resistance when a cone-shape spindle rotates in the solution. The so-called critical polymer concentration, which also corresponds to the selected spinning dope concentration, was estimated by the intercept of the tangent line at the lowest polymer concentration (20 wt%) with the tangent line at the highest polymer concentration, (32 wt%). At this point, significant chain entanglement occurs in the spinning dope and the respective fibers show thin skin layers and minimum surface porosity [15].

2.2.4 Hollow fiber preparation.

P84 hollow fibers were prepared by the dry/wet phase inversion process in a spinning set up described in detail previously [16]. The spinning dope, consisting only of P84 and NMP, was mixed for 8 hours at 50°C in a 2 liter stainless steel vessel by a 150 W IKA® Labortechnik laboratory stirrer (Janke & Kunkel Gmbh&Co.). Then, the polymer solution was filtered through a 15 μm metal filter (Bekipor ST 15Al3, Bekaert S.A., Belgium) into a second stainless steel vessel, under a nitrogen pressure of 5 bar, in order to remove non-dissolved residual material. The bore liquid was a mixture of NMP and deionized water (Milli-Q, 18 MΩ.cm). The polymer dope and the bore liquid were allowed to degas for at least 2 days before spinning. By using gear pumps,

both solutions were simultaneously fed through a tube-in-orifice spinneret. The inner and outer diameters of the spinneret were 200 and 500 μm, respectively. The extruded fibers passed first through an air-gap of 10 cm before entering the coagulation bath filled with tap water at room temperature. P84 fibers were extended with a certain velocity by means of a pulling wheel and collected in a reservoir filled with tap water. In order to remove residual NMP, produced fibers were washed thoroughly with tap water, then solvent exchanged with ethanol for 4 hours, and dried overnight in the atmosphere.

2.2.5 Scanning Electron Microscopy (SEM).

The geometrical characteristics and the morphology of the developed P84 hollow fibers were determined by using a Jeol JSM-T220 Scanning Electron Microscope. Membrane samples were first immersed in ethanol, freeze fractured using liquid nitrogen and sputtered with a thin layer of gold using a Balzers Union SCD 040 sputtering apparatus.

2.2.6 Hollow fiber modules preparation and post-treatment.

About 4-5 P84 hollow fibers, each 10 to 15 cm long, were potted from the one side into 3/8 in. stainless steel holders, while sealing the other side by using a regular epoxy resin. Defects on the membrane surface were plugged by immersing the hollow fiber bundle, after potting, for 5 minutes into a solution of 3 wt% PDMS in n-hexane solution, followed by curing at 65 °C for 4 hours.

2.2.7 Gas permeation experiments.

The N_2, O_2, CO_2, and He permeability coefficients and permeance values of the developed P84 flat sheet and hollow fibers, respectively, as well as the separation performance of a CO_2/N_2 80/20% mixture, were measured as function of feed temperature and feed pressure. Experiments were performed in two different permeation units, operating either at low (max. 10 bar) or high (max. 60 bar) pressure. Pure gas permeability coefficients and permeance values were calculated from the steady state pressure increase with time in a calibrated volume at the permeate side by using the following formula:

$$\frac{\boldsymbol{P}}{l} = \frac{V \cdot 273.15 \cdot (p_t - p_0)}{A \cdot T \cdot \frac{(P_t + P_0)}{2} \cdot 76 \cdot t} \cdot 10^6 \ , \qquad (1)$$

where the ideal gas law is assumed to be valid and t [s] is the time, p_t [bar] is the pressure at the permeate side at time t, where p_0 is the permeate pressure at t = 0 , P [bar] is the feed pressure, T [K] is the temperature, V [cm^3] is the calibrated permeate volume, and A [cm^2] the total membrane area. the gas permeance P/l is expressed in GPU, i.e. 10^{-6} cm^3cm^{-2} s^{-1} $cmHg^{-1}$. Multiplying the gas permeance with the thickness of dense membranes, l [μm], gives the permeability coefficient in Barrer. Dividing the intrinsic gas permeability (Barrer) with the obtained permeance (GPU) of asymmetric hollow fiber membranes gives the thickness of the top layer in μm. The ideal selectivity was determined from the ratio of pure gas permeabilities or permeances measured at the same experimental conditions.
Gas diffusion coefficients of flat sheet membranes were determined by using the time lag method and the following formula:

$$D = \frac{l^2}{6\theta}, \qquad (2)$$

where D is the diffusion coefficient [cm^2s^{-1}], l is the membrane thickness [cm], and θ is the time lag [s].

For plasticization experiments, the detailed experimental protocol included: (1) thorough membrane degassing and evacuation, (2) determination of pure N_2 and CO_2 permeability or permeance at 4 bar respectively, (3) increase of CO_2 feed pressure from 4 to 30 bar (flat sheet) or 18 bar (hollow fibers) with a step of 2-4 bar, (4) overnight membrane degassing and (5) repeating step No.2. In experiments with the CO_2/N_2 80/20% binary mixture, the residue flow rate was kept constant and equal to 30 cm^3(STP)/min, at any feed pressure, in order to have relatively low stage cut values and uniform feed composition across the membranes. Feed and permeate compositions were analyzed by means of a Perkin Elmer Gas Chromatograph equipped with a Porapak Q column. The pure N_2 and CO_2 permeance values were calculated by using the feed and permeate compositions and the total gas mixture permeance. The real CO_2/N_2 selectivity was determined by the ratio of CO_2 and N_2 mole fractions in the permeate and feed stream. The high pressure permeation unit was fully automated and controlled by means of Lab View Software. The temperature was kept constant and equal to 35°C.

2.3 Results and discussion.

P84 flat sheet membranes

2.3.1 Gas permeability and diffusivity measurements.

Figure 2 shows the natural logarithms of the permeability (2a) and the diffusion coefficient (2b) versus 1000/T of N_2, O_2, CO_2, and He through P84 flat sheet membranes as a function of temperature at 4 bar.

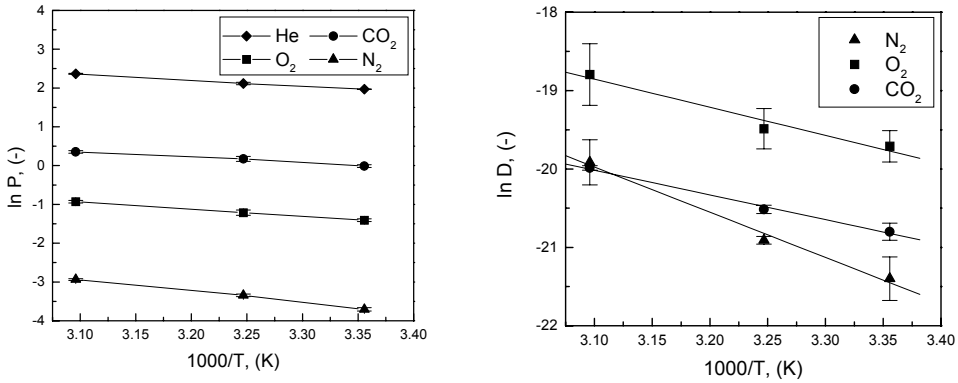

Fig. 2(a, b): Natural logarithms of permeability (2a) and diffusion coefficients (2b) of He (◆), CO_2, (●) O_2 (■), and N_2 (▲) versus 1000/T for dense P84 membranes at 4 bar.

Gas permeabilities are relatively low, for example He: 7.2 Barrer and CO_2: 1 Barrer at 25°C and 4 bar. As expected, permeability coefficients for all gases increase with temperature. Especially, the permeability and diffusion coefficients of N_2 are strongly dependent on temperature, which is also shown in Table 1 where the activation energies for permeation and diffusion are presented. The activation energy for permeation and diffusion of N_2 are 24.5 and 47.9 kJ/mol, respectively, almost two times higher compared to the other gases. The diffusion coefficient of He could not be determined accurately by time lag experiments even at very low feed pressures.

Table 1. E_{act} for permeation and diffusion of He, CO_2, O_2, and N_2 through P84 membranes.

	He	CO_2	O_2	N_2
E_{act} for permeation (kJ/mol)	12.7	11.6	15.3	24.5
E_{act} for diffusion (kJ/mol)	-	26.2	29.8	47.9

Table 2. Permeability and selectivity for P84 and Matrimid 5218. (25 °C).

	P_{He} [Barrer]	P_{He}/P_{N2} [-]	P_{CO2} [Barrer]	P_{CO2}/P_{N2} [-]	P_{O2} [Barrer]	P_{O2}/P_{N2} [-]
P84	7.2	292	0.99	40.2	0.24	10.0
Matrimid 5218	22.5	122	8.7	37.8	1.32	7.2

The effect of temperature on the ideal selectivity coefficients of He, CO_2, and O_2 over N_2 is displayed in Figure 3. The selectivity decreases somewhat with temperature, but generally remains very high. For example the ideal selectivity of He/N_2 is about 292 and that of CO_2/N_2 about 40. Table 2 summarizes the separation properties of the developed P84 flat sheet membrane in comparison with data reported for polyimide, Matrimid 5218, membranes [12, 17]. It is clear that P84 membranes, though less permeable, exhibit significantly higher ideal selectivity coefficients.

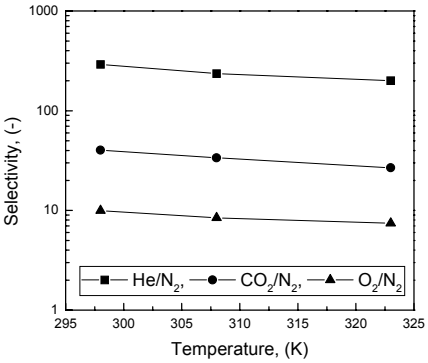

Fig. 3: Ideal selectivity factors of He (■), CO_2 (●), and O_2 (▲) over N_2 versus the temperature for dense P84 membranes at 4 bar.

2.3.2 CO_2 plasticization of P84 flat sheet membranes.

To investigate the plasticization behavior of P84 flat sheet membranes, the CO_2 permeability was measured at feed pressures up to 30 bar. As can be seen in Figure 4, the CO_2 permeability reduces gradually with increasing feed pressure. For comparison reasons, in the same figure the permeability coefficient measured for N_2 at 4 and 20 bar is given. Although the increase of feed pressure results in a slight decrease of ideal selectivity, it is clear that the P84 flat sheet membrane does not show the steep increase of CO_2 permeability typical for plasticization, not even at a CO_2 feed pressure of 30 bar [8].

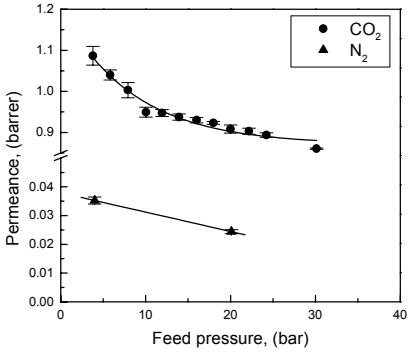

Fig. 4: Permeability of CO_2 (●) and N_2 (▲) versus the feed pressure for dense P84 membranes at 35 °C.

Asymmetric P84 hollow fiber membranes

2.3.3 Viscosity measurements and hollow fiber morphology.

Figure 5 shows the effect of P84 concentration on solution viscosity at three different temperatures. As expected, increase of polymer concentration and decrease of temperature results in higher spinning dope viscosity values. However, a significant increase is observed at a critical concentration of about 28.5 wt% and this value was chosen for the formulation of the spinning dope. The exact spinning conditions are given in Table 3. Figures 6 (a-c) show the geometrical characteristics and the structure of PDMS coated P84 asymmetric hollow fiber membranes. These fibers exhibit a typical asymmetric structure; a top layer supported by a sponge-like porous substructure, which contain some sporadic macrovoids.

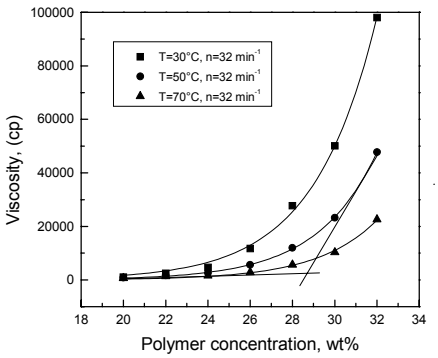

Fig. 5: Effect of P84 concentration on dope viscosity.

Table 3. Spinning conditions and process parameters.

Parameter	Value
Outer diameter of inner orifice, (mm)	0.2
Inner diameter of the 1st orifice, (mm)	0.5
P84 concentration in NMP, wt%	28.5
Viscosity, (cp)	14030
Dope fluid rate (ml/min)	1.98
Take up velocity, (m/min)	8.9
Spinning temperature, (°C)	50
Bore fluid composition (NMP/H_20, wt%)	80/20
Bore fluid flowrate, (ml/min)	0.96
Type of Coagulant	Water
Coagulant bath temperature, (°C)	23
Air Gap, (cm)	10
Room Temperature, (°C)	23
Room Humidity, (%)	55

The outer diameter and the wall thickness are 510 and 95 μm, respectively. The PDMS coating layer shows a good adhesion on the supporting P84 membrane and a uniform thickness of about 0.5-1 μm.

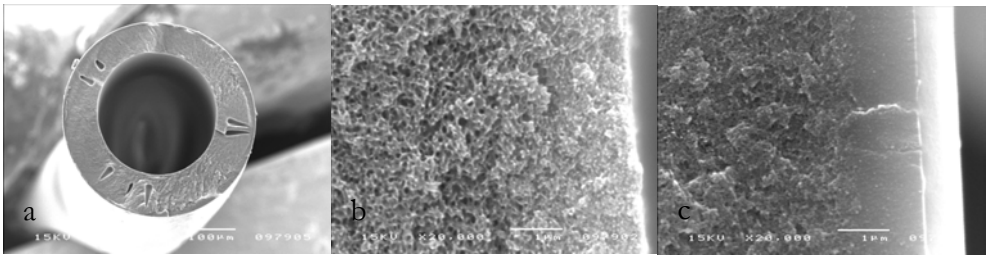

Fig. 6(a-c): SEM pictures of P84 hollow fiber membranes; cross section, (6a : fiber structure, 6b : bore side, 6c : P84 skin layer/PDMS coating).

2.3.4 Permeation properties of pure gases.

Tables 4 summarizes the permeation properties of N_2, O_2, CO_2, and He for as-spun uncoated and PDMS coated hollow fibers, measured at 4 bar and 25°C. In general, P84 hollow fiber exhibit relatively low gas permeance values, while the equivalent skin thickness is in the range of 0.5±0.05 μm. Despite their low productivity, the developed hollow fibers show very high ideal selectivity coefficients. From the values in Table 4 the average ideal selectivity coefficients

can be calculated. For the gas pairs CO_2/N_2, O_2/N_2, and He/N_2 they are 46, 8.6, and 301 respectively, which are amongst the highest reported ever for glassy polymers.

Table 4. Gas permeance of uncoated and PDMS coated P84 hollow fibers.

Gas	Permeance, (GPU) Uncoated	Permeance, (GPU) PDMS coated	Skin layer Av. Thickness, (μm)
N_2	1.5±0.5	0.047±0.005	0.526
O_2	2.0±0.5	0.41±0.03	0.585
CO_2	4.9±1.2	2.2±0.2	0.454
He	21.1±3.0	14.3±1.2	0.502

Figure 7 depicts the effect of feed pressure on CO_2 permeance of P84 hollow fiber membranes. Contrary to the case of flat sheet membranes (Figure 4), P84 hollow fibers show pronounced plasticization behaviour for feed pressures higher than 7-8 bar. Apart from the dependence of CO_2 permeance on feed pressure, the plasticization becomes evident from the reduction of the ideal separation factors, (Step 5. of the experimental protocol), which is 14% for CO_2/N_2. The reduction of the ideal CO_2/N_2 selectivity is due to the fact that, during experiments with CO_2 at high feed pressures (20 bar), the membrane swells. A residual undesired swelling remains after degassing [18]. As a consequence, in a subsequent permeation experiment, the permeance of the low permeating gas, N_2, is also increased.

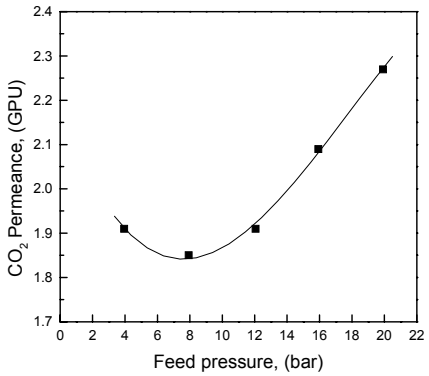

Fig. 7: Effect of feed pressure on pure CO_2 permeance of P84 hollow fiber membranes.

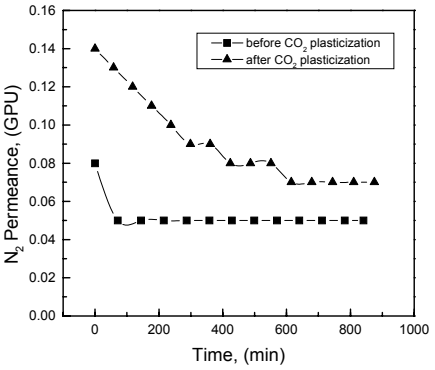

Fig. 8: Time dependence of N_2 permeance for virgin and plasticized P84 hollow fiber membranes.

This is also demonstrated in Figure 8 where the time dependence of N_2 permeance before and after CO_2 plasticization is depicted. In virgin samples, the steady state N_2 permeance value is achieved almost immediately while after CO_2 plasticization the N_2 permeance decreases gradually with time and is stabilized after 15 hours at a value, which is higher than the equilibrium permeance of virgin hollow fibers.
Several authors have reported on the difference in molecular ordering of polymers in ultra thin layers. Despotopoulou et. al [19] showed disordering of the backbone and hindered crystallization by using UV adsorption, fluorescence, and IR spectroscopy. Jones et. al. [20] used small angle neutron scattering to investigate chain structure and conformation. According to Shishatskii et. al. [21] the solubility coefficient of CO_2 is reversibly proportional to the membrane thickness. As the polymer film becomes thinner, its density increases, the specific volume, V_s, decreases, the molar cohesion energy, E_{coh}, remains constant and consequently the cohesive energy density ($CED=E_{coh}/V_s$) of the material is also increased. An increasing density leads to a reduced fractional free volume, hence one expects the gas solubility to reduce as well. However, polymer-penetrant interactions correlate with the CED in such a way that higher CED values lead to a stronger affinity between the polymer and the penetrant. A more densely packed glassy material with the same chemical structure, therefore, dissolves more gas. Asymmetric (0.1-0.5 μm) hollow fibers could exhibit higher CO_2 sorption capacity and, therefore, accelerated plasticization behavior.

2.3.5 Performance of P84 flat sheet and hollow fiber membranes in the separation of a CO_2/N_2 80/20% binary mixture.

Apart from the permeation properties of pure gases, the developed flat sheet and hollow fiber P84 membranes were tested for their performance in the separation of a CO_2/N_2 80/20% mixture. A high CO_2 concentration in the feed gas (80%) was chosen in order to reduce the permeation time needed to collect a sufficient sample for GC analysis. Both flat sheet and hollow fibers were studied in the same permeation set-up, simultaneously and in parallel, at three different feed pressures, 10, 20 and 30 bar. Figure 9 shows the effect of feed pressure on the CO_2 permeability coefficient and CO_2 permeance value of dense flat sheet and hollow fiber P84 membranes, respectively. In the same figure, the stage cut values applied at each feed pressure are also reported. Since the dense membrane was significantly thicker than the asymmetric hollow fiber (20 μm vs. 0.5 μm) and the applied residue flow rate was the same in both cases, 30 cm^3(STP)/min, the obtained stage cut (sc) values were

significantly lower in dense membranes. Similar to the permeation measurements of pure CO_2 in dense membranes (Figure 4), the CO_2 permeability measured from the separation of the binary mixture reduces slightly with feed pressure. From both curves it can be concluded that no plasticization takes place.

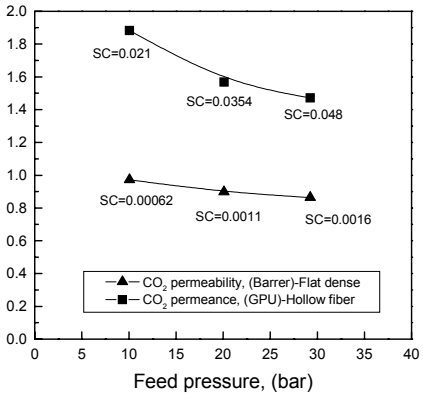

Fig. 9: Effect of feed pressure on CO_2 permeability coefficient (▲) and CO_2 permeance value (■) for dense and asymmetric hollow fiber P84 membranes.

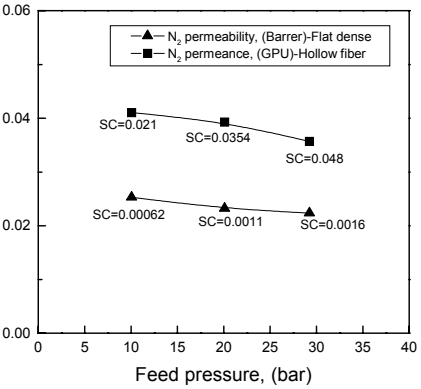

Fig. 10: Effect of feed pressure on N_2 permeability coefficient (▲) and N_2 permeance value (■) for dense and asymmetric hollow fiber P84 membranes.

Figure 10 demonstrates the effect of feed pressure on the N_2 permeability coefficient and N_2 permeance value. In both cases, increase of pressure leads to a decrease in N_2 permeance, further emphasizing the resistance of both structures to high pressures of CO_2. Compared to the permeability coefficients and permeance values reported in Figure 4 and Table 4, the CO_2 and N_2 values for both flat sheet and hollow fibers are slightly lower. This difference can be attributed to the physical ageing of P84 membranes in the time period between the pure gas permeation and gaseous mixture experiments. In agreement with previous studies, the phenomenon of physical ageing is more pronounced for the asymmetric hollow fibers [11].

The slight reduction of CO_2 permeance with feed pressure in the CO_2/N_2 80/20 mixture can be interpreted by considering not only the CO_2 plasticization effect but also the competition phenomena operative due to the presence of a second permeating gas, N_2. The gradual saturation of unrelaxed

sorption sites by molecules of two different gases can affect both solubility and diffusivity coefficients. This competition can result in lower local penetrant concentration, reduced driving force difference across the membrane and therefore lower gas permeance values [22].
Finally, Figure 11 shows the effect of feed pressure on CO_2/N_2 real selectivity for P84 flat sheet and hollow fiber membranes. The real CO_2/N_2 selectivity remains almost constant with feed pressure for dense membranes. This behavior can be attributed to the negligible effect of feed pressure on pure gas permeability coefficients. However, in the case of P84 hollow fiber membranes, the CO_2/N_2 selectivity is reduced with pressure from 46 to 40. This reduction can be partially attributed to the fact that at high feed pressure the stage cut is also higher, leading to lower permeate purity and therefore lower selectivity values. Independent of the stage cut, the real CO_2/N_2 selectivity coefficient obtained for asymmetric hollow fibers is slightly higher than the respective value for dense P84 membranes. This discrepancy in behavior can be explained by differences in polymer chain packing in thick films compared to thin films. It has been reported previously that ultra thin glassy polymer films show accelerated physical ageing, while thicker films from the same material show no such effects. The severe reduction of gas permeabilities in thin films or hollow fibers can lead to gas selectivities higher than the respective dense membranes [11, 23].

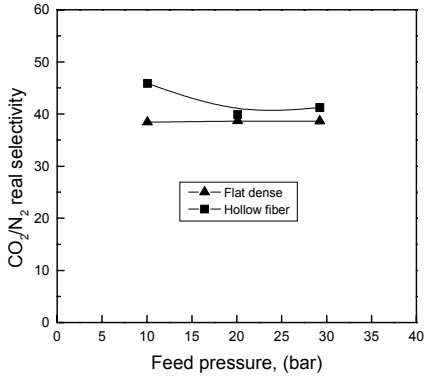

Fig. 11: Effect of feed pressure on real CO_2/N_2 selectivity coefficients for dense (▲) and asymmetric hollow fiber (■) P84 membranes.

2.4 Conclusions.

We investigated the permeation properties and the separation performance of flat sheet and hollow fiber membranes based on co-polyimide BTDA-TDI/MDI (P84). This material exhibits excellent separation properties for He/N_2, CO_2/N_2, and O_2/N_2, with ideal selectivities in the range of 285-300, 45-50, and 8.3-10 respectively, which are among the highest ever reported for polymeric membranes. Although the CO_2 permeability was found to be relatively low, (~1 Barrer at 25°C), the flat sheet membranes showed no evidence of plasticization at CO_2 feed pressures up to 30 bar.
P84 hollow fiber membranes, prepared by the dry/wet phase inversion process, were also investigated and compared with dense flat sheet membranes, with regard to gas permeance, selectivity, and the plasticization behavior for both pure gases and a binary gaseous mixture. While the obtained ideal selectivities were comparable with those measured for dense membranes, the plasticization behavior was quite different. P84 asymmetric hollow fibers showed severe plasticization effects, starting immediately at low pure CO_2 feed pressures. However, plasticization phenomena were suppressed when instead of pure CO_2, a gaseous mixture consisting of CO_2/N_2, 80/20%, was used. Although an expected decrease of selectivity with pressure was observed, no increase of CO_2 permeability with feed pressure could be seen.
These results indicate that P84 co-polyimide is a promising material for the preparation of gas separation membranes with extremely high selectivity coefficients. Its relatively low permeability can be compensated by the optimization of the spinning procedure and the formation of ultra-thin asymmetric hollow fibers.

2.5 References.

[1] W. J. Koros, G. K. Fleming, Membrane-Based Gas Separation, J. Membr. Sci. 83 (1993) p1-80.

[2] A. Bos, I. G. M. Punt, M. Wessling, H. Strathmann, CO2-induced plasticization phenomena in glassy polymers, J. Membr. Sci. 155 (1999) p67-78.

[3] J. J. Krol, M. Boerrigter, G. H. Koops, Polyimide hollow fiber gas separation membranes: preparation and the suppression of plasticization in propane/propylene environments, J. Membr. Sci. 184 (2001) p275-286.

[4] R. W. Baker, Future directions of membrane gas separation technology, Ind. Eng. Chem. Res. 41 (2002) p1393-1411.
[5] A. Bos, I. G. M. Punt, M. Wessling, H. Strathmann, Plasticization-resistant glassy polyimide membranes for CO2/CO4 separations, Sep. Purif. Technol. 14 (1998) p27-39.
[6] C. Staudt-Bickel, W. J. Koros, Improvement of CO2/CH4 separation characteristics of polyimides by chemical crosslinking, J. Membr. Sci. 155 (1999) p145-154.
[7] A. Bos, I. G. M. Punt, M. Wessling, H. Strathmann, Suppression of CO2-plasticization by semiinterpenetrating polymer network formation, J. Polym. Sci. Pt. B-Polym. Phys. 36 (1998) p1547-1556.
[8] A. Bos, I. Punt, H. Strathmann, M. Wessling, Suppression of gas separation membrane plasticization by homogeneous polymer blending, Aiche J. 47 (2001) p1088-1093.
[9] G. C. Kapantaidakis, S. P. Kaldis, X. S. Dabou, G. P. Sakellaropoulos, Gas permeation through PSF-PI miscible blend membranes, J. Membr. Sci. 110 (1996) p239-247.
[10] J. L. Keddie, R. A. L. Jones, R. A. Cory, Size-Dependent Depression of the Glass-Transition Temperature in Polymer-Films, Europhys. Lett. 27 (1994) p59-64.
[11] P. H. Pfromm, W. J. Koros, Accelerated Physical Aging of Thin Glassy Polymer-Films - Evidence from Gas-Transport Measurements, Polymer 36 (1995) p2379-2387.
[12] M. Wessling, M. L. Lopez, H. Strathmann, Accelerated plasticization of thin-film composite membranes used in gas separation, Sep. Purif. Technol. 24 (2001) p223-233.
[13] R. Wang, S. L. Liu, T. T. Lin, T. S. Chung, Characterization of hollow fiber membranes in a permeator using binary gas mixtures, Chem. Eng. Sci. 57 (2002) p967-976.
[14] G. C. Kapantaidakis, G. H. Koops, M. Wessling, Preparation and characterization of gas separation hollow fiber membranes based on polyethersulfone-polyimide miscible blends, Desalination 145 (2002) p353-357.
[15] T. S. Chung, S. K. Teoh, X. D. Hu, Formation of ultrathin high-performance polyethersulfone hollow-fiber membranes, J. Membr. Sci. 133 (1997) p161-175.
[16] G. C. Kapantaidakis, G. H. Koops, High flux polyethersulfone-polyimide blend hollow fiber membranes for gas separation, J. Membr. Sci. 204 (2002) p153-171.

[17] D. T. Clausi, W. J. Koros, Formation of defect-free polyimide hollow fiber membranes for gas separations, J. Membr. Sci. 167 (2000) p79-89.
[18] M. Wessling, I. Huisman, T. van der Boomgaard, C. A. Smolders, Dilation Kinetics of Glassy, Aromatic Polyimides Induced by Carbon-Dioxide Sorption, J. Polym. Sci. Pt. B-Polym. Phys. 33 (1995) p1371-1384.
[19] M. M. Despotopoulou, R. D. Miller, J. F. Rabolt, C. W. Frank, Polymer chain organization and orientation in ultrathin films: A spectroscopic investigation, J. Polym. Sci. Pt. B-Polym. Phys. 34 (1996) p2335-2349.
[20] R. L. Jones, S. K. Kumar, D. L. Ho, R. M. Briber, T. P. Russell, Chain conformation in ultrathin polymer films, Nature 400 (1999) p146-149.
[21] A. M. Shishatskii, Y. P. Yampolskii, K. V. Peinemann, Effects of film thickness on density and gas permeation parameters of glassy polymers, J. Membr. Sci. 112 (1996) p275-285.
[22] B. J. Story, W. J. Koros, Comparison of 3 Models for Permeation of Co2/Ch4 Mixtures in Poly(Phenylene Oxide), J. Polym. Sci. Pt. B-Polym. Phys. 27 (1989) p1927-1948.
[23] I. Pinnau, M. W. Hellums, W. J. Koros, Gas-Transport through Homogeneous and Asymmetric Polyestercarbonate Membranes, Polymer 32 (1991) p2612-2617.

Chapter 3

Intermediate polymer to carbon gas separation membranes based on Matrimid PI*.

J.N. Barsema, S.D.Klijnstra, N.F.A. van der Vegt, G.H. Koops, and M. Wessling

Abstract

Matrimid polyimide gas separation membranes were exposed to different heat treatments between 300 and 525°C to investigate the intermediate structures that evolve between annealing and carbonization. The exposure time was either 5 or 30 minutes, while the atmosphere was N_2. It was found, using TGA and FTIR, that below 425°C no thermal decomposition takes place. At higher temperatures thermal decomposition leads to the formation of intermediate structures as the process of carbonization starts. Gas permeation measurements with He, N_2, O_2, CO_2, and C_3H_6 show that the structure becomes more dense at treatments below the T_g of the polymer, whereas above the T_g a concurrent formation of charge transfer complexes takes place. A steep increase of permeability was found at heat treatments above 475°C, attributed to the thermal decomposition and the transition to carbon membranes. All heat-treated membranes showed a good resistance to plasticization by C_3H_6, although the permeability decreased, when compared to untreated membranes. Membranes treated at 475°C for 30 min showed no plasticization combined with sustained permeation rates.

* Submitted to J. Membr. Sci .

3.1 Introduction.

Over the last decades, polymeric membranes have proven to operate successfully in industrial gas separations [1]. To obtain membranes that combine high permeability and high selectivity together with thermal stability, new polymers, so called high performance polymers were developed like polyimide (PI), poly(phenyl oxide) (PPO), poly(trimethylsilylpropyne) (PTMSP), and Polytriazole. The commercially produced polyimide Matrimid 5218 has shown promising properties when separating gas mixtures like O_2 and N_2, CO_2 and CH_4, CO_2 and N_2, and C_3H_6 and C_3H_8 [2-4]. Combined with the ability to prepare asymmetric integrally skinned hollow fiber membranes with ultra thin top layers, these membranes allow the preparation of gas separation membrane modules for large scale industrial applications[2,4]. Lab scale experiments with dense flat sheet membranes, however, show a major side effect. When the feed gas mixture contains condensable gases like e.g. CO_2 or C_3H_6 [4-7] a minimum is observed in the permeability vs. feed pressure curve followed by a steep increase in permeability combined with a decrease in selectivity when exceeding a certain feed pressure. This effect has been explained by the occurrence of plasticization of the polymer above the plasticization pressure. The membrane structure swells and permeability of all components in the feed increases significantly. Wessling *et.al.* [8] have shown for dense flat sheet membranes prepared from Matrimid 5218 that the plasticization pressure decreases with film thickness. This was recently confirmed by Barsema *et.al.* [9] showing that asymmetrical integrally skinned membranes of P84 co-polyimide with thin top layers showed severe plasticization, whereas for their relatively thick dense flat sheet counterparts, no plasticization effects were observed.
In literature, many articles can be found reporting different procedures to reduce the extent of plasticization phenomena in glassy polymer membranes. Methods used are: 1) heat treatment (e.g. annealing) [4], 2) thermally induced cross-linking [3], 3) chemical cross-linking [10], 4) inter-penetrating network formation [11], and 5) polymer blending [12, 13].

A relatively recent development in gas membrane separation is the preparation of Carbon Molecular Sieve membranes. These membranes are generally produced by pyrolysis of polymeric precursors and can potentially achieve high selectivity while sustaining the permeability and more important they do not show any plasticization phenomena. However, these membranes have two distinct disadvantages. Firstly, they are expensive compared to their polymeric

counterparts. Secondly, and of greater significance, it is quite difficult to produce large defect free surface areas with sufficient mechanical strength for commercial application.

Much research focuses on separate parts of the temperature range: annealing around the T_g, to prevent plasticization or carbonization at temperatures well above 500 °C. Little systematic information exists for the intermediate region of the polymer-to-carbon transition. This paper discusses the intermediate structures that evolve in-between annealing and carbonization. These structures combine properties of both polymers and carbons. This work will focus on the effects of heat treatment, extended considerably over the T_g of the material, on the chemical composition, the molecular structure, the permeation properties, and the plasticization phenomena using Matrimid 5218 polyimide membranes.

3.1.1 Background.

Polymeric membranes are heat treated by allowing the membrane to be exposed to a heated atmosphere. This atmosphere can be either reacting (e.g. O_2, air, or CO_2), inert (e.g. N_2, Ar), or vacuum. When a reacting atmosphere is applied the membrane is annealed, but thermo-chemical cross-linking and decomposition can take place [3], depending on the thermal resistance of the polymer, at relatively low temperatures. In inert or vacuum atmospheres the heat treatment of polymers can be classified into three processes: 1) annealing 100 – 400°C [14], 2) pyrolysis forming carbon 500 – 1000°C [15], and 3) an intermediate state 400 – 500°C; where decomposition starts but no carbon structure is formed yet.

During the annealing step the polymer membrane undergoes an accelerated physical ageing, reducing permeability by relaxation of the frozen glassy structure. Concurrently, in the case of polyimides, the formation of charge transfer complexes (CTC) can occur [4, 14, 16]. CTC's are weak, intra and inter molecular, bonds between the electron rich aromatic ring and the electron deficient imide ring of the polyimide, formed by the donation of π-electrons. As the temperature of the annealing process increases (most significantly above the T_g of the polymer), a higher mobility of the molecules allows for a more dense (energetic more favorable) chain packing and ultimately to a higher density of the polymer [17].

As the temperature is raised above the glass transition temperature also rejuvenation can occur counteracting the effects of physical ageing, increasing the free volume of the polymer.

If a polyimide membrane is subjected to temperatures over 500°C in an inert atmosphere, decomposition to carbon takes place [18]. The weight of the polymer decreases rapidly, while pyrolysis gases, like CO_2, CO, H_2, CH_4, and N_2, evolve from the polymer. The resulting material consists of aromatic carbon with a turbostratic graphite or vitreous carbon structure. These materials combine high permeability with molecular sieve properties and are promising membrane materials [15].
In the temperature range of 400 – 500°C the polymer structure is damaged and an intermediate material is formed.

3.2 Experimental Section.

3.2.1 Materials.

As membrane material, a BTDA-AAPTMI polyimide (Matrimid 5218, Ciba Specialty Chemicals Corp.) was used. The chemical structure is shown in Figure 1. This polyimide has a Tg of 322°C.

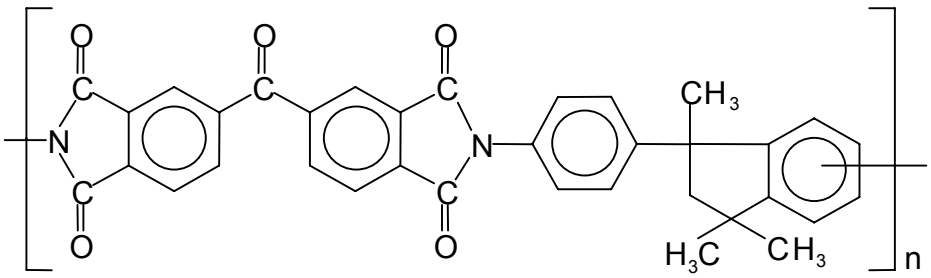

Fig. 1: Structure of Matrimid polyimide.

N-methyl-pyrrolidone (NMP), Merck 99 %, was used as the solvent. All gases used for heat treatment and gas permeation experiments had a purity of at least 99.5 %.

3.2.2 Membrane preparation.

All membranes prepared were based on a solution of 13 wt% Matrimid in NMP. The solutions were allowed to dissolve overnight and were subsequently filtered over a 25 μm metal filter to remove non-dissolved residual material.
The solutions were cast on glass plates using a 250 μm casting knife and placed in a dry N_2 box for three days, then placed in a N_2 oven for a further two days

at 150 °C to remove most of the solvent. The obtained precursor film had a thickness of approximately 25 μm. All membranes used for permeation and plasticization experiments were treated at 350°C for 120 minutes to remove any thermal and physical history.

3.2.3 Heat treatment procedure.

The heat treatment is preformed using a Carbolite® TZF 12/100 High Temperature Tube Furnace, mounted with an Eurotherm 2408CP temperature controller. Figure 2 gives a schematic overview of the furnace set-up.

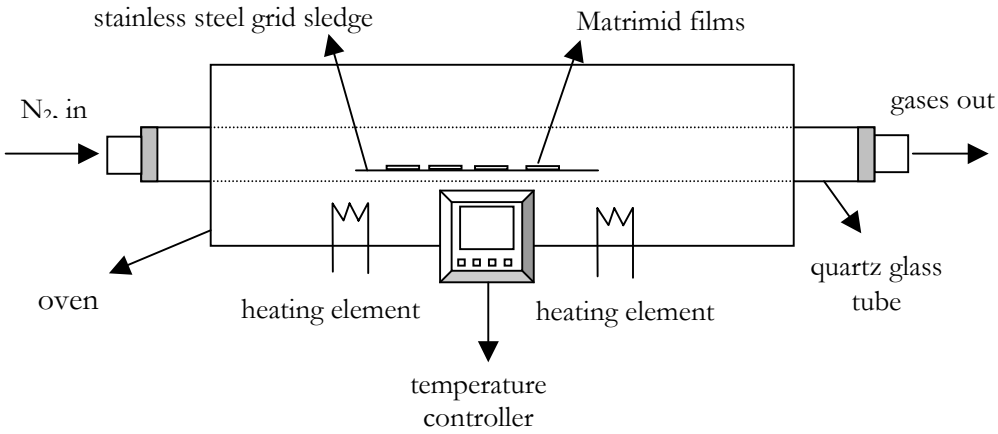

Fig. 2: A schematic overview of the furnace set-up.

The membrane is placed in a quartz glass tube, using a stainless steel grid or a quartz glass as sledge. The atmosphere in the quartz tube during pyrolysis was N_2, with a flow rate of 10 cm^3/min. Heat treatment procedures allowed the temperature to rise from room temperature to 150°C with a heating rate of 50°C/min. Subsequently, this temperature was held for 15 min to remove any adsorbed water. From 150°C until 350°C the temperature was raised with a rate of 5°C/min, thereafter the temperature increase was controlled at 1°C/min.

After reaching the end temperature, the membranes were kept at this temperature for either 5 or 30 minutes, before being quenched to room temperature in an external stainless steel double-hulled cooler containing a nitrogen atmosphere. The membranes were cooled by tap water flowing through the outer hull of the cooler.

3.2.4 Analysis.

Weight loss. The weight loss during heat treatment was determined using Thermo Gravimetric Analysis (TGA). The TGA experiments were preformed using a Perkin-Elmer TGA 7 with a N_2 atmosphere and flow rates of 20 cm^3/min. Heating routes were based on heat treatment procedures.

Density. For the density measurements, an AccuPyc 1330 Pycnometer with a 0.1 cm^3 sample insert was used. The AccuPyc measures the amount of displaced gas. The pressures observed upon filling the sample chamber and then discharging it into a second empty chamber allow computation of the sample solid phase volume. Gas molecules rapidly fill the tiniest pores of the sample; only the truly solid phase of the sample displaces the gas.
SF_6 was chosen as pressure gas, because of its large molecule size and its inert nature, in order to prevent adsorption of the pressure gas inside (the pores of) the membranes as much as possible.

Chemical structure. The changes in the chemical structure during the heat treatments were followed, using Fourier Transformed Infra Red Spectroscopy (FTIR). Heat treated Matrimid powders were mixed with KBr powder at low concentrations and then compressed into discs. These discs were placed into a Biorad Digilab FTS60 FT-IR Spectrometer. The IR absorption spectra were measured at room temperature from 4000 cm^{-1} to 500 cm^{-1} with a spectral resolution of 8 cm^{-1} and averaged over 64 scans.

Gas permeation. To elucidate the effect of the heat treatment on the permeability and selectivity of the membranes, the pure gas He, CO_2, O_2, N_2, and C_3H_6 permeability was determined. Brittle membranes were glued into metal discs, using an Araldit two component adhesive, to prevent cracking of the membranes by the rubber ring seals. The gas permeation experiments were done at the temperature of 25 °C, using a variable permeate pressure set-up. In the experimental set-up, a vacuum was applied on the permeate side, whereas the other side was brought into contact with the feed gases. All measurements were taken after the fluxes became constant in time. A more extensive description of the determination of both permeability and selectivity can be found elsewhere [9]. The reported results are based on measurements performed on two or more membranes.

Plasticization. Besides permeation experiments using C_3H_6 as plasticizing agent, permeation experiments were conducted on pre-plasticized membranes.

The membranes were plasticized, after heat treatment, by 56 bar of CO_2 in a pressure chamber at room temperature for 120 minutes and subsequently the He permeability was followed in the time.

CO_2 sorption. The CO_2 solubility in a number of heat treated samples, at 25°C, was determined using a Rubotherm magnetic suspension balance operated by MessPro software. This balance has an accuracy of 1 μg and a reproducibility of 2 μg. The samples were evacuated to a pressure below 10 Pa, before the CO_2 was applied. The obtained data were corrected for buoyancy effects, which were experienced because of the increased gas density at higher pressures. Besides the solubility of CO_2, the average diffusion coefficient of CO_2 was determined. In case of CO_2 in a glassy polymer, both coefficients are concentration dependent. When the permeability (P_i) is defined as the flux (J_i) normalized for the pressure difference across the membrane ($p_{feed,i}$-$p_{permeate,i}$) and membrane thickness (l), one can write down an equation for the permeability:

$$P_i = \frac{J_i}{\left(p_{feed,i} - p_{permeate,i}\right)/l} = \frac{-D(c_i)\partial c_i/\partial x}{\left(p_{feed,i} - p_{permeate,i}\right)/l}, \tag{1a}$$

and

$$J_i = -D(c_i)\frac{\partial c_i}{\partial x}, \tag{1b}$$

where P_i is the permeability [Barrer], J_i the flux [$cm^3(STP)cm^{-2}s^{-1}$], and $D(c_i)$ a local concentration-dependent diffusion coefficient of a penetrant at any arbitrary point between the feed and permeate side of the membrane [cm^2s^{-1}] with $\partial c_i/\partial x$ the local concentration gradient at the same point in the membrane [19].
Because the steady-state permeability is a constant for fixed feed and permeate conditions, the product of $D(c_i)$ and $\partial c_i/\partial x$ is constant at each point in a membrane. Integration of Equation (1a) over the membrane thickness ($x = 0 \rightarrow x = l$) gives:

$$\left(p_{feed,i} - p_{permeate,i}\right)\frac{P_i}{l}\int_0^l dx = -\int_{c_{permeate,i}}^{c_{feed,i}} D(c_i)\,dc_i \,, \tag{2}$$

which results in Equation (3) for negligible permeate pressure.

$$P_i = \frac{1}{p_{feed,i}}\int_0^{c_{feed,i}} D(c_i)dc_i \,. \tag{3}$$

Multiplying the numerator and denominator of Equation (3) by $c_{feed,i}$ gives for the permeability (P_i):

$$P_i = \left(\int_0^{c_{feed,i}} \frac{D(c_i)\,dc_i}{c_{feed,i}}\right)\left(\frac{c_{feed,i}}{p_{feed,i}}\right) = \overline{D_i}\cdot S_i \,, \tag{4}$$

where $\overline{D_i}$ is the *average* diffusion. If the permeability coefficient and solubility coefficient are determined at the same pressure and temperature, an average diffusion coefficient can be calculated from the ratio of the permeability and average solubility coefficients.

3.3 Results and discussion.

3.3.1 Thermal degradation followed by TGA.

The membranes and Matrimid samples prepared in this research are labeled by their end temperature and residence time, so the membrane treated at 425°C for 30 minutes is labeled 425/30.

Figure 3 shows the thermally induced weight loss of Matrimid versus time and temperature as measured by TGA. Also, the first derivative, the decomposition rate ($rate_{dec}$, wt%/min) is depicted.

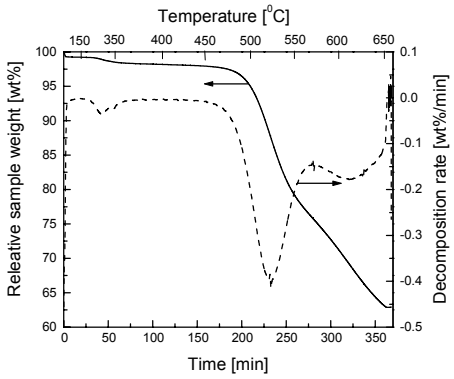

Fig. 3: Relative sample weight vs. time and temperature and decomposition rate vs. time.

Upto 350°C the weight loss is minimal and should be attributed to residual solvent and adsorbed water in the sample. When looking at Figure 3 the sample weight remains almost constant ($rate_{dec}$: ≈0 wt%/min) from 350°C up to approximately 450 °C. At this temperature, $rate_{dec}$ starts to increase, until a maximum is reached at approximately 520 °C ($rate_{dec}$: - 0.4 wt%/min). A second maximum occurs at approximately 610 °C ($rate_{dec}$: - 0.175 wt%/min). Above 610 °C $rate_{dec}$ decreases, although at 650 °C the weight still decreases significantly. According to Inagaki et.al. [18]:

- up to 450 °C, relative low weight loss caused by evaporation of residual water and solvents;
- 450 – 650 °C, rapid decrease of weight caused by degradation of the polymer, while H_2, CO, CO_2, and CH_4 evolve from the sample;
- 650 °C and higher, slow decrease in weight, caused by the evolving of residual non-elementary carbon components, primarily N_2.

From Figure 3, it seems that up to 450 °C no decomposition takes place, however, different TGA-measurements suggest that the first decomposition starts at 425 °C. The weight decrease of a sample held for 3200 minutes at 425 °C, was 10%. This weight loss cannot be explained by water and solvent evaporation only. Decomposition reactions are already occurring at 425 °C , even though the reaction rate is extremely low. From approximately 450 °C,

the rate of the first decomposition reaction is high enough to be detected for samples heated at a rate of 1 °C/minute.
In Figure 4, the loss weight of the Matrimid samples after different heat treatments is followed for samples heat treated up to 650 °C. There is a gradual decrease in final weight for samples treated up to 475 °C for 30 minutes. Although the sample 475/30 clearly shows a lower final weight than the samples treated at lower temperatures, the weight loss is relatively small. Samples treated at temperatures of 525 °C and higher show an increasing weight loss as they are carbonized.

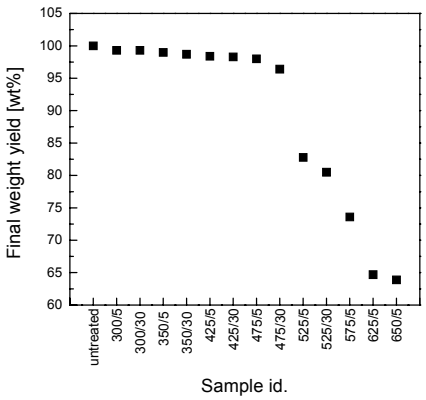

Fig. 4: Final weight yield after heat treatment.

3.3.2 Thermal degradation followed by FTIR.

The chemical changes taking place going through the transformation from polymer to carbon can be observed by FTIR. Figure 5 shows a FTIR spectrum of the pretreated Matrimid (350/120). Table 1 gives an overview of band assignments and wave numbers for the IR spectrum of Matrimid powder, heat-treated for 120 minutes at 350 °C.

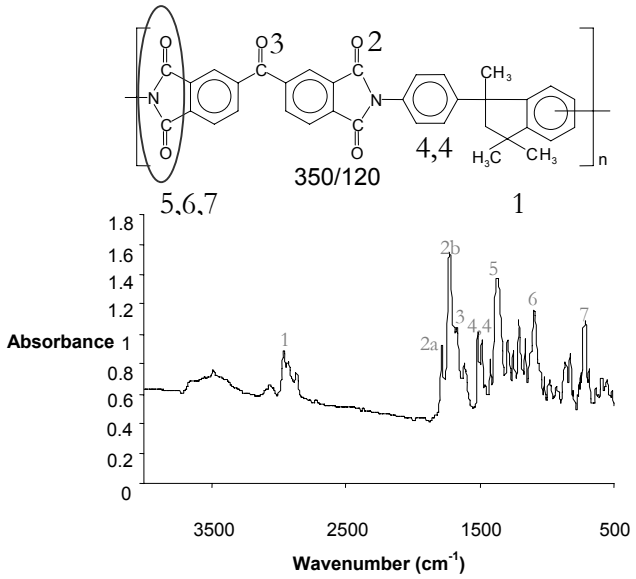

Fig. 5: IR spectrum of Matrimid powder, heat-treated for 120 minutes at 350 °C.

Table 1. Overview of band assignments and wave numbers for IR spectrum of Matrimid powder, heat-treated for 120 minutes at 350 °C.

Number	ν (cm^{-1})	Band assignment
1	2960-2860	ν (C-H) stretch of methyl groups
2a	1779	ν (C=O) symmetric stretch
2b	1725	ν (C=O) anti-symmetric stretch
3	1673	ν (C=O) stretch of benzophenone carbonyl
4 and 4'	1512 and 1488	ν (C=C) aromatic stretching
5	1374	ν (CNC) axial stretch
6	1096	ν (CNC) transverse stretch
7	717	ν (CNC) out-of-plane bending

Figure 6 shows the evolution of the chemical structure, visualized by FTIR spectra.

It becomes obvious from Figure 6 that the absorption spectrum changes with the intensity of the heat treatment (350/120 to 475/780). Generally, the absorption intensity decreases with a more intense heat treatment, as the

concentration of the functional groups, responsible for a specific peak, decreases.

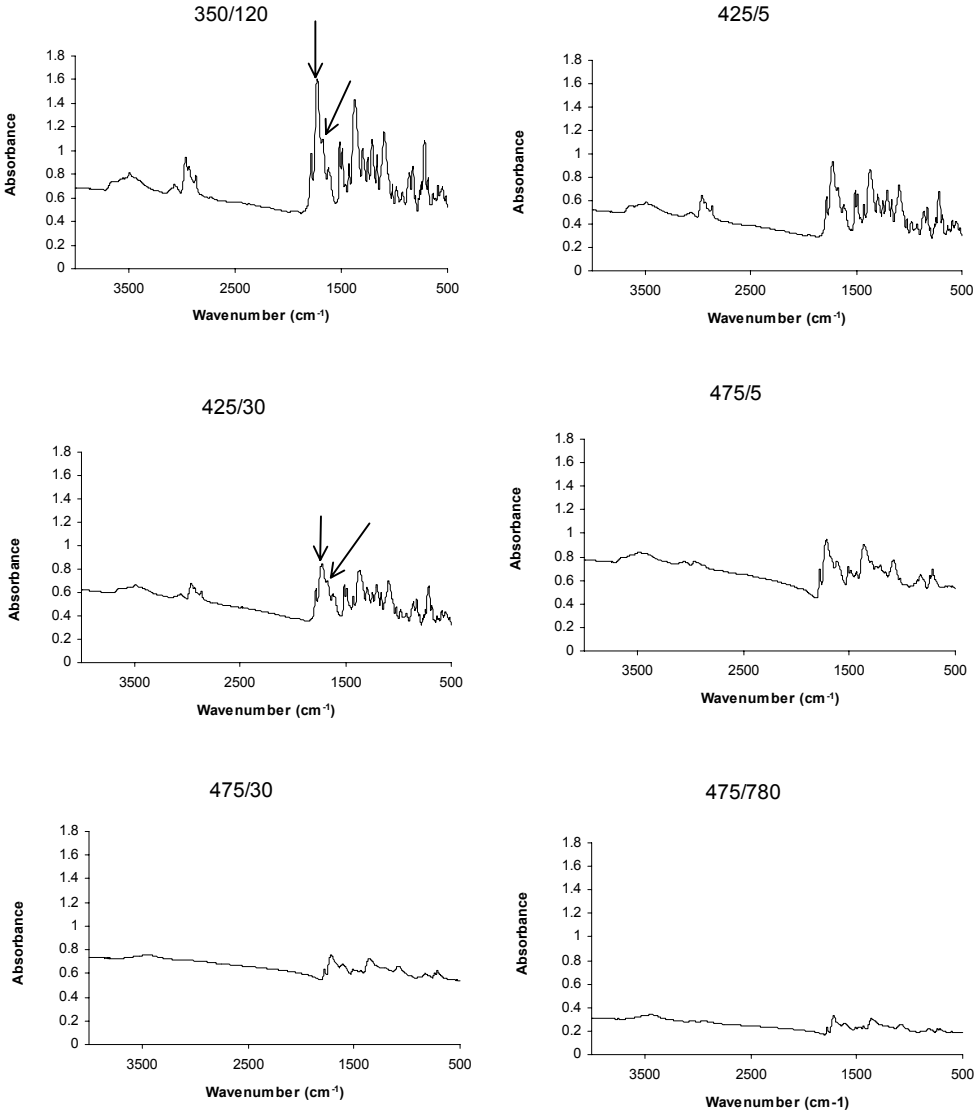

Fig. 6: IR spectra of Matrimid powder after different heat treatments (350 – 475°C).

When comparing 425/30 with 350/120, the ratio of peak intensity of the anti-symmetric stretch peak of the imide carbonyl group (1725 cm^{-1}) to the stretch peak of the benzophenone carbonyl group (1673 cm^{-1}) decreases from 1.8 to 1.4. The peaks are pointed out in Figure 6 for 350/120 and 425/30 by arrows. This is an indication that the imide carbonyl group concentration is decreasing compared to the benzophenone carbonyl group, pointing towards imide ring cleavage, resulting in destruction of the imide C=O groups. Whereas the Matrimid sample treated for 5 minutes at 475 °C still shows comparable absorption intensities when compared to membranes treated at 425 °C. The membrane treated for 30 minutes at 475 °C shows lower absorption intensities. The sample treated for 780 minutes at 475 °C, shows even lower absorption intensities. After 475/780 some imide rings are still present in the Matrimid sample, indicating the reaction has not ended entirely.

3.3.3 Density measurements.

The density was determined of Matrimid membranes (pretreated for 120 minutes at 350°C) heat-treated between 350 and 525 °C. The results are shown in Figure 7; the density increases slightly for membranes treated at 425 °C, as compared to the pretreated membranes. Thermal annealing results in a higher concentration of CTCs, which in turn results in a more dense chain packing and a, although minimal, higher density. As the Matrimid membranes are treated at temperatures of 475 °C and higher, the density increases significantly, due to the onset of carbonization.

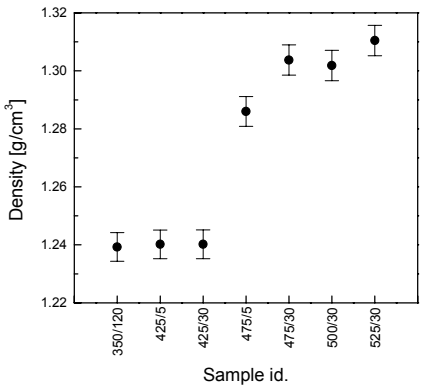

Fig. 7: Density of Matrimid membranes after different heat treatments.

The membranes treated up to 425 °C are dense polymeric membranes; they have lower densities and possess polymeric properties. The membranes treated at 500°C and higher are carbon membranes, they have a higher density (1.5 – 2.3 gcm^{-3} [20]) and possess carbon properties. The membranes treated at 475 °C show densities in between the polymeric and the carbon membranes. They cannot be described in terms of polymer membrane or carbon membrane only.

3.3.4 Permeation properties.

The effect of heat treatment on the permeation properties is shown in Figure 8 to 10, displaying the permeability of N_2, O_2, and CO_2 for different heat treatments at 2, 3, and 5 bar feed pressure. The lines are to guide the eye. All membranes have been pre-treated at 350°C for 120 minutes to obtain membranes with the same thermal history. It is clear that although the heat treatment has a large effect on the permeability, the effect is comparable for all feed pressures, most evident in Figure 10, indicating that the shape of the solubility curve is not significantly altered by the applied heat treatment. We will enlarge on this in a later section.

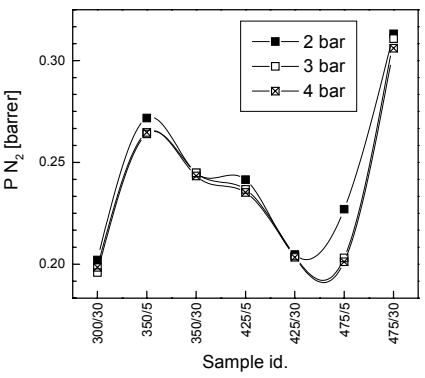

Fig. 8: N_2 permeabilities at different pressures for different membranes treated up to 475°C (2 bar ■, 3 bar □, 5 bar ☒). T = 25 °C.

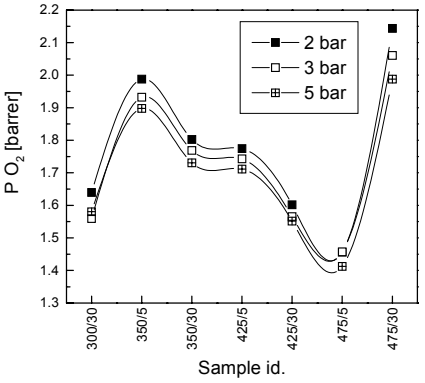

Fig. 9: O_2 permeabilities at different pressures for different membranes treated up to 475°C (2 bar ■, 3 bar □, 5 bar ☒). T = 25 °C.

For N_2 and O_2 (Figure 8 and Figure 9, respectively) the effect of the heat treatment is similar. The 300/30 membrane shows a depression of the permeability caused by annealing of the structure when treated at a

temperature below the T_g of the polymer. Prolonged treatments (30 min vs. 5 min) at 350 and 425°C lead to a depression of the diffusion coefficient, since the solubility is not effected by the heat treatment (see figure 11), and therefore the permeability, most likely caused by the formation of CTC's, through the increased chain mobility. As the membranes are exposed to a temperature of 475°C we observe an initial decrease of the permeability at short treatment times (475/5), but as decomposition reactions commence, the permeability shows a steep increase (475/30). Further exposure to temperatures higher than 475°C lead to a continuous increase in permeability, as we will show later. The permeability of CO_2 (Figure 10) shows significantly different behavior when compared to N_2 and O_2. The membrane 300/30 shows a decrease of permeability, but not to the extent seen in Figure 8 and Figure 9.

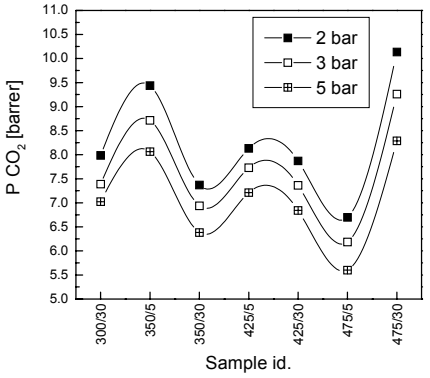

Fig. 10: CO_2 permeabilities at different pressures for different membranes treated up to 475°C (2 bar ■, 3 bar □, 5 bar ⊠). T = 25 °C.

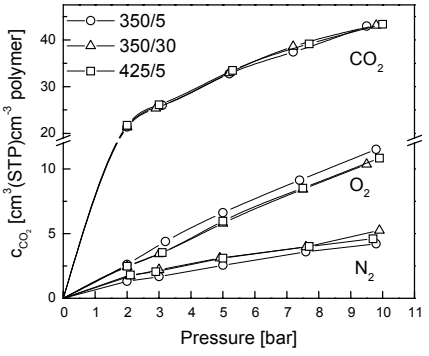

Fig. 11: CO_2 concentration in heat-treated Matrimid membranes (350/5 ○, 350/30 △, and 425/5 □) vs. the pressure. T = 25 °C.

More surprising is the increase in CO_2 permeability of the 425°C (425/5 and 425/30) treated membranes compared to the membrane 350/30. Figure 11 shows that the absolute solubility and the shape of the sorption curve of CO_2 are hardly affected by the heat treatment. However, comparing the average diffusion coefficients for samples treated at 350/5, 350/30, and 425/5 determined from equation (4), Figure 12, clearly shows that the diffusion coefficient increases after reaching a minimum at 350/30, for all feed

pressures, resulting is a relative high permeability of CO_2 through the 425/5 membrane as compared to the membrane treated at 350/30.

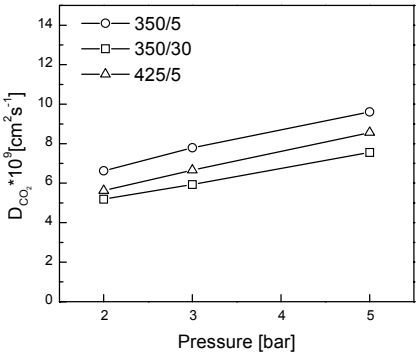

Fig. 12: Average diffusion coefficients of CO_2 in heat-treated Matrimid membranes vs. the pressure (350/5 ○, 350/30 △, and 425/5 □). T = 25 °C.

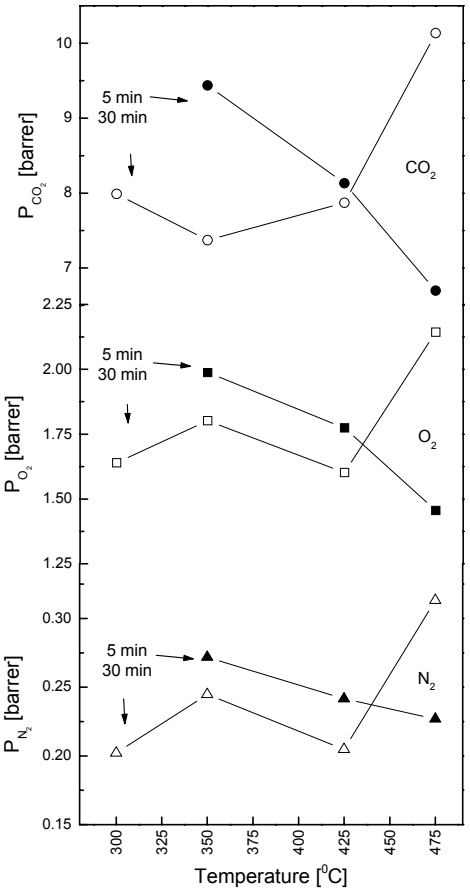

Fig. 13: N_2, O_2, and CO_2 permeability for membranes heat-treated for 5 min (closed symbols) and 30 min (open symbols) vs. the heat treatment end temperature.

A further indication for the different polymer-penetrant interaction of CO_2 as compared to O_2 and N_2 is seen in Figure 13.
Here we split the permeation results, obtained at a feed pressure of 2 bar, for the different gases for membranes treated at the end temperature for 5 min and 30 min. We can clearly see two different trends. The membranes treated for 5 min show a constant decrease of the permeability for all gases. The

curves for the membranes treated for 30 min, however, do not show such an unambiguous trend. All membranes show a sharp increase of their N_2, O_2, and CO_2 permeability when treated at 475 °C. This is caused by the onset of thermal decomposition. The trend in the CO_2 permeability differs substantially from the trend seen for O_2 and N_2. The permeability decreases, going from heat treatment temperatures of 300 to 350 °C, opposite to the trend seen for O_2 and N_2. Secondly the trends for O_2 and N_2 show a distinct minimum in the permeability at a heat treatment temperature of 425°C, absent in the permeability trend of CO_2.

Table 2 shows the permeability and the selectivity of a number of membranes heat-treated at temperatures up to 525°C. It is clear that with increasing temperature of treatment the permeability increases exponentially, but leads, however, to a decrease in selectivity. This can be attributed to the increased thermal decomposition as the first stages of carbonization commence, also visibly observed by the blackening of the membranes during exposure. A side effect of the heat treatment at 475°C and above is that the membranes become increasingly brittle and difficult to handle. The O_2 permeability reported in Table 2 for the membranes treated between 300 and 350°C, is relatively high, although similar values have been reported [4], this may be attributed to the rejuvenation taking place during the pretreatment.

Table 2. Permeability and selectivity for heat-treated Matrimid membranes (2 bar, 20 °C).

Membrane	P_{N2} [Barrer]	Po_2 [Barrer]	Pco_2 [Barrer]	$\alpha(O_2/N_2)$ [-]	$\alpha(CO_2/N_2)$ [-]
300/30	0.20	1.64	7.99	8.20	39.93
350/30	0.24	1.80	7.37	7.51	30.71
425/30	0.20	1.60	7.87	8.01	39.36
475/30	0.31	2.14	10.13	6.91	32.70
500/30	1.18	6.67	32.90	5.65	27.88
525/30	8.74	40.2	190	4.60	21.75

It has been found [4] that heat treatments beneficially affect the plasticization resistance of polymeric films. To investigate the effects of the heat treatment on the plasticization behavior, permeation experiments were conducted using propylene as the feed gas. Figure 14 shows the permeability of propylene versus the feed pressure for the subsequent heat treatments. The untreated membrane in Figure 14 was not pretreated at 350°C. It is clear that the

plasticization is successfully suppressed by applying a heat treatment between 300 and 475°C.

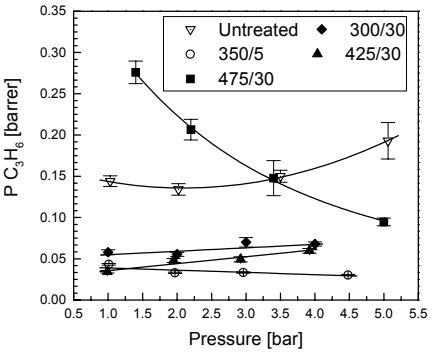

Fig. 14: Propylene permeabilities at different pressures for different membranes treated up to 475 °C. T = 25 °C.

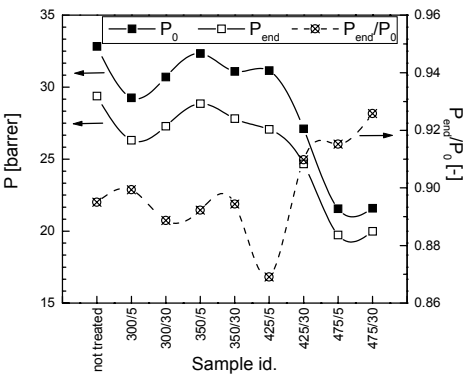

Fig. 15: He permeability (P_0 ■, P_{end} □) of pre plasticized Matrimid membranes and plasticization resistance (⊗). T = 25 °C.

An unfavorable effect is the reduction of permeability over 50%. However, the membrane 475/30 shows no plasticization effects combined with retained permeability. The thermally induced changes to the molecular structure provide a resistance to the swelling of the membrane by propylene.

To investigate the resistance of the membranes to plasticization by CO_2, the membranes were exposed to severe plasticization conditions, 56 bar CO_2 for 2 hours. Immediately after conditioning, the membranes were transferred from the pressure cell to the permeation set-up. Figure 15 shows the He permeability of the membranes immediately after conditioning with CO_2 (P_0) together with the He permeability after the membranes have reached equilibrium permeability (P_{end}). The effect of the heat treatments on the He permeability is comparable to that of N_2 except for the low He permeability of the 475/30 membrane. However, these are pre-swollen membranes and this low permeability can be explained by high resistance to plasticization of the 475/30 membrane. The ratio of P_{end} over P_0 is a measure of the ability of the membrane to resist swelling and is shown in Figure 15. The resistance to swelling is stable for membranes treated up to 350°C, then goes through a significant minimum at 425/5, and finally shows a increasing resistance to plasticization with increasing temperature of the heat treatment.

3.4 Conclusions.

In this experimental study we show that intermediate pre-carbonization gas separation membranes based on polyimides, possess challenging properties. We have shown that heat treatment of Matrimid flat sheet dense membranes, in an inert atmosphere, can alter the membranes properties as well as the molecular structure. Below 425°C the effect of exposure to a heated atmosphere is restricted to annealing and the formation of CTC's. Prolonged (30 min vs. 5 min) exposure to a temperature of 425°C leads to thermal decomposition of the polymer chains. However, the extent of this decomposition is relatively small. TGA experiments show a weight loss with a maximum of 3.6 wt% (475°C for 30 min). FTIR measurements show clearly that the chemical structure is altered beyond a treatment of 425/30.
The permeability of non-condensable gases (N_2, O_2) were measured at different pressures (2, 3, and 5 bar) and found to be depressed by heat treatments below the T_g of the polymer. Above the T_g of the polymer, increasing formation of CTC's and resulting densification of the polymer structure leads to a gradual decrease of the permeability. A significant increase in permeability was found if the membranes are exposed to temperatures above 475°C, caused by the onset of thermal decomposition.
The permeability curve of CO_2 presented vs. the heat treatment conditions is similar to that of N_2 and O_2 with a distinct deviation for the more dense membranes treated at 300 and 425°C. This is attributed to the higher diffusion coefficient of CO_2 in these membranes structures.
Plasticization by propylene is successfully suppressed by heat treatments over 300°C, however, a significant decrease of the permeability is observed. Heat treatment at a temperature of 475°C not only suppresses the plasticization, but shows sustained permeation rates compared to untreated membranes. The ability to resist the swelling by a condensable gas was also shown by measuring the He permeability through pre-conditioned membranes (56 bar CO_2, 2 hours), showing good resistance to swelling for membranes treated over 425 °C (30 min). From the different experiments conducted in this research it becomes obvious that the membranes treated at 425°C for 5 min show a divergent behavior as compared to differently treated membranes. Both TGA and FTIR show that the onset of thermal degradation is located at 425 °C. Although the density and CO_2 sorption remain unchanged, the CO_2 permeation and swelling experiments show an increased affinity for CO_2, this makes this membranes an interesting subject for further investigation.

3.5 References.

[1] W. J. Koros, G. K. Fleming, Membrane-Based Gas Separation, J. Membr. Sci. 83 (1993) p1-80.

[2] D. T. Clausi, W. J. Koros, Formation of defect-free polyimide hollow fiber membranes for gas separations, J. Membr. Sci. 167 (2000) p79-89.

[3] A. Bos, I. G. M. Punt, M. Wessling, H. Strathmann, Plasticization-resistant glassy polyimide membranes for CO2/CO4 separations, Sep. Purif. Technol. 14 (1998) p27-39.

[4] J. J. Krol, M. Boerrigter, G. H. Koops, Polyimide hollow fiber gas separation membranes: preparation and the suppression of plasticization in propane/propylene environments, J. Membr. Sci. 184 (2001) p275-286.

[5] A. Bos, I. G. M. Punt, M. Wessling, H. Strathmann, CO2-induced plasticization phenomena in glassy polymers, J. Membr. Sci. 155 (1999) p67-78.

[6] M. Wessling, I. Huisman, T. van der Boomgaard, C. A. Smolders, Dilation Kinetics of Glassy, Aromatic Polyimides Induced by Carbon-Dioxide Sorption, J. Polym. Sci. Pt. B-Polym. Phys. 33 (1995) p1371-1384.

[7] W. J. Koros, M. R. Coleman, D. R. B. Walker, Controlled Permeability Polymer Membranes, Annu. Rev. Mater. Sci. 22 (1992) p47-89.

[8] M. Wessling, M. L. Lopez, H. Strathmann, Accelerated plasticization of thin-film composite membranes used in gas separation, Sep. Purif. Technol. 24 (2001) p223-233.

[9] J. N. Barsema, G. C. Kapantaidakis, N. F. A. van der Vegt, G. H. Koops, M. Wessling, Preparation and characterization of highly selective dense and hollow fiber asymmetric membranes based on BTDA-TDI/MDI co-polyimide, J. Membr. Sci. 216 (2003) p195-205.

[10] C. Staudt-Bickel, W. J. Koros, Improvement of CO2/CH4 separation characteristics of polyimides by chemical crosslinking, J. Membr. Sci. 155 (1999) p145-154.

[11] A. Bos, I. G. M. Punt, M. Wessling, H. Strathmann, Suppression of CO2-plasticization by semiinterpenetrating polymer network formation, J. Polym. Sci. Pt. B-Polym. Phys. 36 (1998) p1547-1556.

[12] A. Bos, I. Punt, H. Strathmann, M. Wessling, Suppression of gas separation membrane plasticization by homogeneous polymer blending, Aiche J. 47 (2001) p1088-1093.

[13] G. C. Kapantaidakis, S. P. Kaldis, X. S. Dabou, G. P. Sakellaropoulos, Gas permeation through PSF-PI miscible blend membranes, J. Membr. Sci. 110 (1996) p239-247.

[14] H. Kawakami, M. Mikawa, S. Nagaoka, Gas transport properties in thermally cured aromatic polyimide membranes, J. Membr. Sci. 118 (1996) p223-230.

[15] A. B. Fuertes, D. M. Nevskaia, T. A. Centeno, Carbon composite membranes from Matrimid (R) and Kapton (R) polyimides for gas separation, Microporous Mesoporous Mat. 33 (1999) p115-125.

[16] F. J. Dinan, W. T. Schwartz, R. A. Wolfe, D. S. Hojnicki, T. Stclair, J. R. Pratt, Solid-state C-13-nmr spectral evidence for charge-transfer complex-formation in aromatic diimides and dianhydrides, J. Polym. Sci. Pol. Chem. 30 (1992) p111-118.

[17] T. Hasegawa, K. Horie, Photophysics, photochemistry, and optical properties of polyimides, Prog. Polym. Sci. 26 (2001) p259-335.

[18] M. Inagaki, T. Ibuki, T. Takeichi, Carbonization behavior of polyimide films with various chemical structures, J. Appl. Polym. Sci. 44 (1992) p521-525.

[19] W. J. Koros, R. T. Chern, Separation of gaseous mixtures using polymer membranes in Handbook of separation process technology, R. W. Rousseau ed., John Wiley & Sons, New York, 1987, p862-953.

[20] H. O. Pierson, Handbook of carbon, graphite, diamond, and fullerenes. Properties, processing and applications., 1st Edition, Noyes Publications, Park Ridge, 1993,

Chapter 4

Preparation of Carbon Molecular Sieve membranes from P84 co-polyimide precursor.

Abstract

The co-polyimide P84 was used to prepare carbon molecular sieve membranes for the separation of He, CO_2, O_2, and N_2. Using a stainless steel grid covering the precursor membranes during pyrolysis, in a N_2 atmosphere, flat strain free CMS membranes were obtained at (pyrolysis) end temperatures between 350 and 900 °C. By quenching the prepared membranes to room temperature immediately after reaching the pyrolysis end temperature, rather than allowing the membranes remain at the end temperature for a period of time, an improved permeability was obtained.

A maximum permeability for all gases was obtained using a membrane prepared at a pyrolysis end temperature of 600 °C. However, depending on the gas pair, a maximum selectivity was obtained at different pyrolysis end temperatures. For O_2/N_2 the membrane prepared at T_{end}: 750 °C had a P_{O2} of 8.3 Barrer and a selectivity of 10.4, for CO_2/N_2 the maximum selectivity was reached with the membrane prepared at a T_{end} :600 °C, P_{CO2} of 276 Barrer and a selectivity of 35.4, and for He/CO_2 this was obtained for at a T_{end} : 900 °C, resulting in a P_{He} of 17.35 Barrer and an α of 34.0.

4.1 Introduction.

Gas separation is an energy consuming process [1]. In the industrial separation of gases, processes like distillation and pressure swing adsorption [2] are commonly used. However, in the last decade, polymeric membranes have been developed for large-scale separation of gases and are presently applied as an alternative for the conventional processes [3]. It has been shown that heat treatment of polymeric membranes affects the permeability of gases. Moderate heat treatments in inert atmosphere at temperatures below 400°C have shown to be beneficial for the improvement of the resistance of these membranes against plasticization [4]. However, further elevation of the temperature leads to thermal degradation and ultimately carbonization of the polymer (pyrolysis). Whereas temperature treatments below 400°C generally show a reduction of the permeability, a steep increase of permeability accompanied by a decrease of the selectivity is seen when the polymeric membranes are exposed to temperatures between 400 and 550 °C, see chapter 3. Pyrolysis at higher temperatures leads to complete carbonization of the polymer membrane and Carbon Molecular Sieve (CMS) membranes are formed. Carbon Molecular Sieves have shown permeation and separation properties exceeding those of their polymeric precursor membranes [5-7].
Extensive research on precursor material selection [8-11], pyrolysis conditions, and pyrolysis trajectories [12] has led to a good understanding of the important parameters that influence the quality of the resulting CMS membrane. We have chosen the co-polyimide P84 as a precursor to produce CMS membranes, this co-polyimide has a relative high T_g, a high aromatic carbon content, and good thermal stability. Different pyrolysis end temperatures were investigated, whereby the membranes were quenched upon reaching the pyrolysis end temperature, allowing for examination of the carbonization process during the controlled heating step rather than during the uncontrolled cool down period. An extensive explanation of the choices made in the configuration of the pyrolysis conditions and trajectory will be given.

4.2 Experimental Section.

4.2.1 Materials.

The precursor membranes were prepared from the commercial, thermally stable, co-polyimide (BTDA-TDI/MDI) P84 from Lenzing. The structure of the polymer is shown in Fig. 1. The T_g of this polymer was determined with

Differential Scanning Calorimetry, second run and 30 °C/min, and found to be 315 °C.

N-methyl-pyrrolidone (NMP), Merck 99 %, was used as the solvent. All gases used for pyrolysis and gas permeation experiments had a purity of at least 99.5 %.

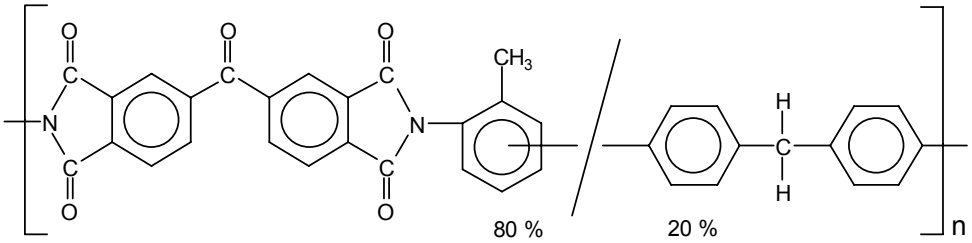

Fig. 1: Structure of P84 polyimide.

4.2.2 Precursor preparation.

All precursor membranes were prepared based on a solution of 13 wt% P84 in NMP. The solutions were allowed to dissolve overnight and were subsequently filtered over a 25 μm metal filter.

The solutions were cast on glass plates using a 200 μm casting knife and placed in a dry N_2 box for three days, then placed in a N_2 oven for a further three days at 50 °C to remove most of the solvent. The relatively low temperature during the removal of the solvent was chosen for reasons described in chapter 6. The obtained precursor film had a thickness of approximately 20 μm.

4.2.3 Pyrolysis.

For pyrolysis of the membranes, a Carbolite® TZF 12/100 High Temperature Tube Furnace was used. The furnace is equipped with an Eurotherm 2408CP temperature controller and programmer and an Eurotherm 2132 over-temperature controller.

Heat treatment procedures allowed the temperature to rise from room temperature to 150°C with a heating rate of 50°C/min. Subsequently, this temperature was held for 15 min to remove any adsorbed water. From 150°C to 350°C the temperature was raised by a rate of 5°C/min, thereafter the temperature increase was controlled at 1°C/min.

After reaching the end temperature, the membranes were quenched.

4.2.4 Analysis.

Weight loss. The weight loss during heat treatment was determined using Thermo Gravimetric Analysis (TGA). The TGA experiments were preformed using a Perkin-Elmer TGA 7 with a N_2 atmosphere and flow rates of 20 cm^3/min. Heating routes were based on heat treatment procedures.

Chemical composition. To verify the chemical composition of the (pre-)carbons, X-ray Photoelectron Spectroscopy (XPS) was performed, using a Quantum 2000 Scanning Esca Probe of Physical Electronics, on samples at different stages in the pyrolysis. The experiments were carried out on the etched (500 eV Ar) surface of the carbonized samples as some oxidation from air always takes place during storing [10].

Gas adsorption. The adsorption of gases in the carbon samples was determined using a Rubotherm magnetic suspension balance operated by MessPro software. This balance has an accuracy of 1 μg and a reproducibility of 2 μg. The samples were evacuated to a pressure below 10 Pa, before the gas pressure was applied. The obtained data were corrected for buoyancy effects, induced by the increased gas density at higher pressures.

Gas permeation. To elucidate the effect of the heat treatment on the permeability and selectivity of the membranes, pure gas He, CO_2, O_2, and N_2 permeability was determined. The membranes were glued into metal discs, using an Araldit two component adhesive, to prevent cracking of the membranes by the rubber ring seals. The gas permeation experiments were done, using a variable permeate pressure set-up. In the experimental set-up, a vacuum was applied on the permeate side, whereas the other side was brought into contact with the feed gases. All measurements were taken after the fluxes became constant in time. A more extensive description of the determination of both permeability and selectivity can be found elsewhere [13]. The reported results are based on measurements performed on two or more membranes.

4.3 Results and discussion.

4.3.1 Pyrolysis.

Figure 2 shows the weight loss caused by the pyrolysis between room temperature and 850 °C. Heating trajectories were based on the same procedures used for preparing CMS membranes, as mentioned above. The dashed line at 54.2 wt% indicates the value of the theoretical carbon yield, which coincides with the total aromatic carbon content in the monomer.
The weight loss curve shows thee distinct trends [14]:

- up to 450 °C, relative low weight loss caused by evaporation of residual water and solvents;
- 450 – 650 °C, rapid decrease of weight caused by degradation of the polymer, while H_2, CO, CO_2, and CH_4 evolve from the sample;
- 650 °C and higher, slow decrease in weight, caused by the evolving of residual non-elementary carbon components, primarily N_2.

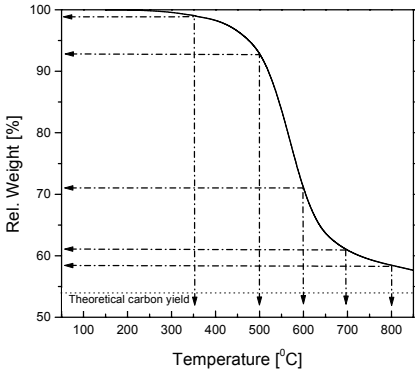

Fig. 2: Weight loss vs. pyrolysis temperature for P84 co-polyimide.

4.3.2 Gas permeation.

To determine the effect of the pyrolysis on the permeability and selectivity of single gases, gas permeation experiments were done using He, CO_2, O_2, and N_2. Choosing these specific gases enables us to cover several properties of the produced membranes. We use He (2.6 Å) and CO_2 (3.3 Å), although they differ 0.6 Å in size, the comparison between these gases is interesting as with increasing carbonization of the membrane the affinity of CO_2 for the membrane increases. This allows the CO_2 to adsorb on the pore walls and

diffuse though pores smaller than its kinetic diameter. O_2 (3.46 Å) and N_2 (3.64 Å) enable us to follow the development of the separation properties of the membranes for molecules that differ only 0.18 Å in size.

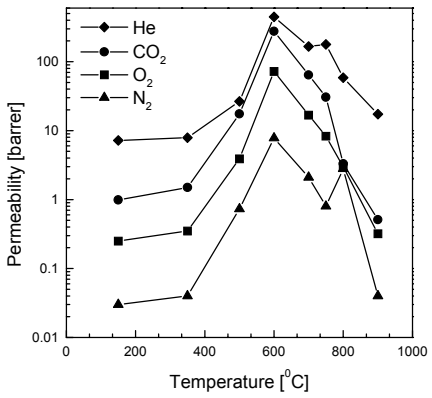

Fig. 3: Permeability vs. pyrolysis temperature of He (◆), CO_2 (●), O_2 (■), and N_2 (▲).

Table 1. Permeation properties of MP membranes treated at different pyrolysis temperature for He, CO_2, O_2, and N_2.

Membrane	$T_{pyrolysis}$ [°C]	Soak time [min]	P_{He} [Barrer]	P_{CO2} [Barrer]	P_{O2} [Barrer]	P_{N2} [Barrer]
MP	150	2 (days)	7.2	0.99	0.25	0.03
MP	350	0	7.9	1.5	0.35	0.04
MP	500	0	26.5	17.5	3.9	0.73
MP	600	0	447	276	72.2	7.8
MP	700	0	166	64.1	16.8	2.1
MP	750	0	178	30.6	8.3	0.8
MP	800	0	58.5	3.3	3.0	2.8
MP	900	0	17.4	0.51	0.32	0.04
MP_{120} [a]	700_{120}	120	37.0	2.4	0.46	0.14

[c] *The membrane was allowed to soak for 120 min at 700°C, before quenching.*

As the temperature of pyrolysis increases, so does the permeability of the obtained membranes. At 600 °C the permeability reached a maximum value for all gases after which the permeability reduces strongly. The occurrence of this maximum is in accordance with results reported by other authors [6] and can

be explained taking two counteracting processes into account. Firstly, precursor mass burns off by the increase of temperature leading to an increased micro porosity and thus an increased permeability. Secondly, the structure densifies as it is exposed to high temperatures, thereby reducing porosity and permeability. In the first stages of the pyrolysis, the first process dominates as the rate of weight loss is high (see Figure 2) above 600 °C the weight loss rate decreases and the influence of densification becomes prominent. It is important to keep in mind that porosity and pore size can change independent of each other. The pores are formed at the intersection of non-parallel positioned graphite crystals. Changes in packing density and crystal orientation can influence the free volume between the crystals (porosity) without changing the dimensions of the intercept (pore size).

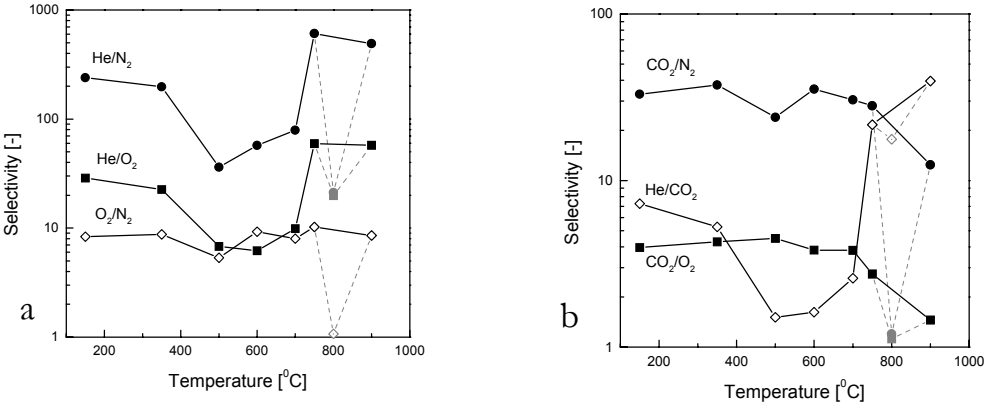

Fig. 4: a- He over O_2 (■), He (●) and O_2 (◇) over N_2 and b- He over CO_2 (◇), CO_2 over N_2 (●) and O_2 (■) selectivity vs. pyrolysis temperature.

The selectivity, as shown in Figure 4a and b for the different conceivable gas pairs does, however, not show such an unambiguous maximum. When the gas pairs are split into inert pairs (Figure 4a) and those were affinity for the carbon matrix is present (Figure 4b), we can follow the evolution of the pore size. Discarding the points for the membranes prepared at 800 °C, these will be treated in the following paragraph, we see from Figure 4a that the selectivity for O_2 over N_2 remains virtually unchanged, where the selectivity of the smaller

He molecule over O_2 and N_2 rises substantially. Obviously, the ratio of pores larger than 3.46 Å (accessible to O_2) and pores larger 3.64 Å (accessible to N_2) remains constant, although the porosity decreases, as seen from the lowered permeability (Figure 3). The densification must lead to a shift of the mean pore size to smaller pores as we observe a relative increase of the He permeance. The selectivity of CO_2 over N_2 and O_2 (see Figure 4b) remains relatively constant at low pyrolysis temperatures, but decreases as the temperature increases, again discarding the point at 800 °C. This, again, indicates the shift of the mean pore size to lower diameters, excluding CO_2. This becomes even more evident when the selectivity of He over CO_2 is considered. The selectivity drops significantly after the transition from polymer to carbon, caused by the increased affinity of the CO_2 for the membrane. However, at higher pyrolysis temperatures a strong increase in selectivity points toward densification of the structure [9] and subsequent CO_2 exclusion from the small pores.

An important observation in Figure 4 is the selectivity of the membranes prepared at a pyrolysis temperature of 800 °C. This approaches 1, i.e. no selectivity, for both CO_2 and O_2 over N_2. Although these results seem to be an artifact, they have been measured for over eight separate membranes. The He over CO_2 selectivity remains high, whereas the He over N_2 deceases by two orders of magnitudes, see Table 1. This, together with the observed O_2 over N_2 selectivity (= 1.1), can only be explained by the existence of two pore sizes having radii of $r_{He} < r_1 < r_{CO2}$ and $r_2 > r_{N2}$. At 800 °C residual N atoms in the carbon matrix are removed during the pyrolysis, leading to structural rearrangements resulting in a change of the pore size distribution. The dissipation of N atoms from the carbon matrix is confirmed by XPS analysis. Figure 5 shows the ratio of carbon to nitrogen atoms. Initially, at relative low pyrolysis temperatures (<700 °C) the ratio varies little. However, starting from 800 °C the ratio increases significantly, indicating the loss of N atoms.

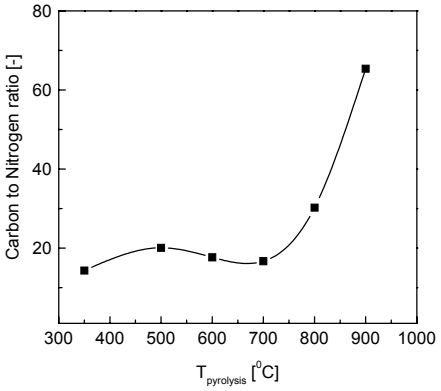

Fig. 5: Ratio of carbon to nitrogen atoms vs. the pyrolysis temperature obtained by XPS.

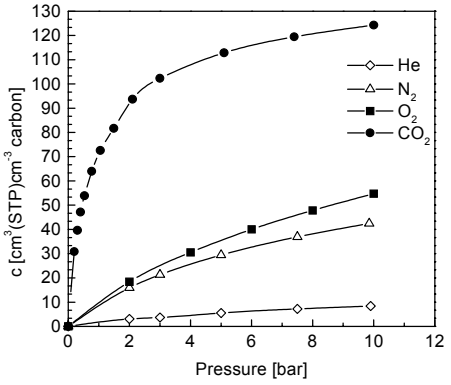

Fig. 6: Equilibrium gas concentration (He ◇, N_2 △, O_2 ■, and CO_2 ●) in MP700 vs. the pressure.

To explain the relatively high selectivity of CO_2 over O_2, as they only differ 0.16 Å in diameter we must consider the affinity of the separate molecules for the carbon matrix. The sorption characteristics, of He, N_2, O_2, and CO_2, of the CMS membranes prepared at 700 °C were determined. Figure 6 shows the sorption curves of the equilibrium sorption concentration measured between 0 and 10 bar.
The difference between the sorption behavior of CO_2, as compared to the other gases is striking. The selectivity of CO_2 over O_2 is influenced significantly by the sorption selectivity of the carbon matrix. The CO_2 curve is strongly concave, hence, although both the O_2 and N_2 curves in Figure 6 are also concave, it is clear that with increasing pressure the sorption selectivity, and thus the overall selectivity, will decrease. This will come back in chapter 5.

To really assess the performance of the prepared membranes, we should look at the obtained selectivities as a function of the permeation rates. Figure 7a, b, and c show these graphs (α vs. P) for O_2 - N_2, CO_2 - N_2, and He - CO_2, respectively. Where in the case of both O_2 - N_2 and CO_2 - N_2 the membranes prepared between 600 and 750 °C perform the best, for the separation of He over CO_2 CMS membranes prepared at higher temperatures show optimal properties, i.e. high permeability and selectivity.

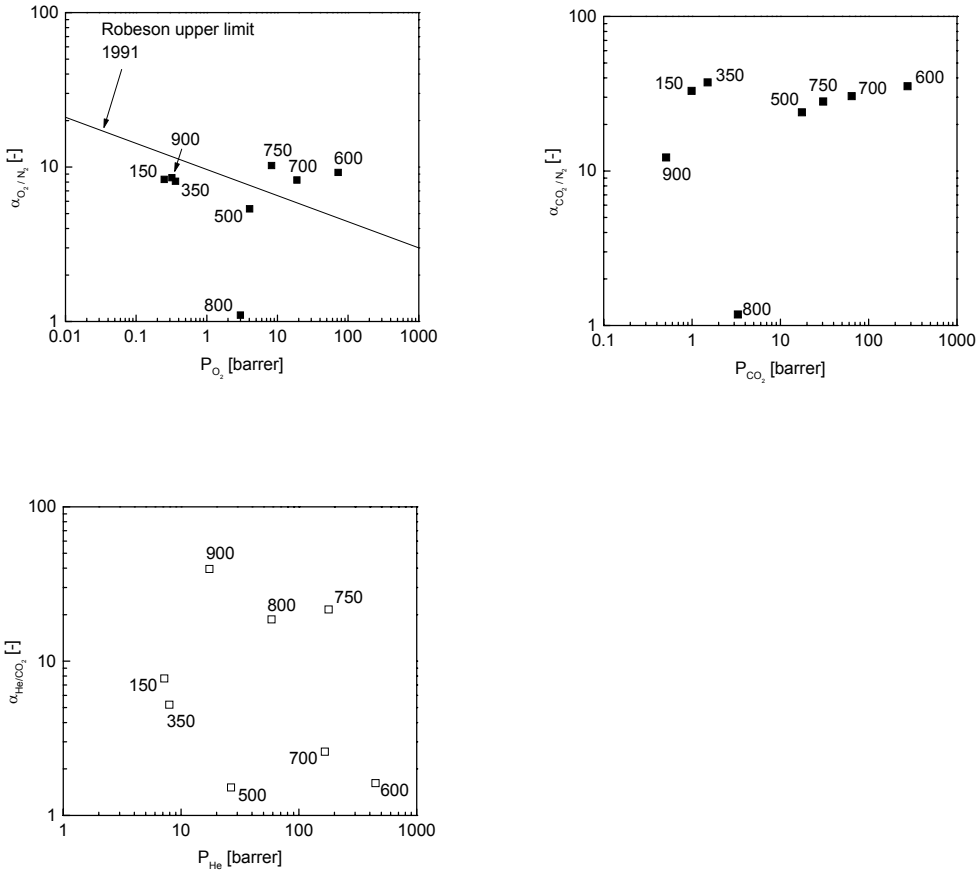

Fig. 7: Overview of membrane performance (α vs. permeability) for a - O_2 over N_2, b - CO_2 over N_2, and c - He over CO_2.

The effect of quenching the CMS membranes is seen in Figure 8, where the selectivity of the different gas pairs is depicted. From Table 1 it is already clear that the permeability decreases considerably, comparing the CMS700 membranes quenched immediately and after 120 minutes. However, the extent of decrease differs for the different gases, which is obvious from Figure 8.
Both the selectivity of CO_2 and O_2 over N_2 decrease considerably, whereas the selectivity of He over CO_2, O_2, and N_2 increases. This indicates that the pore size distribution shifts, explaining the loss of selectivity among the larger

molecules. The carbon becomes more dense, thereby reducing the porosity, while the average pore size moves to smaller sizes, as seen from the reduced permeability and the increased He over CO_2 selectivity. The observed increase of the CO_2 over O_2 selectivity is attributed to small changes in the ratio between pores accessible to CO_2 and O_2 respectively.

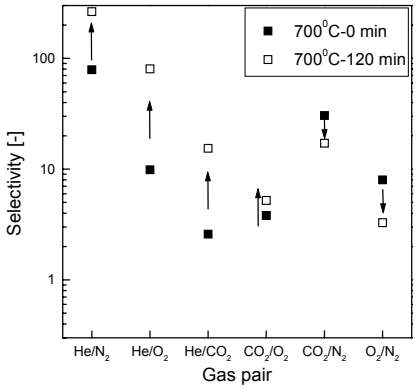

Fig. 8: Comparison selectivity for membranes prepared at 700 °C with (■) and without temperature soak (□).

4.4 Conclusions.

We have shown that P84 co-polyimide is a suitable material for the preparation of carbon molecular sieve membranes. This polyimide has a T_g of 315 °C and is thermally stable in inert atmospheres upto approximately 400 °C. Using the described furnace set-up (CMS-) membranes were prepared at temperatures between 350 and 900 °C and subsequently quenched to room temperature using the described method. By covering the precursor films with a stainless steel grid, flat strain-free CMS membranes are obtained. The permeation properties of the prepared membranes were examined using pure He, N_2, O_2, and CO_2. The membranes prepared at 600 °C showed the maximum permeability for all tested gases, although maximum selectivities were obtained at different pyrolysis temperatures depending on the desired separation. For O_2/N_2 the maximum is reached with the membrane prepared at 750 °C (P_{O2}: 8.3 barrer, α: 10.4), for CO_2/N_2 this was 600 °C (P_{CO2}: 276 barrer, α: 35.4), and for He/CO_2 900 °C (P_{He}: 17.35 barrer, α: 34.0).

The membranes prepared at 800 °C showed abnormal behavior, losing the separation ability for CO_2, O_2, and N_2, but retaining the selectivity of He over CO_2. The abnormal behavior was explained by a bimodal pore size distribution in this membrane, arising from the dissipation of N atoms from the carbon matrix at this temperature as shown by XPS.
Finally, it was shown that a temperature soak at the pyrolysis end temperature (700 °C, 120 min), in contrast to an immediate quench after reaching the pyrolysis end temperature, led to a reduction of the overall permeability.

4.5 References.

[1] R. W. Spillman, Economics of Gas Separation Membranes, Chem. Eng. Prog. 85 (1989) p41-62.
[2] D. M. Ruthven, S. Farooq, K. S. Knaebel, Pressure swing adsorption, 1st Edition, VCH Publishers, Inc., New York, 1994.
[3] R. W. Baker, Future directions of membrane gas separation technology, Ind. Eng. Chem. Res. 41 (2002) p1393-1411.
[4] J. J. Krol, M. Boerrigter, G. H. Koops, Polyimide hollow fiber gas separation membranes: preparation and the suppression of plasticization in propane/propylene environments, J. Membr. Sci. 184 (2001) p275-286.
[5] A. Singh-Ghosal, W. J. Koros, Air separation properties of flat sheet homogeneous pyrolytic carbon membranes, J. Membr. Sci. 174 (2000) p177-188.
[6] T. A. Centeno, A. B. Fuertes, Supported carbon molecular sieve membranes based on a phenolic resin, J. Membr. Sci. 160 (1999) p201-211.
[7] M. B. Rao, S. Sircar, Nanoporous Carbon Membrane for Gas Seperation, Gas Seperation & Purification 7 (1993) p279-284.
[8] M. B. Rao, S. Sircar, Nanoporous Carbon Membranes for Separation of Gas-Mixtures by Selective Surface Flow, J. Membr. Sci. 85 (1993) p253-264.
[9] J. Petersen, M. Matsuda, K. Haraya, Capillary carbon molecular sieve membranes derived from Kapton for high temperature gas separation, J. Membr. Sci. 131 (1997) p85-94.
[10] C. W. Jones, W. J. Koros, Carbon Molecular-Sieve Gas Separation Membranes .1. Preparation and Characterization Based on Polyimide Precursors, Carbon 32 (1994) p1419-1425.

[11] A. B. Fuertes, D. M. Nevskaia, T. A. Centeno, Carbon composite membranes from Matrimid (R) and Kapton (R) polyimides for gas separation, Microporous Mesoporous Mat. 33 (1999) p115-125.

[12] V. C. Geiszler, W. J. Koros, Effects of polyimide pyrolysis conditions on carbon molecular sieve membrane properties, Ind. Eng. Chem. Res. 35 (1996) p2999-3003.

[13] J. N. Barsema, G. C. Kapantaidakis, N. F. A. van der Vegt, G. H. Koops, M. Wessling, Preparation and characterization of highly selective dense and hollow fiber asymmetric membranes based on BTDA-TDI/MDI co-polyimide, J. Membr. Sci. 216 (2003) p195-205.

[14] M. Inagaki, T. Ibuki, T. Takeichi, Carbonization behavior of polyimide films with various chemical structures, J. Appl. Polym. Sci. 44 (1992) p521-525.

Chapter 5

Carbon Molecular Sieve membranes prepared from porous fiber precursor*.

J.N. Barsema, N.F.A. van der Vegt, G.H. Koops, and M. Wessling

Abstract

Carbon Molecular Sieve (CMS) membranes are usually prepared from dense polymeric precursors that already show intrinsic gas separation properties. The rationale behind this approach is that the occurrence of any kind of initial porosity will deteriorate the final CMS performance. We will show that it is not necessary to produce a non-porous precursor in order to obtain a selective CMS membrane. We used tight ultra-filtration fiber membranes as a precursor. These fibers did not have any gas separation properties before the pyrolysis treatment, nor were coatings applied to these fibers before, or subsequent to, the pyrolysis. After a heat treatment in air followed by a pyrolysis in a nitrogen atmosphere, CMS fiber membranes were obtained. The CMS fibers were analyzed using Scanning Electron Microscopy, Thermo Gravimetrical Analysis, and gas permeation. From the permeation rates and permselectivity values measured for He, H_2, CO_2, Ar, O_2, N_2, CH_4, C_2H_4, C_2H_6, C_3H_6, C_3H_8, and SF_6, the evolution of the mean pore diameter was investigated. It was found that the pore diameter increases with pyrolysis temperature up to 800 °C, but decreases as the temperature is raised to 900 °C. The overall porosity reaches its highest value at 900 °C.

* Published as 'J.N. Barsema *et.al.*, J. Membr. Sci. 205 (2002) p239-246'.

5.1 Introduction.

Gas separation is an energy consuming process. In the industrial separation of gases, processes like distillation and pressure swing adsorption are commonly used. However, in the last decade, polymeric membranes have been developed for large-scale separation of gases and are presently applied as an alternative for the conventional processes. Carbon Molecular Sieves (CMS) have shown permeation and separation properties exceeding those of their polymeric precursor membranes. This has led to an extensive research into the field of CMS, with an emphasis on precursor material selection [1-4], and pyrolysis trajectories [5]. Many authors have reported on the preparation procedure of the polymeric precursor. This precursor can be either a supported or an unsupported polymeric membrane. In the first case the polymeric membranes are supported by e.g. flat or tubular configurations of porous inorganic materials, carbon, or sintered stainless steel. The polymer can be applied to the support by ultrasonic deposition [6], dip coating [7], spin coating [8], and other comparable methods. Because of the shrinkage of the polymer material during pyrolysis, the coating procedure has to be repeated until a defect free CMS is obtained [9]. In the latter case of unsupported CMS's, the best precursors were found to be asymmetric fibers with a thin top layer. Here the asymmetric support structure provides strength, whereas the top layer has gas separation properties [10]. Until now much effort has gone into the preparation of fibers with defect free top layers, as defects in the top layer are expected to lead to decreased selectivities of the resulting CMS. Others have used commercial gas separation fibers [11, 12], however, this placed restrictions on the choice of polymers. We, in contrast, have tried to avoid this time consuming procedure by taking on a different approach, starting with tight ultra-filtration (UF) fiber membranes, without coatings. The UF membranes have no intrinsic gas separation properties and show gas permeabilities up to 10^5 GPU[#] for N_2. Preparation of CMS membranes from porous precursors has been reported [13], but to obtain good separation values, the precursor was coated before pyrolysis. We applied no coatings to the fibers before or after the pyrolysis.

[#] 1 GPU = 10^{-6} $cm^3(STP)cm^{-2}s^{-1}cmHg^{-1}$

5.2 Experimental Section.

5.2.1 Materials.

The precursor UF membranes were prepared from the commercial, thermally stable, co-polyimide (BTDA-TDI/MDI) P84 from Lenzing. The structure of the polymer is shown in Fig. 1.

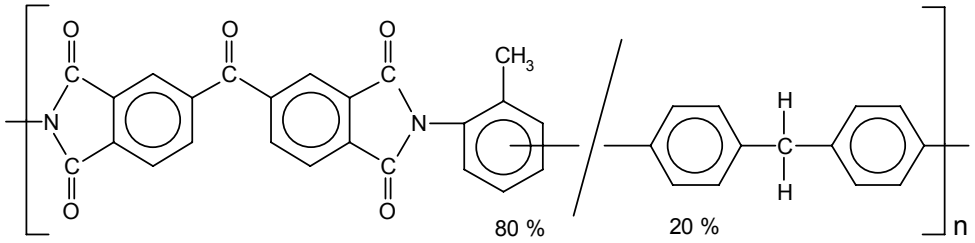

Fig. 1: Structure of P84 co-polyimide.

The T_g of this polymer was determined with Differential Scanning Calorimetry, second run and 30 °C/min, and found to be 315 °C. The theoretical carbon yield of this polymer is 54.2 %, equal to the aromatic carbon content.
N-methyl-pyrrolidone (NMP), Merck 99 %, was used as the solvent, whereas the coagulant was water. As additives polyvinylpyrrolidone (PVP), Acros M_w 58000, and glycerol, Merck > 99 %, were added.
All gases used for pyrolysis and gas permeation experiments had a purity of at least 99.5 %.

5.2.2 Precursor preparation and pretreatment.

The hollow fiber membranes were spun from a dope, which consisted of 71 % N-methyl-pyrrolidone (NMP) and 18 % P84, containing polyvinylpyrrolidone (PVP) and glycerol as additives. Water was used as a coagulation medium. The bore solution was chosen, so that the UF top layer was situated on the bore side. The fibers were immersed overnight in a 10 % glycerol in water solution to prevent pore collapse and afterwards dried in air. The addition of PVP and glycerol improves the porosity of the top layer.
The obtained fibers were given a pretreatment in an air atmosphere for one hour at 300 °C. Subsequently, they were allowed to cool in ambient conditions.

5.2.3 Pyrolysis procedure.

The pyrolysis is performed using a Carbolite® TZF 12/100 High Temperature Tube Furnace, mounted with an Eurotherm 2408 CP temperature controller. The precursor is placed in a quartz glass tube, using a stainless steel grid as sledge. The atmosphere in the quartz tube during pyrolysis was N_2, with a flow rate of 10 cm^3/min. Fig. 2 gives a schematic overview of the furnace set-up.

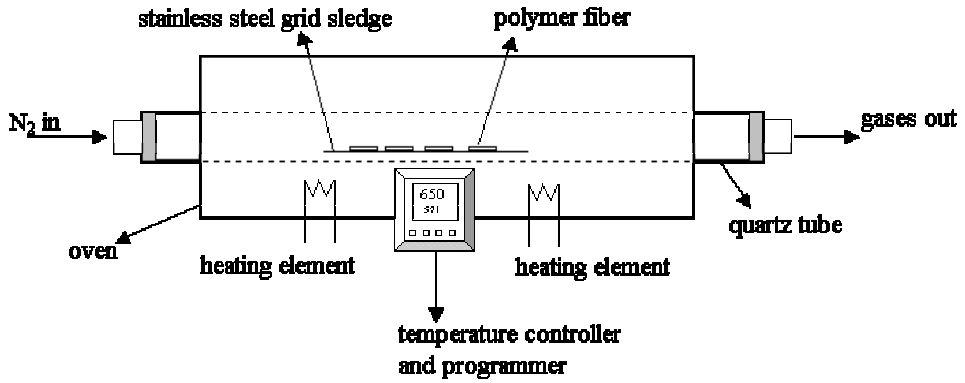

Fig. 2: A schematic overview of the furnace set-up.

The pyrolysis was conducted according to the following procedure; the fibers were heated to 150 °C at a rate of 50 °C/min and kept at this temperature for 15 min to remove residual water and solvent, subsequently the temperature was raised to 350 °C at a rate of 5 °C/min. Above 350 °C the polymer material is in the rubbery state and a lower heating rate is chosen to allow all pyrolysis processes now starting in the polymer to commence. Heating rates from 1 to 13.3 °C/min have been reported [14]. In this case the final temperature was reached with a temperature ramp of 1 °C/min. The end temperature was held for one hour, after which the fiber was allowed to cool in the oven to ambient conditions.

5.2.4 Analysis.

Thermo-gravimetrical analysis. The carbon yield, defined as the weight relative to the initial precursor weight, was determined using Thermo Gravimetric Analysis (TGA). The TGA experiments were preformed using a Perkin-Elmer TGA 7 with an air or N_2 atmosphere and flow rates of 20 cm^3/min. Heating routes were based on pyrolysis procedures.

Scanning electron microscopy. To investigate the effects of the pyrolysis on the structure of the porous asymmetric support layer of the fibers, Scanning Electron Microscopy (SEM) was used. The micrographs were obtained using a JEOL JSM T220A SEM for magnifications up to 25.000x and a JEOL JSM 5600 LV SEM for higher magnifications. The precursor polymeric materials were coated with platinum in an argon atmosphere using a JEOL JFC 1300 (20 mV, 90 sec.) before they were placed in the microscope.

Gas permeation. To further elucidate the CMS microstructure, pure gas permeation experiments were conducted. The fibers, together with a PVC support rod, were potted in stainless steel cylinders using a polyurethane resin. To allow for removal of the permeate gases, one side was left open. This module was fitted in a permeation cell using Teflon gaskets. The gas permeation experiments were done, using a variable permeate pressure set-up. In the experimental set-up a vacuum was applied on the bore side, whereas the shell side was brought into contact with the feed gases. All measurements were taken after the fluxes became constant in time. The permeance $\boldsymbol{P}/l$ (in GPU) was determined from the pressure rise following

$$\frac{\boldsymbol{P}}{l} = \frac{V \cdot 273.15 \cdot (p_t - p_0)}{A \cdot T \cdot \frac{(P_t + P_0)}{2} \cdot 76 \cdot t} \cdot 10^6 \; GPU \,, \tag{1}$$

where the ideal gas law is assumed to be valid and t [s] is the time, p_t [bar] is the pressure at the permeate side, P [bar] is the feed pressure, T [K] is the temperature, V [cm^3] is the cell volume, and A [cm^2] the total fiber area. The selectivity was determined as the ratio of permeabilities

$$\alpha_{x/y} = \frac{\boldsymbol{P}_x}{\boldsymbol{P}_y}, \tag{2}$$

with $\alpha_{x/y}$ [-] is the selectivity of x to y, typically a value larger than unity.
For the gas permeation experiments a number of gases were used, differing in size and affinity to adsorb onto the carbon pore wall. As low affinity gases He (2.6 Å), Ar (3.4 Å), O_2 (3.46 Å), N_2 (3.64 Å), CH_4 (3.8 Å), C_2H_6 (4.0 Å), C_3H_8 (4.3 Å), and SF_6 (5.02 Å) were used. H_2 (2.89 Å), CO_2 (3.3 Å), C_2H_4 (3.9 Å), and C_3H_6 (4.5 Å) were used as high affinity gas.

5.3 Results and discussion.

The precursor fibers showed a pure water flux of 1.6 l/m^{2}hr bar and a molecular weight cut-off of approximately 15000 Da. The observed pure water flux is low for tight UF fibers, however these fibers contain a significant amount of PVP. The PVP swells when brought into contact with water, leading to a reduction of the pore size and observed clean water flux. The gas permeabilities were determined to be over 10^5 GPU. These fibers have an inner UF top layer of approximately 2.7 μm (Fig. 3 a, b, c). No gas selectivity was observed. Bos *et.al.* [15] reported ideal CO_2 over CH_4 selectivities of 89 for P84 dense membranes, which indicates that we are indeed using porous fibers. The pretreatment in air led to an expected partial cross-linking of the co-polyimide [12, 16] This could also be determined from the fact that the fiber did not dissolve completely in the initial solvent after this heat treatment. The fibers were allowed to dissolve in NMP for 96 hours. After this period, the material remained partially non-dissolved.

5.3.1 Pyrolysis.

Table 1. Pyrolysis properties, carbon yield, inner diameter, wall thickness, and selective layer thickness of the membranes.

No.	Temperature [°C]	Carbon yield [w%]	Inner diameter [μm]	Wall thickness [μm]	Layer thickness [μm]
1.	No treatment		678	212	2.7
2.	300[a]	96.0	579	196	2.6
3.	600	86.5	511	173	2.4
4.	700	66.0	475	154	2.3
5.	800	59.5	454	150	2.4
6.	900	56.0	433	147	2.6

[a] *Except for fiber 2, which was treated in an air atmosphere, all pyrolysis took place in an N_2 atmosphere*

The pretreated precursor fibers were pyrolysed at temperatures between 600 and 900 °C. In table 1 the weight loss with increasing temperature for the different pyrolysis end temperatures is reported.

5.3.2 Scanning electron microscopy.

To reveal the structure of the resulting membranes SEM micrographs were taken, as seen in Fig. 4 a, b, c. Table 1 summarizes the physical properties of the obtained CMS membranes. Although fiber dimensions decrease considerably, no large changes in the porous morphology can be observed. Kusuki *et. al.* [12] report a nodular structure in the selective top layer of both the precursor and the CMS. When comparing the structure of the UF top layer of the precursor (Fig. 3c) with that of the CMS top layer (Fig. 4c), we see similarities. Apparently, part of the precursor structure is retained in the selective layer of the CMS.

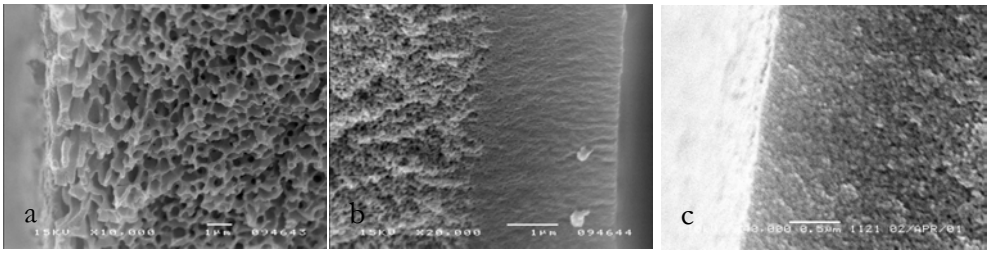

Fig. 3 a, b, c: Outer, inner, and top layer structure of the precursor.

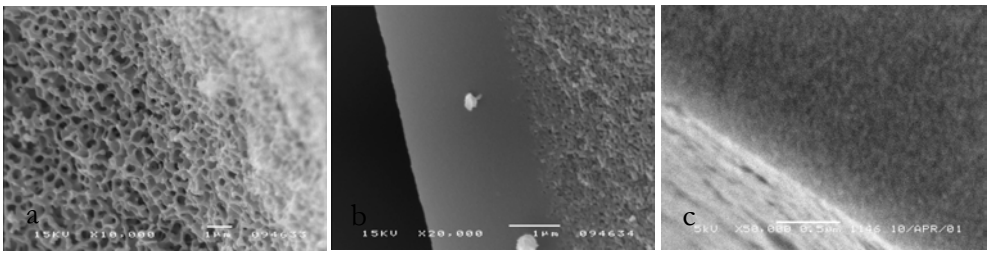

Fig. 4 a, b, c: Outer, inner, and top layer structure of the CMS pyrolysed at 700°C.

5.3.3 Gas permeation through CMS fibers.

In Fig. 5 an overview is given of the permeabilities of all the measured gases through the CMS membranes, at a feed pressure of 2.1 bar. Gas permeation and separation through micro-structured membranes can take place via three main mechanisms. Which mechanism is best to describe the process, depends

on the pore size of the microstructure. According to Way *et. al.* [17], in pores larger than 50 Å the main mechanism is Knudsen diffusion. Upon deceasing the pore size below 50 Å the molecules, which adsorb strongly on the pore surface, can diffuse more readily by surface diffusion [18]. However, the selectivity will decrease with increasing pressure due to the concave shape of the sorption isotherm [14]. In the case of very strong adsorbing or non-permanent gases pore blocking can occur, resulting in high selectivities [18]. When pore sizes approach molecular diameters (< 6 Å) the separation is mainly determined by molecular sieving, not depending on the pressure.

Fig. 5 shows that, as the temperature of pyrolysis increases, the permeance of the CMS increases, best observed for the smaller gas molecules. This can be explained by an increase of the pore size, an increase of the number of pores, or a combination of both.

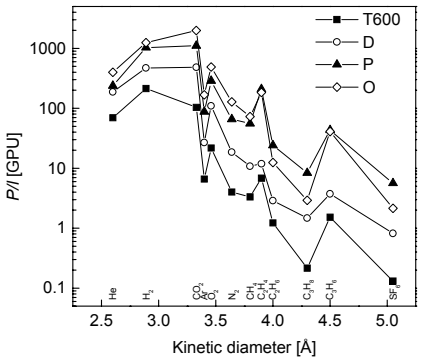

Fig. 5: Permeation of high and low affinity gases against the kinetic diameter, through CMS membranes prepared at different pyrolysis temperatures. (feed pressure 2.1 bar). ■ - 600 °C, ○ - 700 °C, ▲ - 800 °C, ◇ - 900 °C.

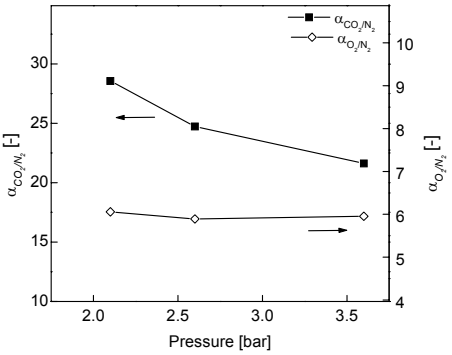

Fig. 6: The selectivities of CO_2 over N_2 and O_2 over N_2 against the feed pressure for a membrane pyrolised at 700 °C. ■ - α CO_2/N_2, ◇ -α O_2/N_2.

In Fig. 6 the selectivities of CO_2 over N_2 and O_2 over N_2 are plotted versus the feed pressure. The decrease of selectivity for CO_2 over N_2 with increasing feed pressure tells us that the main mechanism for separation is based on surface diffusion. For the separation of O_2 and N_2 ($\alpha_{Knudsen}$ = 1.08), however, molecular

sieving is the main mechanism for separation, as can be concluded from the pressure independence of the selectivity.

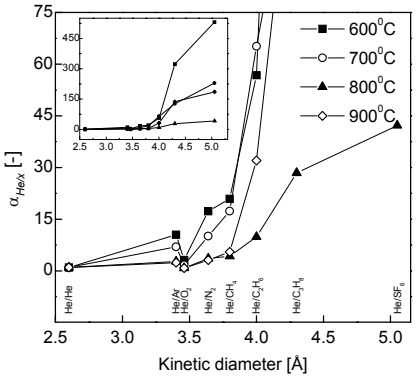

Fig. 7: Selectivity of He towards the low affinity gases against the kinetic diameter (feed pressure 2.1 bar). ■ - 600 °C, ○ - 700 °C, ▲ - 800 °C, ◇ - 900 °C.

To give an estimation of the mean pore size and to follow the effect of pyrolysis on this property, the selectivity of He over the low affinity gases is plotted versus the kinetic diameter of the permeating gases in Fig. 7.
By concentrating on the region where the transition from low to high selectivity occurs, it is possible to describe the processes taking place during pyrolysis. From 600 °C to 700 °C the permeance increases (see Fig 5.), but the mean pore size, however, appears to remain constant, because the transition from low to high selectivity takes place, for both pyrolysis temperatures, at CH_4 ($d_{kinetic}$ = 3.8 Å). Hence, it is likely that only the number of pores increases, rather than their dimensions. A further rise in pyrolysis temperature to 800 °C results in an increase of the permeance and mean pore size, shifting the selectivity transition to propane ($d_{kinetic}$ = 4.3 Å). However, a further increase of the pyrolysis temperature to 900 °C leads to a decrease of the mean pore size (transition at $d_{kinetic}$ = 4.0 Å), while the permeance still increases for the smaller gas molecules, see figure 5. This is an indication that the number of pores is still increasing. Apparently the process of matrix shrinkage overcomes the effect of material loss due to pyrolysis. A similar effect has been reported by Centeno *et. al.* [19], although a shift of the maximum permeability to higher temperatures can be observed . An explanation for this shift is the higher initial porosity present in the precursor compared to the dense precursors used by

many other authors. Remarkably, the curve of the 800 °C CMS membrane is S-shaped suggesting that there is a bimodal distribution of the pore size in this membrane, with a small number of pores with sizes lager than 5.02 Å. It is obvious that our assessment of the mean pore size is qualitatively correct only, yet it does provide a good insight into the effects that changes in carbon density, weight reduction etc. have on porosity and mean pore size during the formation of the CMS membranes.
The permeation rates for all gases decreased as the modules were stored over a period of several weeks. Although the permeation rates decreased the selectivities were unaffected. This effect is most likely caused by adsorption of contaminates, e.g. water, from the air and in the bulk N_2 used to purge the storage container. Similar effects have been reported by Jones *et. al.* [20].

5.4 Conclusions.

We can state, that it is not necessary to start with a gas selective precursor to prepare selective CMS membranes for gas separation. Moreover, porous precursors may be employed, resulting in gas selective CMS membranes exhibiting a formidable gas permeance. We have used UF fibers with high, non-selective, gas fluxes and prepared gas separation membranes, without applying any additional coating layers before or after pyrolysis of the fibers. This greatly benefits the preparation of the precursor for CMS membranes. Fibers prepared from the P84 co-polyimide retain their asymmetric structure in both the support and in the selective top layer. The asymmetric structure provides the fiber with mechanical strength, even after pyrolysis. However, in the top layer, rearrangements of the polymer do take place, providing the appropriate structure for CMS formation. By following the permeation behavior of a large number of high and low affinity gases we could follow the process of CMS formation. We saw that with a continued increase of the permeance the pore size initially increases, but decreases at temperatures higher than 900 °C. This observation suggests that two simultaneously occurring phenomena can be distinguished. A continuous increase of the pore number with increasing pyrolysis temperature and secondly a change in pore size. At first the pore size increases (from 600 – 800 °C) and eventually decreases at higher temperatures (900 °C).

5.5 References.

[1] M. B. Rao, S. Sircar, Nanoporous Carbon Membranes for Separation of Gas-Mixtures by Selective Surface Flow, J. Membr. Sci. 85 (1993) p253-264.

[2] J. Petersen, M. Matsuda, K. Haraya, Capillary carbon molecular sieve membranes derived from Kapton for high temperature gas separation, J. Membr. Sci. 131 (1997) p85-94.

[3] C. W. Jones, W. J. Koros, Carbon Molecular-Sieve Gas Separation Membranes .1. Preparation and Characterization Based on Polyimide Precursors, Carbon 32 (1994) p1419-1425.

[4] A. B. Fuertes, D. M. Nevskaia, T. A. Centeno, Carbon composite membranes from Matrimid (R) and Kapton (R) polyimides for gas separation, Microporous Mesoporous Mat. 33 (1999) p115-125.

[5] V. C. Geiszler, W. J. Koros, Effects of polyimide pyrolysis conditions on carbon molecular sieve membrane properties, Ind. Eng. Chem. Res. 35 (1996) p2999-3003.

[6] M. B. Shiflett, H. C. Foley, Ultrasonic deposition of high-selectivity nanoporous carbon membranes, Science 285 (1999) p1902-1905.

[7] J. Hayashi, H. Mizuta, M. Yamamoto, K. Kusakabe, S. Morooka, Pore size control of carbonized BPDA-pp'ODA polyimide membrane by chemical vapor deposition of carbon, J. Membr. Sci. 124 (1997) p243-251.

[8] A. B. Fuertes, T. A. Centeno, Carbon molecular sieve membranes from polyetherimide, Microporous Mesoporous Mat. 26 (1998) p23-26.

[9] H. Kita, H. Maeda, K. Tanaka, K. Okamoto, Carbon molecular sieve membrane prepared from phenolic resin, Chem. Lett. (1997) p179-180.

[10] V. M. Linkov, R. D. Sanderson, E. P. Jacobs, Highly Asymmetrical Carbon Membranes, J. Membr. Sci. 95 (1994) p93-99.

[11] N. Tanihara, H. Shimazaki, Y. Hirayama, S. Nakanishi, T. Yoshinaga, Y. Kusuki, Gas permeation properties of asymmetric carbon hollow fiber membranes prepared from asymmetric polyimide hollow fiber, J. Membr. Sci. 160 (1999) p179-186.

[12] Y. Kusuki, H. Shimazaki, N. Tanihara, S. Nakanishi, T. Yoshinaga, Gas permeation properties and characterization of asymmetric carbon membranes prepared by pyrolyzing asymmetric polyimide hollow fiber membrane, J. Membr. Sci. 134 (1997) p245-253.

[13] A. S. Damle, S. K. Gangwal, V. K. Venkataraman, Carbon Membranes for Gas Separation - Developmental Studies, Gas Sep. Purif. 8 (1994) p137-147.

[14] H. Suda, K. Haraya, Gas permeation through micropores of carbon molecular sieve membranes derived from Kapton polyimide, J. Phys. Chem. B 101 (1997) p3988-3994.

[15] A. Bos, I. Punt, H. Strathmann, M. Wessling, Suppression of gas separation membrane plasticization by homogeneous polymer blending, Aiche J. 47 (2001) p1088-1093.

[16] S. Kuroda, I. Mita, Degradation of Aromatic Polymers .2. The Crosslinking During Thermal and Thermo-Oxidative Degradation of a Polyimide, Eur. Polym. J. 25 (1989) p611-620.

[17] J. D. Way, D. L. Roberts, Hollow Fiber Inorganic Membranes for Gas Separations, Sep. Sci. Technol. 27 (1992) p29-41.

[18] M. B. Rao, S. Sircar, Nanoporous Carbon Membrane for Gas Seperation, Gas Seperation & Purification 7 (1993) p279-284.

[19] T. A. Centeno, A. B. Fuertes, Supported carbon molecular sieve membranes based on a phenolic resin, J. Membr. Sci. 160 (1999) p201-211.

[20] C. W. Jones, W. J. Koros, Characterization of Ultramicroporous Carbon Membranes with Humidified Feeds, Ind. Eng. Chem. Res. 34 (1995) p158-163.

Chapter 6
Functionalized Carbon Molecular Sieve membranes containing Ag-nanoclusters.

J.N. Barsema, J.Balster, V.Jordan, N.F.A. van der Vegt, and M. Wessling

Abstract

In Carbon Molecular Sieve (CMS) membranes, the separation of O_2 and N_2 is primarily based on the difference in size between the gas molecules. To enhance the separation properties of these CMS membranes, it is necessary to functionalize the carbon matrix with materials that show a high affinity to one of the permeating gas species. Adding Ag-nanoclusters increases the selectivity of O_2 over N_2 by a factor 1.6, compared to a non-functionalized CMS membrane prepared by the same pyrolysis procedure. We have analyzed the structure of Ag-nanocluster ($d_{cluster} \approx 50$ nm) containing membranes produced from different Ag sources, $AgNO_3$ and AgAc, and with different Ag content (0, 6, 25, and 40 wt%). By measuring the pure gas permeabilities of He, CO_2, O_2, and N_2 we have determined the effect of Ag-nanoclusters in the carbon matrix, concluding that, in the case of pure gases, the Ag-nanoclusters act primarily as a spacer at pyrolysis end temperatures up to 600 °C, increasing the O_2 permeability by a factor of 2.4. However, they enhance the separation of O_2 over N_2 at higher pyrolysis end temperatures (700 to 800 °C). It was shown that the build up of an Ag layer on the surface of the membrane reduces the permeability, but does not affect the selectivity.

* Based on 'J.N.Barsema *et.al.*, J. Membr. Sci. 219 (2003) p47-57'.

6.1 Introduction.

Over the last decades, polymeric membranes have proven to operate successfully in industrial gas separations [1]. In certain separations, like the production of oxygen-enriched air, polymeric membranes still lack sufficient selectivity to render their use economically attractive over conventional separations like cryogenic distillation or pressure swing adsorption. Carbon Molecular Sieves (CMS) have shown permeation and separation properties significantly exceeding those of their polymeric precursor membranes. In principle, two concurrently occurring separation mechanisms can be distinguished in CMS membranes. In CMS membranes with pores approaching the molecular diameters of the gases to be separated (< 6Å), the main mechanism is molecular sieving. The separation takes place on the basis of size exclusion and is, therefore, not dependent on pore wall – gas molecule interactions nor on the feed pressure [2]. When the pore sizes of the CMS membrane are below 50Å a transition from Knudsen to surface diffusion takes place [3]. Gas molecules adsorb on the pore wall and travel through the pore by diffusion over the surface of the pore rather than through the free volume of the pore itself. The mechanism of surface diffusion becomes increasingly important as the interaction between the pore wall and the gas molecule increases. In the case of strongly adsorbing gases and small pores, pore blocking can occur through selective adsorption of one of the species, which in certain cases can lead to pore condensation.
The separation of N_2 and O_2 takes place predominantly based on the first mentioned mechanism of molecular sieving. Both gas species posses little to no affinity to the carbon matrix. Precise tailoring of the pore size has resulted in high separation factors for these two gases [4, 5] however, to achieve even higher separation factors, it is necessary to go beyond the tailoring of pore sizes. By functionalizing the carbon matrix with Ag-nanoclusters, we will show that it is possible to increase the selectivity factor for the separation of N_2 and O_2 compared to their non functionalized CMS counterparts. Metallic Ag is well known for its interactions with O_2 and is used in composite inorganic membrane separations at elevated temperatures [6], in thin film Pd/Ag alloy dense metal membranes [7] and as catalyst in many oxidation reactions [8]. In contrary to the above-mentioned work, we will perform the separations at room temperature. In the temperature range from 0 to 100 °C

the interactions between Ag and O_2 can be classified as [9]:

- physical adsorption,
- chemical adsorption,
- solution (absorption),
- bulk compound formation.

In physical and chemical adsorption processes the reaction is confined to the surface of the metal. They are distinguished by the nature of the surface forces. Between temperatures as low as –195 °C to temperatures of 400 °C, O_2 readily chemisorbs onto Ag-surfaces [10]. This implies that in the temperature range between 0 and 100 °C both chemical and physical adsorption take place. Generally, desorption of chemical adsorbed O_2 below 100 °C is negligible [11], however Czanderna [11] showed that even at low temperatures small amounts (<15%) of the O_2 (i.e. chemically and physically adsorbed) easily desorb simply by evacuation. The nature of the oxygen species adsorbed on the Ag-surface is generally believed to be part dissociative and part non-dissociative, e.g. O^-, O^{2-}, O_2, O_2^-, and O_2^{2-} [12]. These oxygen species form activated complexes with a considerably higher mobility, compared to adsorbed oxygen molecules [12].
In solution and bulk compound processes the gas penetrates into the metal lattice. Often it can be very important to distinguish between these four processes, but such a distinction is not always possible.
In this chapter we will present a method for the preparation of CMS membranes containing Ag-nanoclusters. These membranes are characterized and their permeability and selectivity are compared to non-functionalized CMS membranes.

6.2 Experimental Section.

6.2.1 Materials.

Both CMS and Ag containing CMS (AgCMS) membranes were prepared using the commercial, thermally stable, co-polyimide (BTDA-TDI/MDI) P84 from Lenzing as polymer precursor. The structure of the polymer is shown in Fig. 1.

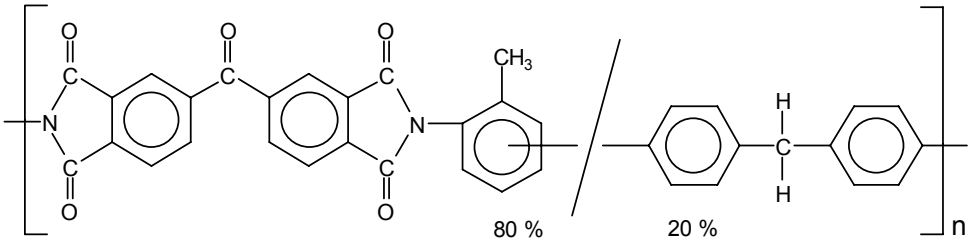

Fig. 1: Structure of P84 co-polyimide.

The T_g of this polymer was determined with Differential Scanning Calorimetry (second run and 30 °C/min) and found to be 315 °C. The theoretical carbon yield of this polymer is 54.2 wt%, equal to the aromatic carbon content.
N-methyl-pyrrolidone (NMP), Merck 99 %, was used as the solvent. As additive TriFluoroacetic Acid (TFA), Merck-Schurchardt 99 %, was used. As Ag source two different Ag salts were used. $AgNO_3$, Merck 99.8 %, and $AgC_2H_3O_2$ (AgAc), Merck 99 %. All gases used for pyrolysis and gas permeation experiments had a purity of at least 99.5 %.

6.2.2 Precursor preparation.

All precursor membranes were prepared based on a solution of 13 wt% P84 in NMP. For the AgCMS precursors, the Ag containing salts were dissolved in the NMP before the P84 was added. In the case of AgAc an equivalent of 1.2 mol TFA per mol of AgAc was added to the solution to facilitate the solvation of AgAc, forming AgTFA [13]. All solutions were made and kept in the absence of light to prevent reduction of the Ag salt by UV radiation. The solutions were allowed to dissolve overnight and were subsequently filtered over a 25 μm metal filter.
The solutions were cast on glass plates using a 200 μm casting knife and placed in a dry N_2 box for three days, then placed in a N_2 oven for a further three days at 50 °C to remove most of the solvent. The relatively low temperature during the removal of the solvent was chosen to prevent any thermal decomposition of the Ag salts prior to the pyrolysis process. The obtained precursor film had a thickness of approximately 20 μm.

6.2.3 Pyrolysis procedure.

The pyrolysis is preformed using a Carbolite® TZF 12/100 High Temperature Tube Furnace, mounted with an Eurotherm 2408 CP temperature controller. Fig. 2 gives a schematic overview of the furnace set-up.

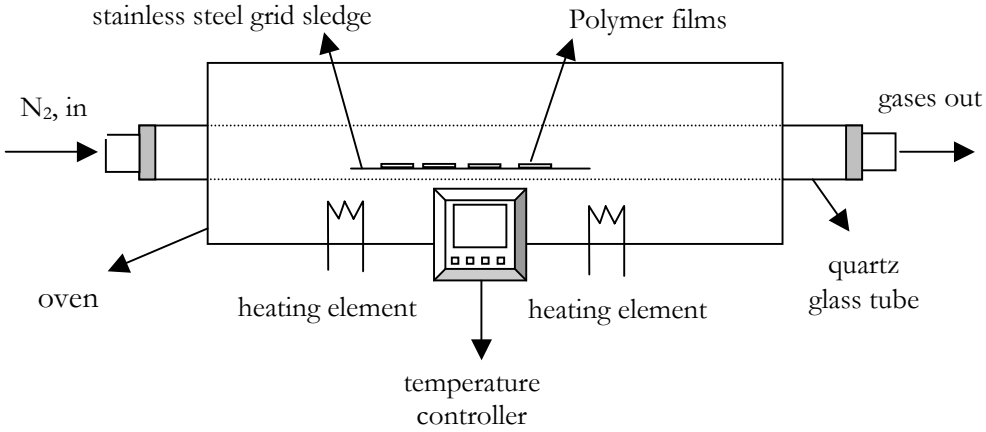

Fig. 2: A schematic overview of the furnace set-up.

The precursor is placed in a quartz glass tube, using a stainless steel grid as sledge. The atmosphere in the quartz tube during pyrolysis was N_2, with a flow rate of 10 cm^3/min.

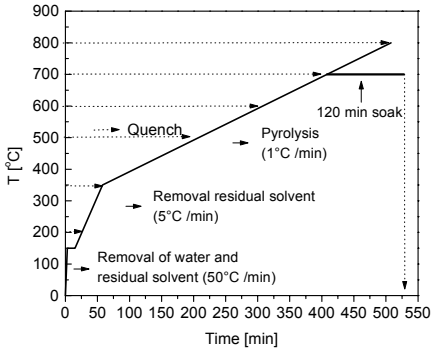

Fig. 3: A schematic overview of the pyrolysis trajectory and the temperatures at which the CMS membranes are quenched.

Fig. 3 shows the pyrolysis trajectory for the preparation of the CMS and AgCMS membranes. Upon reaching the end temperature, the membranes were immediately quenched under N_2 to room temperature in an external stainless steel double-hulled cooler. The membranes are cooled by flowing tap water through the outer hull of the cooler.

6.2.4 Analysis.

Thermo-gravimetrical analysis. The carbon yield, respectively, carbon Ag yield, defined as the weight relative to the initial precursor weight, was determined using Thermo Gravimetric Analysis (TGA). The TGA experiments were preformed using a Perkin-Elmer TGA 7 with a N_2 atmosphere and flow rates of 20 cm^3/min. Heating routes were based on pyrolysis procedures.

Scanning electron microscopy. To investigate the distribution of Ag and Ag-nanoclusters in the AgCMS structure Scanning Electron Microscopy (SEM) was used to look at both the cross-section and surface of the membranes. The micrographs were obtained using a JEOL JSM T220A SEM for magnifications up to 25.000x and a JEOL JSM 5600 LV SEM for higher magnifications. The precursor polymeric materials were coated with platinum in an argon atmosphere using a JEOL JFC 1300 (20 mV, 90 sec.) before they were placed in the microscope. To obtain a more detailed picture of the surface of the produced membranes Atomic Force Microscopy, Nanoscope 3A from Digital Instruments, was used.

X-ray photoelectron spectroscopy. To investigate the presence and chemical nature of Ag, X-ray Photoelectron Spectroscopy (XPS) was performed, using a Quantum 2000 Scanning Esca Probe of Physical Electronics, on samples at different stages in the pyrolysis. The experiments were carried out on the surfaces of the samples despite the occurrence of some oxidation evoked by contact with the air [14].

Gas soption. The adsorption of gases in the carbon samples was determined using a Rubotherm magnetic suspension balance operated by MessPro software. This balance has an accuracy of 1 μg and a reproducibility of 2 μg. The samples were evacuated to a pressure below 10 Pa, before the gas pressure was applied. The obtained data were corrected for buoyancy effects, experienced because of the increased gas density at higher pressures.

Using the Dubinin-Astakhov equation (equation 1) and the sorption isotherm at low equilibrium pressures [15], the total micoporous volume (for a certain probe molecule) can be determined. The Dubinin-Astakhov equation relates the pore volume W to the sorption potential A (equation 1). W is calculated from the volume occupied by the adsorbed molecules, determined by multiplying the number of moles adsorbed per gram adsorbent with the Van der Waals constant b [cm^3mol^{-1}].

$$W = W_0 e^{-\left(\frac{A}{E}\right)^n}, \tag{1}$$

where W is the pore volume [cm^3g^{-1}], W_0 is the total micoporous volume available to the probe molecule [cm^3g^{-1}], E is the characteristic energy of sorption [$Jmol^{-1}$], n [-] is equal to 2 [16], and A is the sorption potential [$Jmol^{-1}$] given by equation 6:

$$A = RT \ln\left(\frac{p_s}{p}\right), \tag{2}$$

with p_s the saturation pressure [bar] and p the equilibrium pressure [bar].
The total microporous volume accessible to the probe gas can now be determined from the y-axis intercept in a plot of ln W versus A^2.

Gas Permeation. To elucidate the CMS and AgCMS microstructure pure gas permeation experiments were conducted. The membranes were glued into metal discs, using an Araldit two component adhesive, to prevent cracking of the membranes by the rubber ring seals. The gas permeation experiments were done, using a variable permeate pressure set-up. In the experimental set-up, a vacuum was applied at the permeate side, whereas the other side was brought into contact with the feed gases. All measurements were taken after the fluxes became constant in time. A more extensive description of the determination of both permeability and selectivity can be found elsewhere [2]. The reported results are based on measurements performed on two or more membranes.

Besides N_2 and O_2, CO_2 and He were used for the gas permeation experiments. Of these gases He (2.6 Å), O_2 (3.46 Å), and N_2 (3.64 Å) have a relatively low affinity to the carbon matrix compared to CO_2 (3.3 Å) [17].

To show the effect of functionalizing the CMS membrane by adding Ag-nanoclusters the results are partly presented as enhancement factors (Ef). This factor is defined in analogy with the facilitation factor in facilitated transport [18], e.g. liquid membranes. The Ef gives the ratio of permeabilities of a specific gas for the functionalized AgCMS over the CMS, eq. (3).

$$Ef = \frac{P_{AgCMS}}{P_{CMS}}, \tag{3}$$

6.3 Results and discussion

In Table 1, an overview is given of the membranes prepared for this research. The membranes containing no Ag are coded MP, whereas the Ag containing membranes are denominated by MAg.

Table 1. Composition of precursor solution, precursor film, and (Ag)CMS membranes.

Name	Ag source	P84 in solution [wt%]	Ag in solution[a] [wt%]	Ag in precursor [wt%][a]	Ag in AgCMS [a,b] [wt%]
MP1	-	13.04	-	-	-
MAg1	$AgNO_3$	12.94	0.49	3.59	6.21
MAg2	$AgNO_3$	12.56	2.36	14.5	24.6
MAg3	$AgNO_3$	12.11	4.56	23.7	39.6
MAg4	AgAc	12.86	0.50	3.63	6.28

[a] *Based only on the Ag content of the silver source.*

[b] *Based on the theoretical carbon yield.*

6.3.1 Thermo-gravimetric analysis.

From the TGA experiments, it is possible to derive the onset of both the reduction of the Ag^+-ions and the pyrolysis of the polymer. Fig. 4a gives the TGA results for all the different precursor compositions and pure P84 powder in the temperature range of 50 to 200 °C. The Ag^+-ions start reducing at approximately 155 °C. Simultaneous to the process of reduction the residual

solvent evaporates from the sample, as can be seen from the differences in the curves for precursors P84 powder and MP1. This evaporation conceals the weight loss caused by the reduction of Ag^+-ions in precursor MAg1, because of the small amount of Ag^+-ions present.

Fig. 4.b shows the weight loss of all the precursors over a temperature range from 150 °C to 700 °C. The TGA curves were corrected for water and solvent loss below 150 °C.

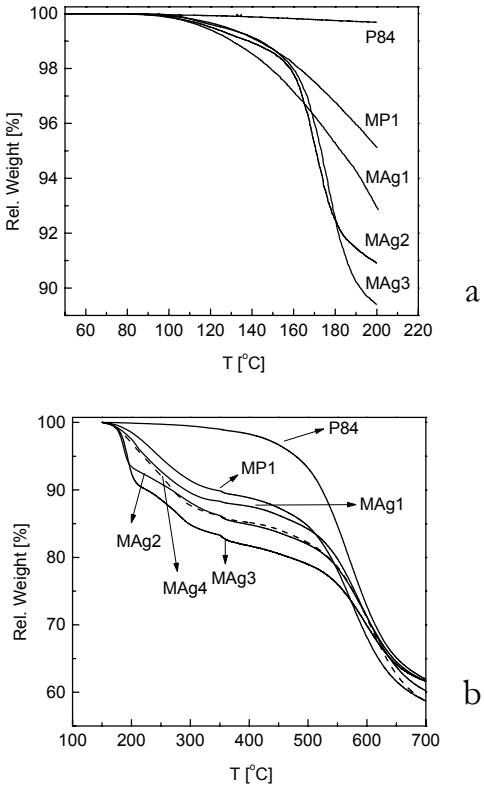

Fig. 4 a, b: TGA micrograph of the reduction process (a) and the total pyrolysis (b) for all precursor membrane compositions.

Although the Ag content in the different precursors differs from 0 to 23 wt%, the final weight loss is in the same range for all samples. A simple mass balance over the pyrolysis can explain this, showing that the weight loss of pyrolysis products and Ag salt counter-ions coincide.

As the heat treatment progresses the physical properties of the membranes change, depending on temperature and Ag content. Table 2 displays the different physical properties of the membranes. The MAg3 membranes with a high Ag content are very brittle. This is attributed to the high amount of Ag distributed in the carbon matrix and on the surface of the membrane.

Table 2. Physical properties of the produced CMS and AgCMS membranes.

Name	200 °C	350 °C	500 °C	600-800 °C
MP1	polymer yellow transparent flexible	polymer yellow transparent flexible	intermediate black brittle	carbon black reflecting brittle
MAg1	polymer yellow/brown transparent/little reflecting flexible	polymer brown mirror flexible	intermediate golden mirror flexible	carbon golden mirror brittle
MAg2	polymer brown transparent/reflecting flexible	polymer silver mirror flexible	intermediate golden mirror flexible	carbon silver mirror brittle
MAg3	polymer silver mirror brittle	polymer silver mat brittle	intermediate silver mat brittle	carbon silver mirror very brittle
MAg4	polymer yellow/brown transparent/little reflecting flexible			carbon silver mirror brittle

6.3.2 Precursor composition and CMS structure.

In Table 1 the composition of the prepared (Ag)CMS is given for different Ag sources before and after pyrolysis. Although the content of Ag is high, it is still below the percolation threshold. Shen *et.al* [19] determined the percolation threshold to be between 33 and 36 wt% for Ag in Bi-Y-O-Ag composites. Although Table 1 contains values of up to 40 wt% of Ag, the percolation threshold is not reached, as a large part of the Ag migrates to the surface of the

membrane. This was verified using XPS showing the presence of Ag on the surface of the membranes. The source of the Ag^+-ions can play an important role in the formation of the functionalized membrane. Southward *et.al.* [13] reported that the formation of conductive Ag layers on polyimide surfaces is affected by the ligands. Depending on the type of ligand, more or less Ag^+-ions are directed to the surface. They found that using AgAc in combination with TFA produced better conductive surfaces, whereas the use of $AgNO_3$ gave brittle and degraded films. Although the use of AgAc as Ag source in carbon molecular sieves has been reported [20], we observed the best results using $AgNO_3$. The observed brittleness of the films produced with $AgNO_3$ reported by Southward [13] is most likely caused by the formation of gaseous products during the reduction of $AgNO_3$. By using thin precursor films and limiting the $AgNO_3$ content, we obtained flexible films with mechanical properties comparable to their non-functionalized counterparts. The different behavior of these two Ag sources can be observed by taking a more detailed look at the cross-section and surface of the functionalized membrane. Fig. 5 and 6, respectively, show the SEM (cross-section) and AFM (surface) micrographs of functionalized membranes (MAg1 and MAg4) pyrolysed at 700°C. We should emphasize that SEM and AFM micrographs show no structure at these resolutions for samples without Ag.

In the case of functionalized membranes prepared with $AgNO_3$ (Fig. 5a), a fine distribution of Ag-nanoclusters, seen as white dots, is observed in the black carbon cross-section.

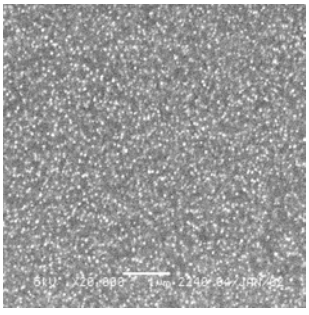

a

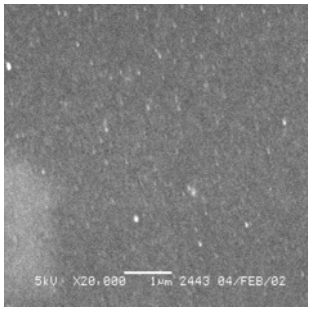

b

Fig. 5: SEM micrographs of the AgCMS membrane cross-section of MAg1 and MAg4 , using $AgNO_3$ (a) or AgAc (b) as Ag source, respectively. (Pyrolysis end temperature 700 °C).

This, in contrary to the AgAc containing samples (Fig. 5b), where virtually no Ag-clusters can be observed. In Fig. 6a and 6b the black regions represent the carbon matrix and the white regions the Ag clusters as obtained by AFM tapping mode. It is evident from the surface pictures that in the case of AgAc (Fig. 6b) a significant part of the Ag diffuses to the surface, resulting in a densely packed layer. This is in agreement with the findings of Southward *et.al.* [13], as they aimed for a layer of Ag on the surface, whereas we aim for a containment of the Ag-nanoclusters in the carbon matrix. For this purpose the $AgNO_3$ is more suitable.

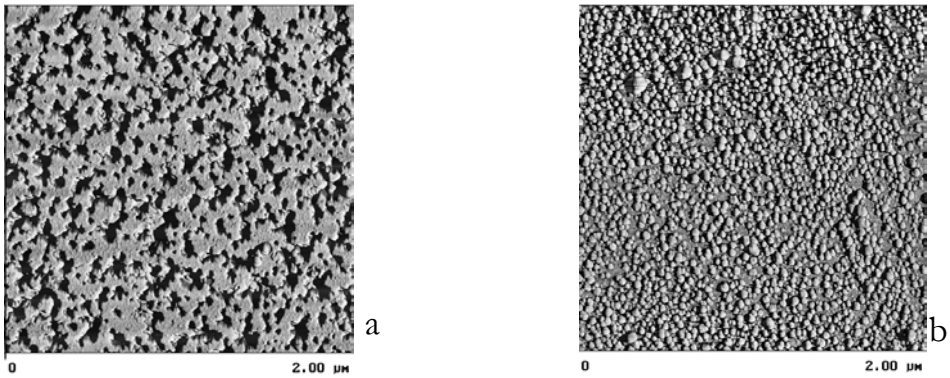

Fig. 6: AFM micrographs of the AgCMS membrane surface of MAg1 and MAg4, using $AgNO_3$ (a) or AgAc (b) as Ag source, respectively. (Pyrolysis end temperature 700 °C).

As the pyrolysis end temperature is increased, the Ag layer on the surface of the MAg1 membrane changes from single Ag clusters to a percolated structure at temperatures above 500 °C. This can be seen by comparing Fig. 6a with Fig 7, which shows the surface of a MAg1 membranes prepared at 350 °C. As the pyrolysis temperature is increased or the end temperature soak is extended, the concentration of Ag on the surface of the membranes increases.

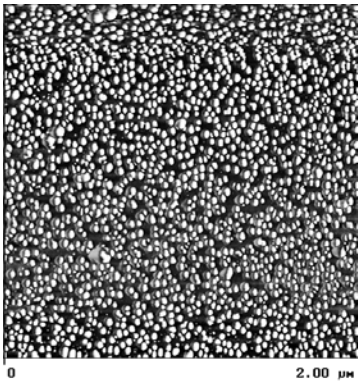

Fig. 7: AFM micrograph of the AgCMS membrane surface of MAg1, using $AgNO_3$ as Ag source. (Pyrolysis end temperature 350 °C).

This continues until an almost dense Ag layer is formed. By reducing the concentration of $AgNO_3$ in the precursor, less Ag diffuses to the surface, resulting in thinner surface layers. The average cluster size reduces from 65 nm to 50 nm for MAg2 and MAg1, respectively, with increasing number of Ag-clusters.

Fig. 8 shows the effect of cluster size on the number of clusters and total cluster surface area calculated for 1 mmol Ag, assuming perfectly spherical clusters with density $\rho(Ag)= 10.5\ g/cm^3$ (293 K). As the diameter decreases the number of particles and their accumulated surface area increase rapidly. It is clear that we should work towards small cluster diameters, to obtain the highest functional area in the functionalized membrane.

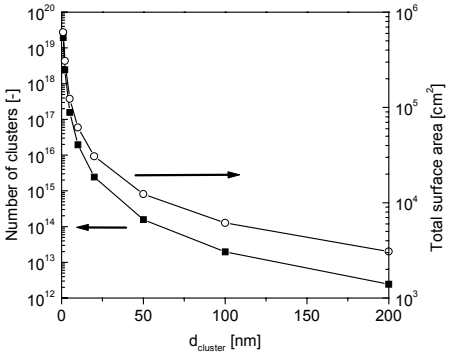

Fig. 8: Number of clusters (○) and total surface area (■) versus the cluster diameter, calculated for 1 mmol Ag assuming perfectly spherical clusters with density ρ(Ag)= 10.50 g/cm³ (293 K).

6.3.3 Gas sorption in AgCMS membranes.

The addition of Ag-nanoclusters to the CMS prepared at 700 °C, leads to a significant increase in both the sorption of the tested gases and the total micro porous volume available to CO_2 (see Figure 9 and 10, respectively).

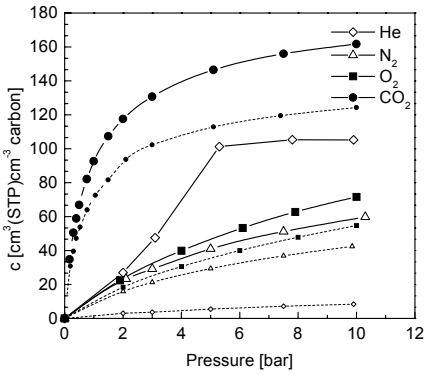

Fig. 9: Gas concentration (He ◇, N_2 △, O_2 ■, and CO_2 ●) vs. pressure for MAg700. Dashed lines represent the MP700 membrane. T = 25 °C.

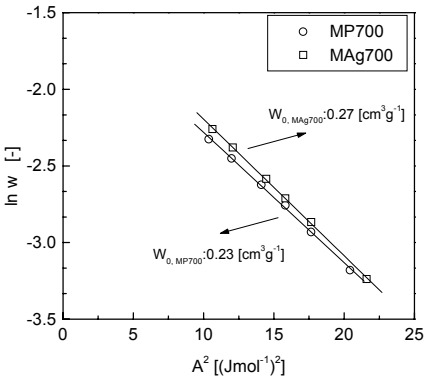

Fig. 10: Dubinin-Astakhov plots for MP700 (○) and MAg700 (□) CMS membranes. T = 25 °C.

The dashed lines in Figure 9 represent the sorption curves measured without Ag-nanoclusters (Figure 11, chapter 4). It is obvious that the sorption increases significantly for all gases. However, the sorption selectivity of O_2 over N_2 does not increase significantly (< 5%). The total micro porous volume available to CO_2, as determined by the Dubinin-Asthakhov equation, increased by more than 17 % from 0.23 to 0.27 cm^3g^{-1} (see Figure 10), providing an explanation for this large sorption increase.
The He concentration in the carbon increases strongly with the addition of Ag-nanoclusters, indicating the creation of new He accessible volume.

6.3.4 Gas permeation through AgCMS membranes.

The effect of functionalizing the carbon matrix with Ag-nanoclusters becomes evident when the pure gas permeabilities are determined. Numerical values are given in Table 3 and the results are interpreted below by plotting the data in various ways.

Table 3. Pure gas permeabilities for the prepared CMS and AgCMS membranes.

Membrane	$T_{pyrolysis}$ [°C]	P_{He} [Barrer]	P_{CO2} [Barrer]	P_{O2} [Barrer]	P_{N2} [Barrer]
MP1	350	7.9	1.5	0.35	0.04
MP1	500	26.5	17.5	3.9	0.73
MP1	600	447	276	72.2	7.8
MP1	700	166	64.1	16.8	2.1
MP1	700_{120}[c]	37.0	2.4	0.46	0.14
MP1	750	179	30.6	8.25	0.80
MP1	800	58.5	3.3	3.0	2.8
MAg1	350	6.5	1.1	0.26	0.05
MAg1	500	42.1	27.5	6.1	1.8
MAg1	600	668	619	170	19.9
MAg1	700	589	290	81.3	6.7
MAg1	700_{120}[c]	366	83.6	30.8	2.5
MAg1	750	372	268	54.1	4.5
MAg1	800	169	12.4	3.0	0.19
MAg2	700	720	284	77.0	8.4
MAg4	700	298	148	39.4	3.9

[c] *The membrane was allowed to soak for 120 min at 700°C, before quenching.*

Fig. 11 displays the selectivity of O_2 over N_2 versus the O_2 permeability. For reference, we have added the Robeson upper limit of 1991 [21]. It is clear that the carbonized membranes (MP1 600 , MP1 700, and MP1 750) show permeability and separation properties exceeding the properties of their polymeric precursors (MP1 350 and MP1 500). The MP1 800 membranes have a selectivity of O_2 over N_2, which approaches 1. This phenomenon was discussed in chapter 4. The addition of Ag nanoclusters to the carbon matrix has a significant effect on the permeability and selectivity of the membranes.

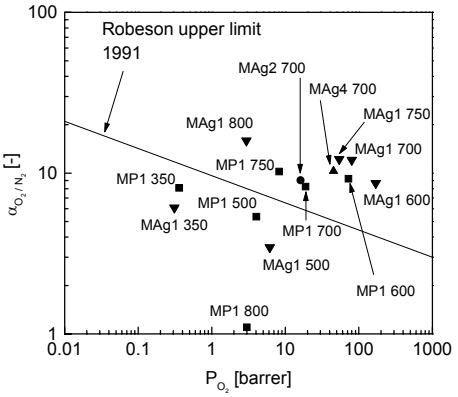

Fig. 11: Selectivity of O_2 over N_2 versus the O_2 permeability for different pyrolysis end temperature, Ag content, and source (298 K, 2 bar).
■ - MP1, ▲ - MAg1, ● - MAg2, ▼ - MAg4.

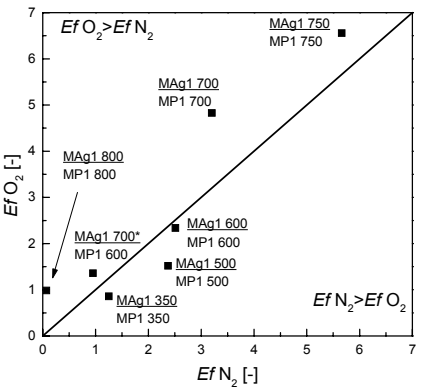

Fig. 12: Enhancement factors for O_2 and N_2 for MAg1 compared to MP1 (298 K, 2 bar).

To quantify the effect of Ag-nanoclusters in the carbon matrix, Fig. 12 shows the enhancement factor for O_2 and N_2, as defined by eq. (3). The line at the angle of 45° indicates that O_2 and N_2 are equally enhanced. Values below the line indicate a preferential N_2 enhancement, whereas values above the line indicate a preferential O_2 enhancement. Considering that the value of the enhancement factor is a measure for the increase of the permeability of a gas, we can derive from Fig. 12 that below 600 °C the Ag acts primarily as a spacer within the carbon matrix, thereby significantly increasing the permeability of the membrane for both gases and simultaneously decreasing the size selectivity. However, at 700 °C the oxygen permeability is enhanced with a factor of 4.8, compared to an enhancement of 3.3 for N_2. This trend is continued in the

membranes prepared at pyrolysis end temperatures of 750 and 800 °C, both showing a higher O_2, as compared to the N_2 enhancement.
The point in Fig. 12 coded MAg700*/MP1600 is displayed because these specific membranes show an *Ef* of 1 for N_2. This indicates that the reported CMS membrane prepared at 600 °C has the same permeability for N_2 as the AgCMS prepared at 700 °C, thus indicating that both have the same pore size. The effect of the Ag-nanoclusters now becomes evident, as the O_2 permeability shows an *Ef* of 1.3.

The spacer effect of the Ag, i.e. adding additional volume for permeation to the carbon, is shown in Fig. 13, where the selectivity of He over CO_2, two gases with low affinity to the functionalized carbon matrix, is plotted versus the He permeability. The arrows indicate membranes treated at the same temperature. The He permeability increases by adding Ag-nanoclusters, whereas the selectivity over CO_2 is lowered, when the same pyrolysis end temperature is considered. The sample in Fig. 13 coded $700_{120\ min}$ was allowed to soak at 700 °C for 120 minutes before the quench.

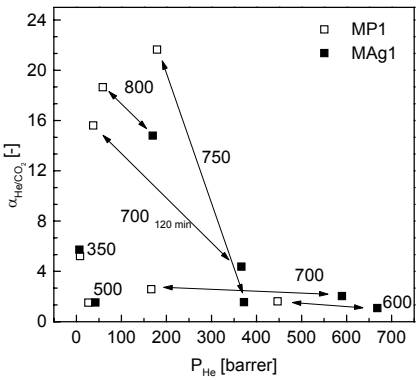

Fig. 13: Selectivity of He over CO_2 versus the He permeability for MAg1 (■) and MP1 (□) (298 K, 2 bar). The arrows indicate membranes treated at the same temperature.

To explain the permeation behavior we should look more closely at the mechanisms for diffusion within the functionalized carbon structure. Fig. 14 shows a schematic representation of the functionalized carbon structure.

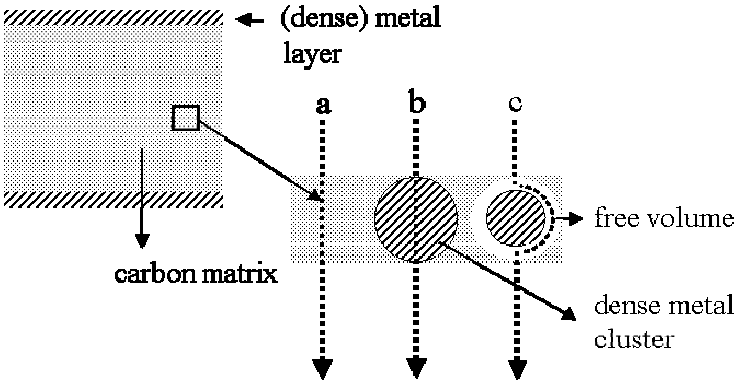

Fig. 14: Proposed diffusion routes through a functional part of a AgCMS membrane. (a) Diffusion through carbon matrix, (b) Diffusion through Ag-cluster. (c) Bypass of Ag-cluster diffusion through free volume.

Three transport routes (Fig. 14 a, b, c) can be proposed for a gas molecule to diffuse through a functional part of the membrane. Independent of the diffusion route through the membrane, the gas molecules must first diffuse through the metal layer on the surface of the membrane before entering or leaving the membrane. In the case of the proposed route *a* where no metal cluster is present, the molecules diffuse through the carbon matrix by micropore diffusion. Following route *b*, the gas molecule diffuses through the metal cluster. From Hwang *et.al.* [22] the permeation rate through dense Ag clusters at a temperature of 25 °C can be estimated to be small ($<10^{-7}$ Barrer). Finally, considering route *c*, the permeating gas molecule can bypass the metal cluster, because of a poor adhesion between the metal cluster and the carbon matrix, similar to the process described by Sakai *et.al.* [23] for Ag clusters in Nafion membranes. Depending on the size of the bypass volume this occurs by macropore diffusion and Knudsen diffusion (< 150 Å) or alternatively by surface diffusion (< 50 Å) in the case of interaction between the gas and the metal cluster, i.e. in this case O_2. As the virgin Ag-nanocluster is exposed to O_2 it will chemisorb most of the O_2 irreversibly onto the surface. Part of the O_2 molecules are weakly bound to the surface by both physical and chemical adsorption and can easily desorb [11]. As the O_2 adsorbs, it can dissociate into atoms allowing it to pass through even smaller bypass areas [12]. Figure 15 shows the measured sorption and desorption isotherms for both the MP700 as the MAg700 membranes for O_2.

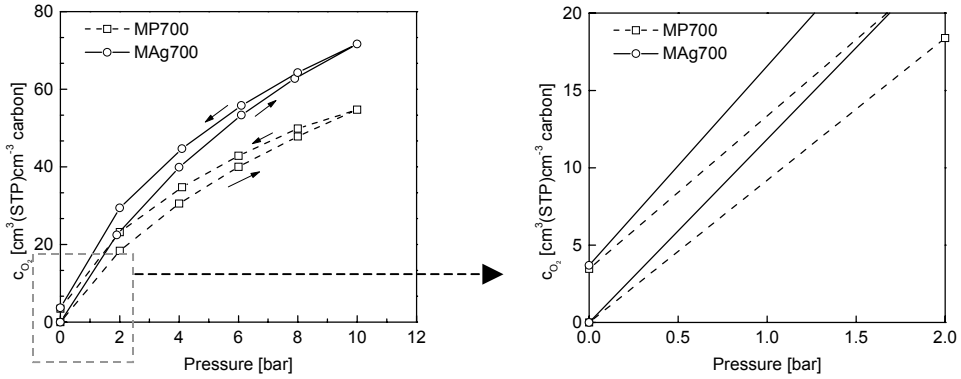

Fig. 15: O_2 sorption and desorption curves vs. the pressure for MP700 (□) and MAg700 (○) membranes. T: 25 °C.

Both isotherms show that not all O_2 is desorbed, although the extent of the hysteresis differs, the residual amount of O_2 is comparable. This suggests that the non-desorbed O_2 has oxidized the carbon matrix rather than chemisorbed onto the Ag.

From the increased permeation rates compared to the non-functionalized carbon matrix and the low permeation rates through dense metal clusters, we conclude that route *c* is the mechanism contributing most to the enhanced permeability. At higher pyrolysis end temperatures, the bypass volume around the Ag-clusters as described in route *c* is reduced, thereby increasing the effect of surface diffusion over the Ag-clusters.

If the choice of mechanism c is a correct one, the bypass formed has, in a two-dimensional view, two walls of a different composition. On the one side Ag and on the other side C, hence, one might also expect an enhancement of permeability of carbon interacting gas species, e.g. CO_2. Indeed if we look at Figure 16, displaying the selectivity of CO_2 over N_2, O_2 over N_2, and CO_2 over O_2, we see a substantial increase in the selectivity of CO_2 over N_2 with increasing temperature of pyrolysis (and thus decrease of bypass diameter) next to the known increase of O_2 over N_2. Importantly, the CO_2 over O_2 selectivity remains virtually unchanged, indicating that both molecules benefit equally from the bypass.

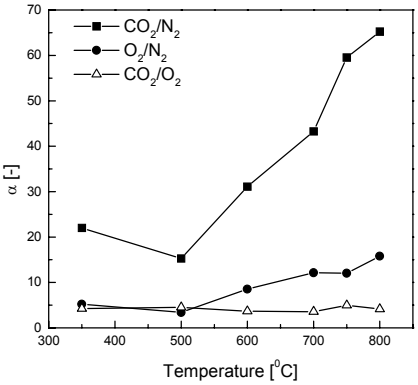

Fig. 16: Selectivity of CO_2 over N_2 (■), O_2 over N_2 (●), and CO_2 over O_2 (△) vs. the pyrolysis temperature for MAg membranes. P: 2 bar, T: 25 °C.

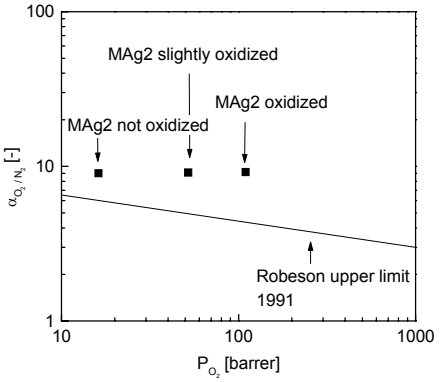

Fig. 17: Selectivity of O_2 over N_2 versus the O_2 permeability for different extent of oxidization of a MAg2 membrane (298 K, 2 bar).

The build up of an Ag layer on the surface of the membrane has a strong effect on the permeability of the membrane. To investigate the properties of this Ag layer we analyzed three middle Ag-content MAg2 membranes. Between reaching the pyrolysis end temperature and start of the quench procedure the membranes were brought into contact with air, resulting in an oxidation of the membrane surface. The extent of oxidation was varied. Fig. 17 shows the effect of the oxidation step on the O_2 over N_2 selectivity and the O_2 permeability.

With prolonged oxidation, the permeability of O_2 increases by approximately 700 % without showing any loss of selectivity. This implies that by oxidizing the membrane we have reduced the Ag layer on the membrane surface, however we have not altered the carbon matrix as suggested by Shusen *et.al.* [24], who increased the mean pore size by post-oxidation of a carbon membrane.

6.4 Conclusions.

We have shown that it is possible to functionalize CMS membranes with Ag. Moreover, we have shown that the addition of Ag-nanoclusters to CMS membranes increases the pure gas O_2 over N_2 selectivity by a factor of 1.6, when compared to its non-functionalized CMS counterpart, at pyrolysis end temperatures of 700 °C and higher. By introducing the enhancement factor E*f* we can clearly show the effect of the functionalization. The permeability of the membranes increases significantly (240 %, 600 °C) for pyrolysis end temperatures below 700 °C, where the Ag-nanoclusters can act as spacers. Above this temperature, an Ag layer develops on the surface of the membrane. Oxidation of this layer has proven beneficial to the permeability, without affecting the selectivity. We have suggested three possible diffusion routes through the AgCMS, opting for the route where the gas molecules pass through the free volume between Ag-nanocluster and the carbon matrix.
We analyzed several Ag contents (0, 6, 25, and 40 wt%) of two different Ag sources ($AgNO_3$ and AgAc), determining that the lower Ag content (6 wt%) with $AgNO_3$ as the source resulted in the most stable AgCMS membrane. This membrane contained Ag-nanoclusters with a diameter of approximately 50 nm and a fine distribution throughout the bulk of the carbon matrix. Using a higher Ag content affects the mechanical stability of the membrane, while both permeability and selectivity are negatively influenced. The micro porous volume is increased significantly by addition of Ag-nanoclusters, resulting in a higher gas solubility, as compared to the non-functionalized material. The addition of AgAc as the Ag source led to the formation of Ag surface layers with an increased coverage of the total surface as compared to $AgNO_3$.

6.5 References.

[1] R. W. Baker, Future directions of membrane gas separation technology, Ind. Eng. Chem. Res. 41 (2002) p1393-1411.

[2] J. N. Barsema, N. F. A. van der Vegt, G. H. Koops, M. Wessling, Carbon molecular sieve membranes prepared from porous fiber precursor, J. Membr. Sci. 205 (2002) p239-246.

[3] J. D. Way, D. L. Roberts, Hollow Fiber Inorganic Membranes for Gas Separations, Sep. Sci. Technol. 27 (1992) p29-41.

[4] M. B. Shiflett, J. F. Pedrick, S. R. McLean, S. Subramoney, H. C. Foley, Characterization of supported nanoporous carbon membranes, Adv. Mater. 12 (2000) p21-25.
[5] H. Suda, K. Haraya, Gas permeation through micropores of carbon molecular sieve membranes derived from Kapton polyimide, J. Phys. Chem. B 101 (1997) p3988-3994.
[6] J. Kim, Y. S. Lin, Synthesis and oxygen permeation properties of ceramic-metal dual-phase membranes, J. Membr. Sci. 167 (2000) p123-133.
[7] H. Amandusson, L. G. Ekedahl, H. Dannetun, Hydrogen permeation through surface modified Pd and PdAg membranes, J. Membr. Sci. 193 (2001) p35-47.
[8] T. Furusawa, K. Seshan, J. A. Lercher, L. Lefferts, K. Aika, Selective reduction of NO to N-2 in the presence of oxygen over supported silver catalysts, Appl. Catal. B-Environ. 37 (2002) p205-216.
[9] D. O. Hayward, Gas adsorption in Chemisorption and reactions on metallic films, J. R. Anderson ed., vol 1, Academic Press, London, 1971, p231.
[10] Gmelig handbuch der anorganischen chemie, Silber: verbindungen, R. Keim, vol B1, 8th Edition, Verlag Chemie GMBH, Weingeim, 1971, p32.
[11] A. W. Czanderna, The adsorption of Oxygen on Silver, J. Phys. Chem. 68 (1964) p2765-2772.
[12] X. E. Verykios, F. P. Stein, R. W. Coughlin, Oxidation of ethylene over silver: adsorption, kinetics, catalyst, Catal. Rev. Sci. Eng. 22 (1980) p197-234.
[13] R. E. Southward, D. W. Thompson, Inverse CVD: A novel synthetic approach to metallized polymeric films, Adv. Mater. 11 (1999) p1043-1047.
[14] C. W. Jones, W. J. Koros, Carbon Molecular-Sieve Gas Separation Membranes .1. Preparation and Characterization Based on Polyimide Precursors, Carbon 32 (1994) p1419-1425.
[15] M. M. Dubinin, The potential theory of adsorption of gases and vapors for adsorbents with energetically nonuniform surfaces., Chem. Rev. 60 (1960) p235-241.
[16] J. Hayashi, M. Yamamoto, K. Kusakabe, S. Morooka, Simultaneous Improvement of Permeance and Permselectivity of 3,3',4,4'-Biphenyltetracarboxylic Dianhydride-4,4'-Oxydianiline Polyimide

Membrane by Carbonization, Ind. Eng. Chem. Res. 34 (1995) p4364-4370.

[17] M. Ogawa, Y. Nakano, Gas permeation through carbonized hollow fiber membranes prepared by gel modification of polyamic acid, J. Membr. Sci. 162 (1999) p189-198.

[18] C. A. Koval, Z. E. Reyes, in Liquid membranes: theory and application, R. D. Noble , J. D. Way ed., American Chemical Society, Washington DC, 1987, p29.

[19] Y. Shen, M. Liu, D. Taylor, S. Bolagopal, A. Joshi, K. Krist, Mixed ionic-electronic conductors based on BI-Y-O-Ag metallic-ceramic system, T. A. Ramanarayanan, W. L. Worrell , H. L. Tuller ed., 2nd International Symposium on ionic and mixed conducting ceramics, vol 94-12, The Electrochemical Society, Pennington, 1994, p574.

[20] H. Suda, K. Haraya, Oxygen/nitrogen permselectivity of silver/carbon nanocomposite membranes, ed., The 6th International Congress on Inorganic Membranes 2000, Montpellier, 2000, p406.

[21] L. M. Robeson, Correlation of separation factor versus permeability for polymeric membranes, J. Membr. Sci. 62 (1991) p165-185.

[22] S.-T. Hwang, K. Kammermeyer, Membranes in separations, 1st Edition, Wiley-Interscience, New York, 1975, p94.

[23] T. Sakai, H. Takenaka, E. Torikai, Oxygen/nitrogen separation by a nafion(R)-Ag microcomposite membrane, J. Membr. Sci. 31 (1987) p227-234.

[24] W. Shusen, Z. Meiyun, W. Zhizhong, Carbon Membranes for Gas Separation, Sep. Sci. Technol. 31(16) (1996) p2299-2306.

Chapter 7

Ion exchange blend polymeric precursors for Ag containing Carbon Molecular Sieve membranes.

J.N. Barsema, N.F.A. van der Vegt, G.H. Koops, and M. Wessling

Abstract

We prepared dense flat sheet Ag functionalized Carbon Molecular Sieve membranes from a blend of P84 co-polyimide and AgSPEEK (sulphonated poly(ether ether ketone) with Ag^+ as counter ion). These blends offer the possibility to produce new precursor structures, which were previously not possible, like integrally skinned asymmetric hollow fibers. Membranes prepared at a pyrolysis end temperature of 800 °C showed a maximum permeability for all tested gases at a Ag content of approximately 2.5 wt% (He: 465 Barrer, CO_2: 366 Barrer, O_2: 91.8 Barrer, N_2: 10.3 Barrer). The maximum achieved selectivity for O_2 over N_2 with CMS membranes based on these blends was $\alpha_{O2/N2}$: 13.5 (Ag content: 4.5 wt%, P_{O2}: 52.7 Barrer). The CO_2 over N_2 selectivity reached a value of 48.9 (Ag content: 4.5 wt%, P_{CO2}: 191 Barrer). These observations are explained by the formation of selective bypasses around Ag-nanoclusters in the CMS carbon matrix.

* based on Barsema *et.al.*, submitted to Adv. Funct. Mat.

7.1 Introduction.

Gas separation is an energy consuming process. In the industrial separation of gases, processes like distillation and pressure swing adsorption are commonly used. However, during the last two decades polymeric membranes have been developed for large-scale separation of gases and are presently applied as an alternative for the conventional processes. Recently developed Carbon Molecular Sieve (CMS) membranes have shown to combine a preferred high permeability while sustaining selectivity [1]. For the separation of O_2 and N_2, membranes were prepared with a selectivity over 30 [2, 3]. However, the permeability was in some cases relatively low. We have recently shown that the selective properties of a P84 co-polyimide based CMS can be improved by functionalization of the CMS through addition of Ag-nanoclusters to the carbon matrix [4]. It was shown that the permeability was not only retained as compared to their non-functionalized counterparts, the permeability even increased substantially for pyrolysis temperatures between 600 and 750 °C. The Ag-nanoclusters were formed by temperature-induced reduction of $AgNO_3$, previously added to the precursor casting solvent. A negative side effect was the formation of large Ag agglomerates at the surface of the CMS membranes, greatly increasing the resistance to permeation. A second disadvantage is the high solubility of $AgNO_3$ in water, which prevents the production of integrally skinned asymmetric hollow fiber membranes by phase inversion, typically using water as the non-solvent [5]. During the phase inversion process, $AgNO_3$ moves with the solvent from the casting solution into the non-solvent phase.
In this work, we will describe a new concept for the preparation and characterization of polymeric precursors containing Ag^+ ions and their CMS counterparts. This concept has the potential to be applicable for phase inversion fiber spinning of an Ag^+ containing polymeric precursor. For this we will utilize polymeric blends containing Ag^+ loaded ion exchange polymers, i.e. sulphonated poly(ether ether ketone) with Ag^+ as counter ion (AgSPEEK).

7.2 Experimental Section.

7.2.1 Materials.

The blended precursor membranes were prepared from the commercial, thermally stable, co-polyimide (BTDA-TDI/MDI) P84 from Lenzing. The structure of the polymer is shown in Figure 1a. The T_g of this polymer was

determined with Differential Scanning Calorimetry, second run and 30 °C/min, and found to be 315 °C.
The second blend component was sulphonated poly(ether ether ketone) (SPEEK), Figure 1b. This polymer is obtained by sulphonation of Poly(Ether Ether Ketone) (PEEK). An extensive explanation of the preparation of SPEEK can be found elsewhere [6].

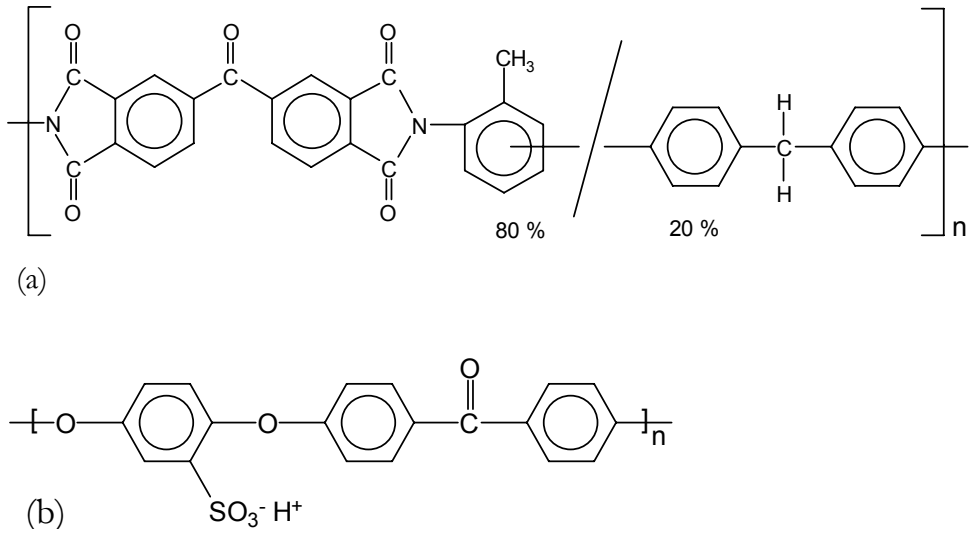

Fig. 1: Chemical Structure of (a) - P84 co-polyimide, (b) – SPEEK.

As Ag source $AgNO_3$, Merck 99.8 %, was used. N-methyl-pyrrolidone (NMP), Merck 99 %, was used as the solvent. All gases used for pyrolysis and gas permeation experiments had a purity of at least 99.5 %.

7.2.2 Precursor preparation.

Ag containing blends can be prepared by two procedures: (a) blending of P84 with H-SPEEK and subsequent exchange of H^+ by Ag^+, (b) direct blending of P84 with Ag-SPEEK.
Ion exchange, for both SPEEK and P84/SPEEK, was performed using the following protocol. The polymer was immersed into 1 M HCl for 1 day to obtain protonated SPEEK, subsequently it was rinsed with de-ionized water, followed by immersion in 4 M $AgNO_3$ for three days. During the last two steps the solutions were renewed three times.

For the characterization of the blends, films were prepared from a solution of 13 wt% polymer in NMP. The solutions were allowed to dissolve overnight and were subsequently filtered over a 25 μm metal filter.
The solutions were cast on glass plates using a 200 μm casting knife and placed in a dry N_2 box for three days. Finally, the films were placed in a N_2 oven for a further three days at 50 °C to remove most of the solvent. The relatively low temperature during the removal of the solvent was chosen to prevent premature reduction of the Ag^+-ions [4]. The obtained precursor film had a thickness of approximately 20 μm.

7.2.3 Pyrolysis procedure.

The pyrolysis is preformed using a Carbolite® TZF 12/100 High Temperature Tube Furnace, mounted with an Eurotherm 2408 CP temperature controller. The precursor is placed in a quartz glass tube, using a stainless steel grid as sledge. The atmosphere in the quartz tube during pyrolysis was N_2, with a flow rate of 10 cm^3/min.
A pyrolysis trajectory consisting of three steps was used for the preparation of the CMS and AgCMS membranes. In the first step, the precursor was heated to 150 °C (50 °C/min) and remained at this temperature for 15 min to remove adsorbed water. Subsequently the temperature was raised with a heating rate of 5 °C/min to 350 °C, after which the pyrolysis end temperature was reached with a heating rate of 1 °C/min. Upon reaching the end temperature, the membranes were immediately quenched into N_2 to room temperature in an external stainless steel double-hulled cooler. The membranes are cooled by flowing tap water through the outer hull of the cooler. The prepared AgCMS membranes were coded MAgS followed by the pyrolysis end temperature and AgSPEEK fraction (wt%), e.g. MAgS700-10.0

7.2.4 Analysis.

Ion exchange capacity. The ion exchange capacity of the prepared blends is determined by indirect titration with 0.1 N NaOH. The samples, approximately 0.7 g , are brought into the proton state by immersion into 250 ml of HCl (1 M) for 1 day. The excess HCl is subsequently removed from the sample by rinsing for three hours using 250 ml of de-ionized water. The rinsing fluid is renewed three times, or until no H^+ can be detected in the waste water, using $AgNO_3$ as indicator.
The protonated polymer is immersed in 50 ml NaCl (2M) or $AgNO_3$ (4M) solution depending on the desired counter ion (Na^+ or Ag^+). The immersion

fluid is replaced three times whereby the immersion fluid is collected for H^+ analysis by titration. In the case of Ag^+ exchange, an equal volume of 4 M NaCl is added to the retained immersion fluid to precipitate the remaining Ag^+ (as this will react with the OH^- of the titration solution) and is removed by filtration. Subsequently the total amount of released H^+ is determined by tritration with 0.1 M NaOH. From the obtained proton concentration, we can determine the degree of sulphonation (SD) and the ion exchange capacity (i.e.c.) of pure SPEEK as well as of the blend using eq. (1):

$$i.e.c. = \frac{1000SD}{x \cdot (M_{nSPEEK} \cdot SD + M_{PEEK} \cdot (1 - SD)) + (1 - x) \cdot M_{P84}}, \quad (1)$$

where i.e.c. is the ion exchange capacity [meqg^{-1}], SD is the degree of sulfonation [-], M is the molecular weight of the monomer [g], x is the SPEEK fraction in the blend [-], and n represents the counter ion in the SPEEK (H^+, Na^+, or Ag^+).

Weight loss. The weight loss during heat treatment was determined using Thermo Gravimetric Analysis (TGA). The TGA experiments were performed using a Perkin-Elmer TGA 7 with a N_2 atmosphere and flow rates of 20 cm^3/min. Heating routes were based on pyrolysis procedures described elsewhere [4].

Differential Scanning Calorimetry. Using Differential Scanning Calorimetry, we can determine the T_g and therefore the (in-)homogeneity of the prepared blends. For the DSC experiments, a Perkin-Elmer Pyris 1 DSC was used. Because the SPEEK will thermally degrade at relatively low temperatures, only one heating run can be applied to the sample. Therefore, we choose to use the temperature modulated DSC option provided by the Perkin-Elmer software (Heating rate 2°C/min, modulation amplitude 4°C, period 60 seconds).

Chemical composition. To investigate the presence and chemical nature of Ag and S, X-ray Photoelectron Spectroscopy (XPS) was performed, using a

Quantum 2000 Scanning Esca Probe of Physical Electronics, on samples at different stages in the pyrolysis. The experiments were carried out on the surfaces of the samples despite the occurrence of some oxidation evoked by contact with the air [7].

Scanning Electron Microscopy. To investigate the distribution of Ag and Ag-nanoclusters in the AgCMS structure, Scanning Electron Microscopy (SEM) was used to look at both the cross-section and surface of the membranes. The micrographs were obtained using a JEOL JSM 5600 LV SEM.

Gas adsorption. The adsorption of gases in the carbon samples was determined using a Rubotherm magnetic suspension balance operated by MessPro software. This balance has an accuracy of 1 μg and a reproducibility of 2 μg. The samples were evacuated to a pressure below 10 Pa, before the gas pressure was applied. The obtained data were corrected for buoyancy effects, experienced because of the increased gas density at higher pressures.

7.3 Results and discussion.

Ag containing polymers can be obtained by species controlled ion exchange with ionomers. We use the well know ionomer SPEEK. This polymer, prepared by sulfonation of PEEK, contains SO_3^- groups that can bind cations, e.g. H^+, Na^+, or Ag^+.
It was shown that P84 co-polyimide is a good precursor for CMS membranes, see chapter 4. By blending P84 co-polyimide with AgSPEEK one can obtain Ag containing polymeric precursors for the preparation of CMS membranes.

7.3.1 Thermo gravimetrical analysis.

The AgSPEEK serves primarily as Ag source while the P84 determines the carbon properties, the pyrolysis behavior of the blend should preferably be close to that of P84.

Figure 2 shows TGA curves for the pure components as well as for three different blend compositions (5, 20, and 50 wt% AgSPEEK). As the AgSPEEK content decreases, the pyrolysis behavior of the blends follows the P84 closely. The AgSPEEK shows a considerably different pyrolysis behavior as compared to P84. AgSPEEK shows a sharp increase in weight loss at temperatures just below 400 °C, then a plateau between 400 and 500 °C, and finally a second weight decrease step starts above 500 °C. Actually there is a substantial difference in pyrolysis behavior between SPEEK molecules with different counter ions. Figure 3 shows the TGA curves for HSPEEK, NaSPEEK, and AgSPEEK. Thermal stability increases following $H^+ < Ag^+ < Na^+$, with Ag^+ reducing to metallic Ag during the heat treatment. Other authors have also shown this strong dependence of the thermal stability on the counter ion [8].

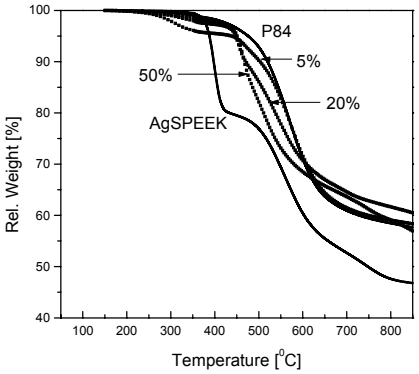

Fig. 2: Relative weight decrease as function of the temperature for various compositions of AgSPEEK/P84 blends.

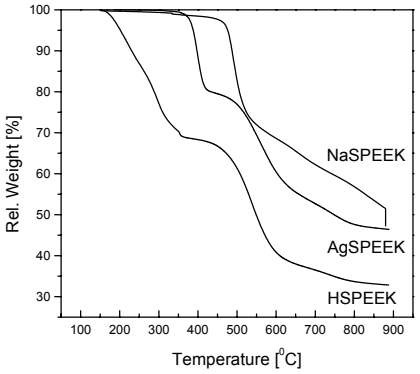

Fig. 3: TGA curves for different counter ion loaded SPEEK.

7.3.2 Ion exchange.

The i.e.c. of the used SPEEK was determined to be 1.61 meqg^{-1}. The counter ion exchange can take place before or after blending with P84. Figure 4 shows the i.e.c. of three blends (5, 20, and 50 wt%), where H^+ is exchanged by Ag^+ after blending, compared to the pure SPEEK. The dashed line shows the real values for the i.e.c., whereas the solid line shows the theoretical value, which would be obtained by blending after ion exchange. Both axes are plotted on a

logarithmic scale to point out the deviation from the theoretical value at low SPEEK content.

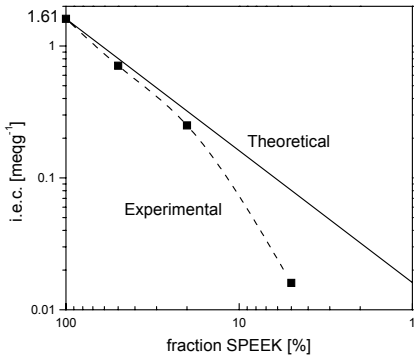

Fig. 4: I.e.c. v.s blend composition for P84/SPEEK blends.

Obviously, the i.e.c. of the obtained blends falls below the theoretically expected value, as it becomes increasingly more hydrophobic with increasing P84 content. The degree of swelling decreases and, therefore, the ion exchange becomes more difficult. Figure 5 depicts the Ag content in the resulting CMS vs. the blend composition. In previous work we have shown that Ag loading in the CMS exceeding 6 wt% is disadvantageous for both permeability and mechanical properties [4]. The area, designated as interesting, in Figure 5 indicates the compositions resulting in an Ag loading of the carbon matrix lower than 6 %. Therefore, the P84/SPEEK should not contain more than 20 wt% of SPEEK. Combining the conclusions, drawn from Figure 4 and Figure 5 we can conclude that blending prior to counter ion exchange will lead to an inefficient use of the Ag source capabilities of the SPEEK, hence we will blend after H^+ is exchanged by Ag^+.

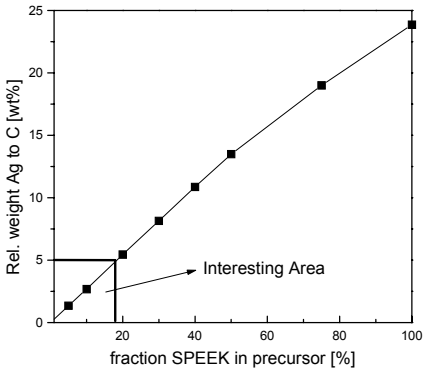

Fig. 5: Ag in CMS vs. P84/SPEEK/Ag blend composition.

7.3.3 Temperature modulated DSC.

To obtain a good distribution of Ag throughout the carbon matrix it is essential to have a homogenous blend of P84 and AgSPEEK. This was verified using temperature modulated DSC (tmDSC). Only one heating run could be conducted as AgSPEEK can undergo chemical alterations due to the applied temperature, i.e. reduction of Ag^+-ions and thermo-chemical degradation [8]. Chun et.al. [9] reported glass transition temperatures between 195 and 210 °C for HSPEEK prepared with different degree of sulfonation. Figures 6a and b show the heat flow (a) and complex Cp (b) of P84, AgSPEEK, and an equi-proportional blend of P84 and AgSPEEK, as obtained by tmDSC. The reduction of Ag^+ to Ag is clearly visible in the heat flow curves of both pure AgSPEEK and the blend as a large increase in heat consumption is observed, starting at approximately 125 °C. The blend curve shows a second temperature region with a high heat consumption beginning at 330 °C, which is also seen in the steep decrease of the Cp, indicating that a subsequent reaction is taking place.

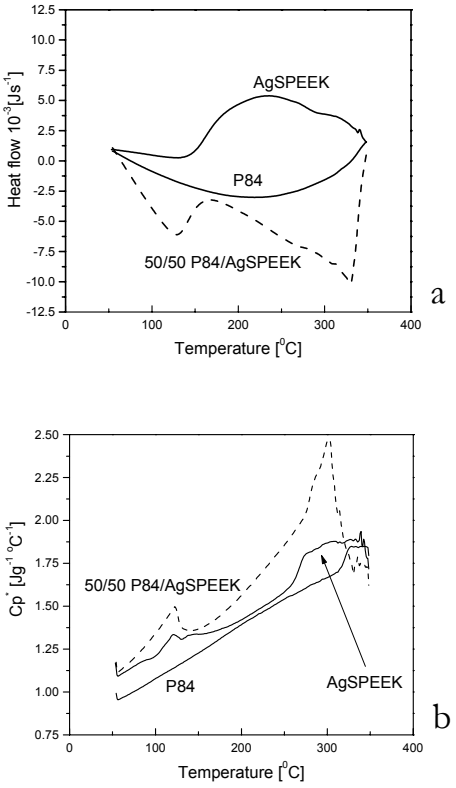

Fig. 6: (a) Heat flow and (b) complex Cp curves for P84, AgSPEEK, and a 50:50 blend of P84 and AgSPEEK obtained by tmDSC.

The T_g of the investigated samples can be derived from the secondary transitions in Figure 6b. The values of the T_g for P84, AgSPEEK, and their equi-proportional blend as determined from the complex Cp curves are 317.2, 266.3, and 287.7 °C, respectively. The blend sample shows only one T_g at a temperature of 287.7, which is in good agreement with the theoretical value of 291.8, obtained by applying the simple mixing rule. A second verification is obtained by plotting the measured i.e.c. versus the fraction SPEEK in the blend (see Figure 7). Wilhelm *et. al.* show that for the inhomogeneous blend of poly(ether sulphone) (PES) and SPEEK, there is a threshold of 40 % SPEEK

before the measured i.e.c of the PES/SPEEK approaches the theoretical predicted i.e.c. [10]. The threshold is explained by the formation of small inaccessible de-mixed regions of SPEEK surrounded by a PES matrix.

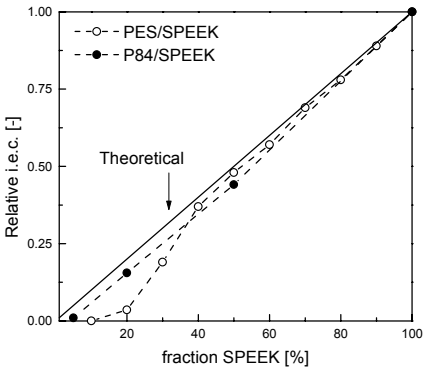

Fig. 7: Relative i.e.c. of PES/SPEEK [10] and P84/SPEEK blends vs. the fraction SPEEK.

Figure 7 shows the relative i.e.c. for two blends, PES/SPEEK [10] and P84/SPEEK, versus the SPEEK fraction. Also the theoretical i.e.c. is added, obtained by applying a simple mixing rule. Where the PES/SPEEK blend shows the mentioned threshold, the P84/SPEEK blend approaches the theoretical i.e.c. over the complete range of blend compositions.
From these observations we can conclude that on a macroscopic level the P84 and AgSPEEK blend is homogeneous.

7.3.4 The presence of Sulfur.

A significant disadvantage of using an ionomer with sulfonic acid as fixed ion is the presence of sulfur. It is well known that sulfur acts as de-activator of Ag in catalysis systems [11, 12], as S readily covalently binds with Ag. Oudar [12] states that a dissociation site for a O_2 molecule on Ag consists of two neighboring surface metal atoms, neither of which is bound to an adsorbed S atom. On either side of this pair of metal atoms, two vacancies must be located capable to receive the dissociated O atoms. These vacancies cannot be in contact with an S occupied site. This requires that a cluster of six adsorbate vacancies is available to dissociate one O_2 molecule. The presence of a small amount of sulfur atoms can thus influence the O_2 on Ag adsorption

significantly. Although, according to literature, the toxicity of the sulfur in R-SO_3^- is reduced by a shielding effect of the surrounding oxygen atoms bonded to the central S atom [11, 13], it would be preferable to remove all S atoms during the pyrolysis. XPS experiments on samples prepared at temperatures between 350 and 800 °C reveal the presence of both Ag as well as S atoms on the surface of the membranes. From the position of the peaks, it is possible to determine the chemical nature of the Ag and S compounds, i.e. whether the sulfur is bound to silver. Figure 8 shows the XPS spectra for (a) - S (2p spectral lines) and (b) - Ag (3d spectral lines) recorded from MAgS-5.0 samples obtained at 350, 600, 700, and 800 °C. They are compared with data obtained from the NIST XPS database [14].

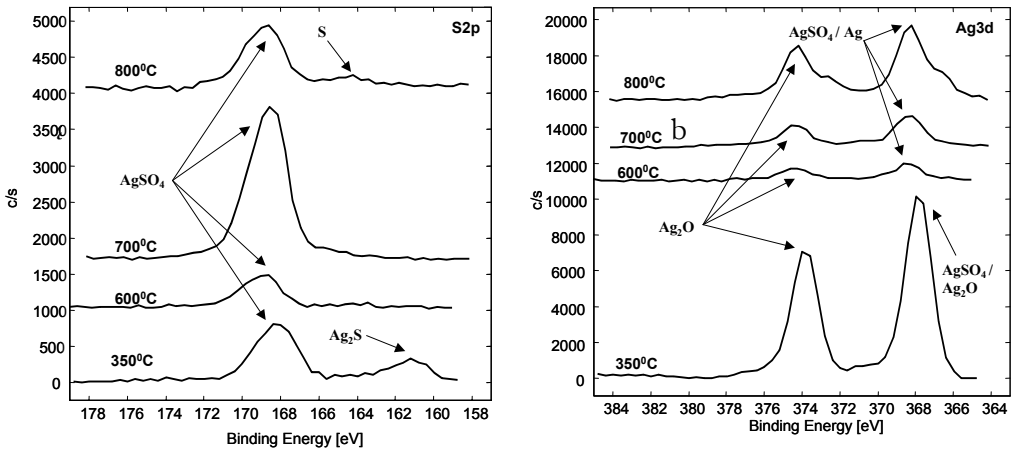

Fig. 8: XPS spectra of MAgS350-800. (a) S (2p), (b) Ag (3d).

From Figure 8(a), the presence of $AgSO_4$ (168.2 – 168.6 eV) is clearly visible. The peak at approximately 160.8 eV represents Ag_2S and is only seen in the sample treated to 350 °C. A small peak is seen in the spectrum obtained from the sample treated to 800 °C, this peak is attributed to pure S (164.0 – 164.8 eV). So it is evident that poisoning of Ag by S molecules is taking place. To find out if there is still active Ag present in the membranes we must look at the spectrum of Ag shown in Figure 8(b). It is less clear which compounds are present as the binding energies overlap. The peak at approximately 368.1 eV (600-800 °C) can be either $AgSO_4$ or pure Ag, whereas the peak (appr. 367.8 eV) in the spectrum of the sample treated upto 350 °C can represent both

Ag_2O and $AgSO_4$. However, the peak seen at 374.0 eV in all spectra can only be attributed to the presence of Ag_2O. The oxidation of Ag is caused by surface to air contact. We can, therefore, conclude that at all temperatures, part of the Ag is deactivated by S poisoning and a reduced enhancement of the O_2 flux by the Ag must be expected.

7.3.5 Scanning Electron Microscopy.

SEM micrographs were taken from MAgS800-5.0, MAgS800-9.1, and MAgS800-16.7 membranes (see Figure 9).

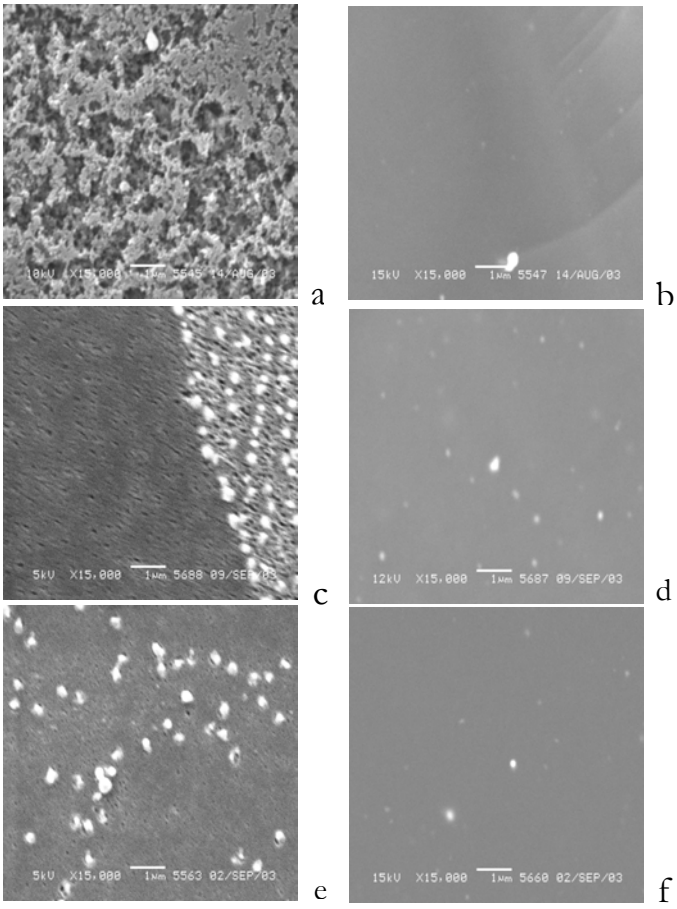

Fig. 9: SEM micrographs of membranes: MAgS800-5.0 (a: surface, b: cross-section); MAgS800-9.1 (c: surface, d: cross-section); MAgS800-16.6 (e: surface, f: cross-section).

We make a distinction between micrographs of the surface (a, c, and e) and the cross-section (b, d, and f), seen in Figure 9. A relatively low concentration of 5 wt% as present in the MAgS800-5.0 membrane (9a), leads to surface structures, comparable to those found on AgCMS membranes prepared using $AgNO_3$ as Ag source, see chapter 6.
In chapter 6, we also concluded that increasing the Ag content in the precursor results in an increased Ag presence on the surface. The surfaces of the MAgS800-9.1 (9c) and MAgS800-16.7 (9e) membranes appear to be dense, although some porous structure resembling irregularities can be found. Some individual Ag clusters, white spheres, are seen on the surface. Significant agglomerations of these Ag clusters (observed as large white stains) were also found on the surface of these membranes, even visible to the eye, as shown in Figure 10, and in more detail at the right side of Figure 9c. The development of these agglomerations is not yet understood, however these regions seem to have a higher porosity than the surrounding surface combined with a high concentration of Ag.

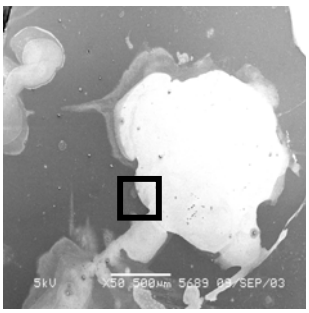

a

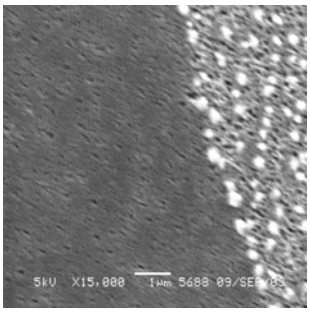

b

Fig. 10: SEM micrographs of the surface of a MAgS800-9.1: (a) low magnification, (b) high magnification.

SEM analysis of the cross-section could not identify large numbers of Ag-nanoclusters, Figure 9b, d, and f. This is a strong indication that the Ag clusters are too small to be observed (< 10 nm) or have not been formed at all.

An interesting side effect is seen on the surface of the MAgS800-9.1 and MAgS800-16.7 samples, where thin pillars or fibers have appeared during pyrolysis, see Figure 11. This is further explained in Appendix II.

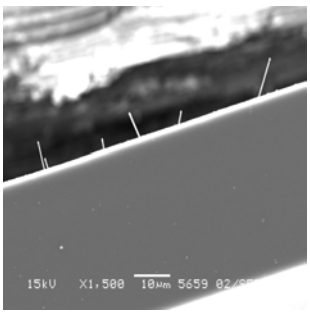

a

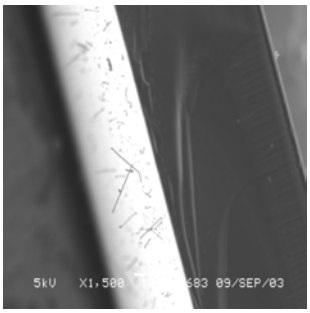

b

Fig. 11: SEM micrograph of carbon fibers on the surface of (a) MAgS800-9.1 and MAgS800-16.6 (b) membranes.

7.3.6 Gas permeation through AgCMS membranes based on P84/AgSPEEK blends.

In Figure 12, we see the effect of Ag content in the CMS on the permeability of He, CO_2, O_2, and N_2. By adding different amounts of AgSPEEK to the precursor, indicated by the number, we varied the Ag content between 1 and 5 wt% of the carbon matrix, see Table 1.

Table 1. Effect of Ag content on permeation properties of He, CO_2, O_2, and N_2 for functionalized CMS membranes. P: 2 bar, T: 25 °C.

Membrane	AgSPEEK content [$wt\%_{in\ poly}$]	Ag content [$wt\%_{in\ CMS}$]	P_{He} [Barrer]	P_{CO2} [Barrer]	P_{O2} [Barrer]	P_{N2} [Barrer]
MP800	0	0	58.5	3.3	3.0	2.8
MAgS800	5.0	1.35	161	83.3	27.5	4.6
MAgS800	9.1	2.46	465	366	91.8	10.3
MAgS800	16.7	4.51	361	191	52.7	3.9
MAg800	6.0*	6.21	169	12.4	3.0	0.19

** $AgNO_3$ was used as Ag source instead of AgSPEEK.*

For comparison, also the results [4] for a CMS membrane containing no Ag (MP800) and an AgCMS membrane based on a P84/$AgNO_3$ (MAg800) precursor were added, see Table 1. We must emphasize that when adding up to almost 20 wt% of AgSPEEK it is questionable whether one can speak of an additive and neglect the effect of the SPEEK on the carbonization process. A

clear maximum permeability is reached at an Ag content of 2.46 wt%. Higher concentrations of Ag lead to the formation of Ag layers on the surface of the membranes, reducing the permeability and thereby counteracting the effect of the Ag clusters on the permeability [4].

When plotting the selectivity of CO_2 over N_2, O_2 over N_2, and CO_2 over O_2 vs. the Ag content (see Figure 13), we observe a trend comparable to that seen in Figure 16, chapter 6, where we could see an increase in selectivity for CO_2 over N_2, and O_2 over N_2 with increasing temperature of pyrolysis. As shown in Figure 13, the same increase in CO_2 over N_2, and O_2 over N_2 selectivity is observed with increasing Ag content. Again, the selectivity of CO_2 over O_2 remains virtually unchanged, indicating that the occurring changes have a comparable effect on the permeation of both molecules. Where the increase of selectivity could be explained by a process of bypass formation and narrowing around Ag-nanoclusters in chapter 6, now the answer must be sought in the increasing number of bypasses, with increasing Ag content. As the number of bypasses increases, so does the number of regions where fast, favorable, surface diffusion of the adsorbed molecules takes place, resulting in a higher selectivity.

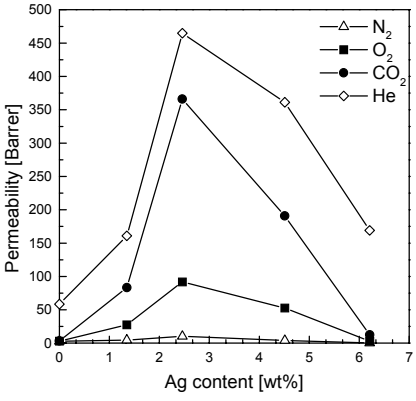

Fig. 12: Permeability of He (◊), CO_2 (●), O_2 (■), and N_2 (△) vs. Ag content. P: 2 bar, T: 25 °C.

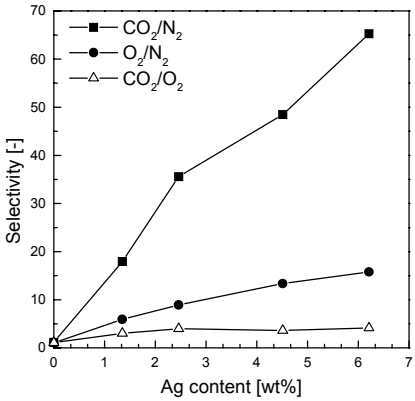

Fig. 13: Selectivity of CO_2 over N_2 (■), O_2 over N_2 (●), and CO_2 over O_2 (△) vs. the Ag content. P: 2 bar, T: 25 °C.

Although we expected a reduced functionality of the Ag present in the membrane, because of S poisoning, this is not backed up by the experimental results. Hence, we over estimated the negative effect of S on the enhancement function of the Ag or, quite possible, the surface composition differs from the bulk composition.

Finally, Figure 14 shows the selectivity versus the productivity for the separation of O_2 and N_2. Depending on the required productivity and purity one can now select the membrane with optimal performance.

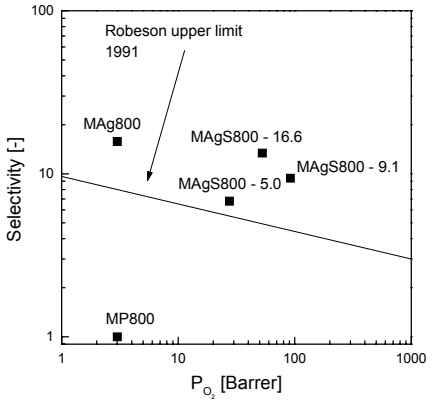

Fig. 14: Selectivity of O_2 over N_2 vs. the O_2 permeability for CMS membranes prepared at 800 °C with different Ag content. P: 2 bar, T: 25 °C.

7.4 Conclusions.

We have shown that dense flat sheet CMS membranes, prepared from blends containing P84 co-polyimide and Ag ion-exchanged SPEEK and pyrolysed at 800 °C, have O_2 over N_2 separation properties exceeding the Robeson 1991 upper limit. By varying the ratio of P84 and AgSPEEK the Ag content in the CMS membranes could be tailored allowing us to find an optimal Ag content to maximize either permeability or selectivity. It was found that a maximum permeability was obtained for CMS membranes containing approximately 2.5 wt% of Ag (P_{O2}: 91.8 Barrer, $\alpha_{O2/N2}$: 8.9), where the selectivity kept increasing

as the Ag content increased (Ag content: 4.5 wt%, P_{O2}: 52.7 Barrer, $\alpha_{O2/N2}$: 13.5). An interesting side effect of the addition of Ag was the increase of the CO_2 over N_2 selectivity reaching a value of 48.9 (Ag content: 4.5 wt%, P_{CO2}: 191 Barrer). These observations were explained by the formation of selective bypasses around Ag-nanoclusters in the CMS carbon matrix.
XPS analysis identified the presence of S compounds on the surface of the CMS prepared from a P84-AgSPEEK blend. Although it is well known that S can deactivate Ag catalyst, no negative effect on the gas separation performance of the membranes was found.
Using temperature modulated DSC and TGA analysis we determined that the blend precursors are homogenous and have thermal properties close to that of P84.
These new blends provide the opportunity to prepare asymmetric structured precursors, containing Ag^+-ions, by phase inversion in aqueous non-solvents. Therefore, the production of Ag functionalized integrally skinned asymmetric CMS hollow fibers is within reach. This could not be obtained with previously proposed precursor composition and preparation methods.

7.5 References.

[1] A. F. Ismail, L. I. B. David, Future direction of R&D in carbon membranes for gas separation, Membrane Technology 2003 (2003) p4-8.

[2] M. B. Shiflett, H. C. Foley, Ultrasonic deposition of high-selectivity nanoporous carbon membranes, Science 285 (1999) p1902-1905.

[3] H. Suda, K. Haraya, Gas permeation through micropores of carbon molecular sieve membranes derived from Kapton polyimide, J. Phys. Chem. B 101 (1997) p3988-3994.

[4] J. N. Barsema, J. Balster, V. Jordan, N. F. A. van der Vegt, M. Wessling, Functionalized carbon molecular sieve membranes containing Ag-nanoclusters, J. Membr. Sci. 219 (2003) p47-57.

[5] J. N. Barsema, G. C. Kapantaidakis, N. F. A. van der Vegt, G. H. Koops, M. Wessling, Preparation and characterization of highly selective dense and hollow fiber asymmetric membranes based on BTDA-TDI/MDI co-polyimide, J. Membr. Sci. 216 (2003) p195-205.

[6] T. He, Composite hollow fiber membranes for ion separation and removal, Edition, Twente University Press, Enschede, 2001.

[7] C. W. Jones, W. J. Koros, Carbon Molecular-Sieve Gas Separation Membranes .1. Preparation and Characterization Based on Polyimide Precursors, Carbon 32 (1994) p1419-1425.

[8] F. Wang, T. L. Chen, J. P. Xu, Synthesis of poly(ether ether ketone) containing sodium sulfonate groups as gas dehumidification membrane material, Macromol. Rapid Commun. 19 (1998) p135-137.

[9] Y. S. Chun, H. S. Kwon, W. N. Kim, H. G. Yoon, Compatibility studies of sulfonated poly(ether ether ketone)- poly(ether imide)-polycarbonate ternary blends, J. Appl. Polym. Sci. 78 (2000) p2488-2494.

[10] F. G. Wilhelm, I. G. M. Punt, N. F. A. van der Vegt, H. Strathmann, M. Wessling, Cation permeable membranes from blends of sulfonated poly(ether ether ketone) and poly(ether sulfone), J. Membr. Sci. 199 (2002) p167-176.

[11] C. H. Bartholomew, Mechanisms of catalyst deactivation, Applied Catalysis A: General 212 (2001) p17-60.

[12] J. Oudar, Sulfur adsorption and poisoning of metallic catalysts, Catalysis Reviews - Science and Engineering 22 (1980) p171-195.

[13] J. B. Butt, E. E. Petersen, Activation, deactivation, and poisoning of catalyst, 1st Edition, Academic Press inc., San Diego, 1988.

[14] NIST X-ray Photoelectron Spectroscopy Database, http://srdata.nist.gov/xps, 28/8/2003.

Appendix I

Optimizing pyrolysis procedure and set-up for the preparation of CMS membranes.

I.1 Introduction.

Although most of this thesis concentrates on the properties of Carbon Molecular Sieve membranes, we must not forget to take a close look at the pyrolysis furnace and the conditions of the pyrolysis process. Important factors such as heat transmission, heat radiation profile, pyrolysis atmosphere, and heating and cooling procedures are treated in this appendix.

I.2 Pyrolysis set up.

For pyrolysis of the membranes, a Carbolite® TZF 12/100 High Temperature Tube Furnace was used. The furnace is equipped with an Eurotherm 2408CP temperature controller and programmer and an Eurotherm 2132 over-temperature controller. Inside the oven two heating elements are located, at approximately one third and two third of the oven. The oven can be heated to temperatures of 1250 °C. The length of the furnace tube is approximately 1 m and the diameter is 10 cm.

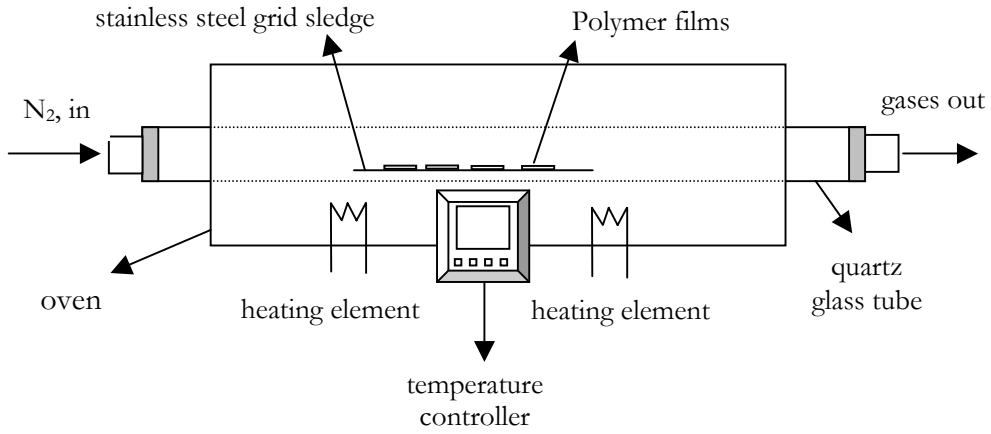

Fig. 1: A schematic overview of the furnace set-up.

The temperature profile inside the furnace is uniform as the heated length is divided into three zones, each with its own temperature controller and thermocouple. The power supplied to the end zones is automatically adjusted to compensate for the heat loss at the ends of the tube, irrespective of whether the ends are left open or have insulation plugs fitted. The uniform temperature zone equals the overall length of the furnace tube minus 1.5 times the diameter at both ends, according to the manufacturer.
Inside the furnace a quartz glass tube is placed. Two quartz glass tubes were used, with the following dimensions:

- ∅: 6,0 cm, l: 140 cm, wall thickness: 3 mm

- ∅: 9,0 cm, l: 140 cm, wall thickness: 3 mm

During pyrolysis the atmosphere in the quartz tube is controlled by flowing an inert gas through the tube using a Brooks 5850 mass flow controller. In literature, a number of different atmospheres, besides vacuum [1, 2], are suggested e.g. N_2 [3, 4], Ar [5, 6], or He [6]. Here N_2 was chosen because of is availability and price. This inert gas flow provides a medium for both the heat transfer and removal of pyrolysis gases [6].

I.3 Heat transfer.

As the gas flows into the tube at room temperature, it is necessary to calculate maximum gas flow rate and the length of the instationary zone where the gas is heated to the furnace temperature. There are three separate sections in the heating process that must be considered. First, the instationary zone of the oven, secondly the time needed to heat the quartz tube, and finally the time necessary to heat the inert gas.

ad. 1 If heating in the instationary zone of the furnace tube is neglected, 1.5 times the diameter of the furnace tube, i.e. 15 cm, will not contribute to the heating of the inert gas.

ad. 2 For the fresh inert gas to reach the temperature of the furnace tube, the inside of the quartz tube must be heated to the temperature of the furnace tube too. If the conduction and convection of heat by the gas atmosphere between furnace and quartz tube are neglected, the quartz tube is heated solely by radiation from the furnace tube. The time necessary for the quartz tube to follow the changes in temperature of the furnace tube can be calculated using eq.1 and 2, which represent the total heat consumption of the quartz tube and the absolute heat flux radiated by the furnace.

$$t = \frac{\Phi_{total,quartz}}{\Phi''_{total,furnace}} = \frac{\Phi_{vol,quartz} \cdot \partial V_{quartz\ tube}}{\Phi''_{furnace} \cdot \partial A_{furnace,||}} = \tag{1}$$

$$\frac{\Phi_{vol,quartz} \cdot \pi \cdot (r_{out,quartz} - r_{in,quartz})^2 \cdot \partial l}{\Phi''_{furnace} \cdot 2 \cdot \pi \cdot r_{furnace} \cdot \partial l} = \frac{\Phi_{vol,quartz} \cdot (r_{out,quartz} - r_{in,quartz})^2}{2\Phi''_{furnace} \cdot r_{furnace}}$$

and:

$$\Phi_{vol,quartz} = \rho_{quartz} \cdot c_p \cdot \left(T_{furnace} - T_{quartz\ tube}\right), \tag{2a}$$

$$\Phi''_{furnace} = \tfrac{1}{2} e \cdot \sigma \cdot T^4_{furnace}, \tag{2b}$$

with t time [s], $\Phi_{total,\ quartz}$ heat uptake quartz tube [J], $\Phi''_{total,\ furnace}$ heat emission furnace [W], $\Phi_{vol,quatrz}$ volumetric heat uptake quartz [Jm^{-3}], Φ''_{tube} the heat emission per area furnace [Wm^{-2}], $\delta A_{tube,||furnace}$ area [m^2], $\delta V_{quartz\ tube}$ quartz tube volume [m^3], r radius [m], c_p heat capacity quartz [$Jkg^{-1}K^{-1}$], $T_{furnace}$ temperature furnace [K], T_{quartz} temperature quartz tube, e the emission efficiency [-], ρ quartz density [kgm^{-3}], and σ the Stefan-Boltzmann constant [$Wm^{-2}T^{-4}$].

Table 1: Constants and calculated values for $\Phi_{total,\ quartz}$, $\Phi''_{total,\ furnace}$, and t.

e	0.8	[-]	[7]
$r_{out,\ quartz}$	0.030	[m]	
$r_{in,\ quartz}$	0.027	[m]	
$r_{furnace}$	0.060	[m]	
ρ	2203	[kgm^{-3}]	[8]
σ	$5.67x10^{-8}$	[$Wm^{-2}T^{-4}$]	

T [K]	Heating rate [$Kmin^{-1}$]	c_p [8] [$Jkg^{-1}K^{-1}$]	$\Phi_{total,\ quartz}$ [J]	$\Phi''_{total,\ furnace}$ [W]	t [s]
300	15	772	4362.34	22.04	197.88
350	15	772	4362.34	40.84	106.81
400	5	964	1815.76	69.67	26.06
500	5	964	1815.76	170.10	10.67
600	5	964	1815.76	352.72	5.15
700	1	964	363.15	653.46	0.56
800	1	1052	396.30	1114.77	0.36
900	1	1052	396.30	1785.64	0.22
1000	1	1052	396.30	2721.60	0.15
1100	1	1052	396.30	3984.69	0.10
1200	1	1052	396.30	5643.51	0.07

Table 1 shows the values for the constants used and the calculated values for $\Phi_{total,\ quartz}$, $\Phi''_{total,\ furnace}$, and t. The temperature steps of the furnace differ in rate at the various stages of the pyrolysis.

From Table 1 it is clear that there is a temperature lag at low furnace temperatures, as the heat radiated by the furnace is still low. This can be overcome by allowing the system to reach temperature equilibrium at 150°C (427 K), also enabling residual adsorbed water to evaporate.

ad. 3 As simple gases like He, N_2 and O_2 are transparent for radiation [7] heating of the fresh inert gas entering the tube at room temperature has to take place by conduction. Because of the applied low flow rates convection is neglected. The time necessary to heat up the inert gas to the temperature of the quartz tube can be estimated using the correlation between the dimensionless temperature Y and the Fourier number Fo for tube configurations [7, 9]:

$$Y = \frac{T_{quartz\ tube} - T_{gas,t}}{T_{quartz\ tube} - T_{gas,t=0}}, \tag{3a}$$

$$Fo = \frac{a \cdot t}{r^2} = \left(\frac{\lambda}{\rho \cdot c_p} \right)_{N_2,T} \cdot \frac{t}{r^2}, \tag{3b}$$

where Y is the dimensionless temperature [-], $T_{quartz\ tube}$ is the temperature of the quartz tube [K], $T_{gas,\ t=0}$ is the temperature of the gas upon entering the tube [K], $T_{gas,t}$ temperature of the gas at time t [K], Fo is the Fourier number [-], a is the thermal conductivity [m^2s^{-1}], t is the time [s], r is the radius of the quartz tube [m], and λ, ρ, and c_p are the heat conductivity coefficient [$Wm^{-1}K^{-1}$], density [kgm^{-3}], and heat capacity [$Jkg^{-1}K^{-1}$] resp. of N_2 at temperature T.
The dimensionless temperature Y is a function of the position in the tube and the time represented by the Fo number. In literature a large number of graphical solutions for the average and hart temperature vs. the Fo number are reported [9]. Using eq. 3 and the correlation between Y and Fo the temperature difference between the quartz tube and the inert gas can be calculated for different times after entering the tube. The results are depicted in Figure 2 and show that the largest deviation is seen at T = 650 K, however, after 60 seconds a temperature difference can no longer be observed.

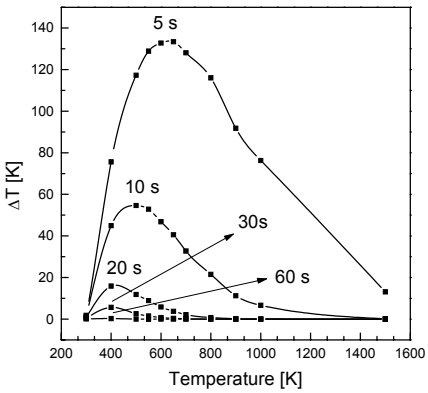

Fig. 2: Temperature lag between furnace and inert gas atmosphere vs. furnace temperature for several time intervals.

The maximum flow rate for a known maximum instationary zone length is given by eq. 4:

$$F_{N_2,\max} = \frac{\Delta x_{\max} \cdot A_{tube,\perp}}{t}, \tag{4}$$

with F_{N2} inert gas flow [m^3/s], Δx length of instationary zone [m], $A_{tube,\perp}$ surface area of the tube entrance [m^3], and t time [s].

I.4 Maximum flow rate.

Before starting any pyrolysis experiments, we must first determine a maximum flow rate of the inert gas. The furnace/quartz tube can be divided into three sections as depicted in figure 3.

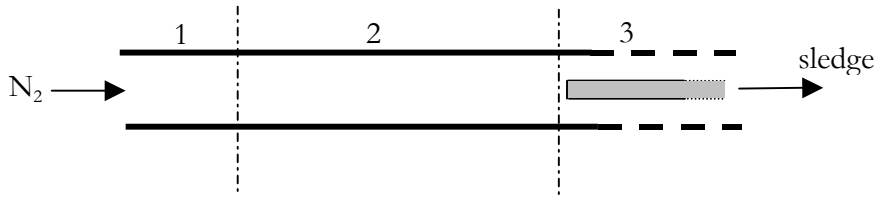

Fig. 3: Schematic overview of the quartz tube divided into sections.

Section 1 is the instationary zone of the furnace and is considered not to contribute to the heating of the atmosphere. As mentioned before, this is 1.5 times the diameter of the furnace, i.e. 1.5 times 10 cm is 15 cm. Section 3 is where the inert gas first encounters the sledge and precursor membranes. Section 2 is the instationary zone where the inert gas atmosphere must be heated from room temperature to the temperature of the furnace. When the sledge is placed in the middle of the furnace/quartz tube, the maximum length of section 3 is half the tube length minus instationary zone furnace, minus half the sledge length, i.e. 50 cm – 15 cm – 25 cm = 15 cm.
Using eq. 4:

$$F_{N_2,\max} = \frac{\Delta x_{\max} \cdot A_{tube,\perp}}{t}, \qquad (4)$$

and the conclusion from figure 2, i.e. the minimum residence time in the tube is 60 s, we can determine the maximum flow rate:

- ∅: 6,0 cm, $F_{N2,\,max}$: 425 ml/min
- ∅: 9,0 cm, $F_{N2,\,max}$: 950 ml/min

We will stay far below the maximum flow by using a flow rate of 10 ml/min.

I.5 Sledge design.

The membranes are inserted into the furnace using a sledge. Two types of materials were used for the construction of the sledge:

- quartz glass,
  dense plate, 3mm thick, low electrical and thermal conductivity,

- stainless steel (SS),
  porous grid, 0.5mm thick, high electrical and thermal conductivity.

The SS grid allows transport of gases (N_2 and pyrolysis products) from both sides of the precursor membrane, whereas in the case of the dense quartz glass sledge, the transport is mainly restricted to the topside of the precursor membrane.
Figure 4. [8, 10] shows a comparison of the thermal conductivity coefficients λ of quartz glass and SS, clearly indicating the significantly higher thermal conductivity of SS.

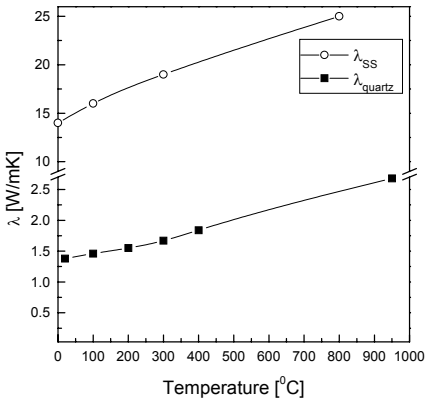

Fig. 4: Heat conduction coefficient vs. the temperature for quartz (■) and SS (○).

The relatively low heat conduction of quartz glass combined with the low gas transport through the sledge can cause temperature differences across the thickness of the precursor, leading to stress creation inside the resulting CMS membrane. Consequently, we have chosen to primarily use the SS grid sledge.
Stress inside the CMS membrane is also introduced by the difference in heat radiation intensity on both bottom- and topside of the precursor during pyrolysis. Figure 5a schematically shows the radiation profile (arrows) inside the furnace. Because of the radial nature of the radiation profile, the radiation intensity increases towards the center of the furnace and consequently differs along the precursor topside surface. On the bottom side the precursor is in contact with the SS grid, which itself is in contact with the quartz tube. The high thermal conductivity of the SS grid leads to a uniform temperature profile along the width of the sledge, creating an uniform heat transfer to the precursor membrane as shown in figure 5a below the membrane. By placing a second SS grid above the precursor (figure 5b) an area of uniform heat (radiation) intensity is created inside the radial radiation field. Again, the high thermal conductivity of the SS grid will lead to a uniform heat transfer, as the grid will produce a radiation field perpendicular to the precursor surface.

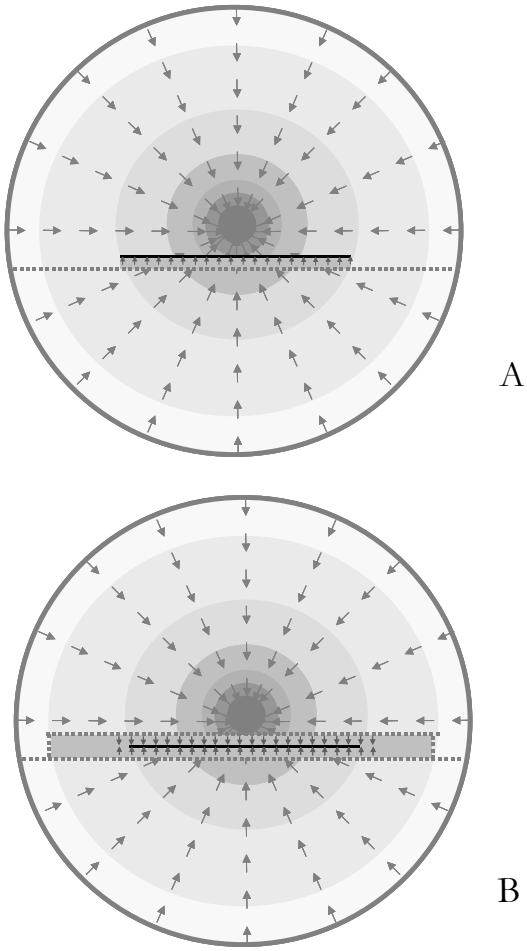

Fig. 5: Radiation density profile in the furnace. A- No SS grid cover, B- SS grid cover.

I.6 Quenching set up.

After pyrolysis, the membranes are quenched to room temperature, using a double hulled SS cooler. It consists of an inner, N_2 flushed, compartment, where the sledge with the carbon membranes is inserted and an outer compartment, through which a cooling agent, tap water, is directed. The dimensions of the inner compartment are 40x8x2 cm and of the outer

compartment 50x9x3 cm. A schematic side view and cross-section of the cooler are given in Figures (6a,b).

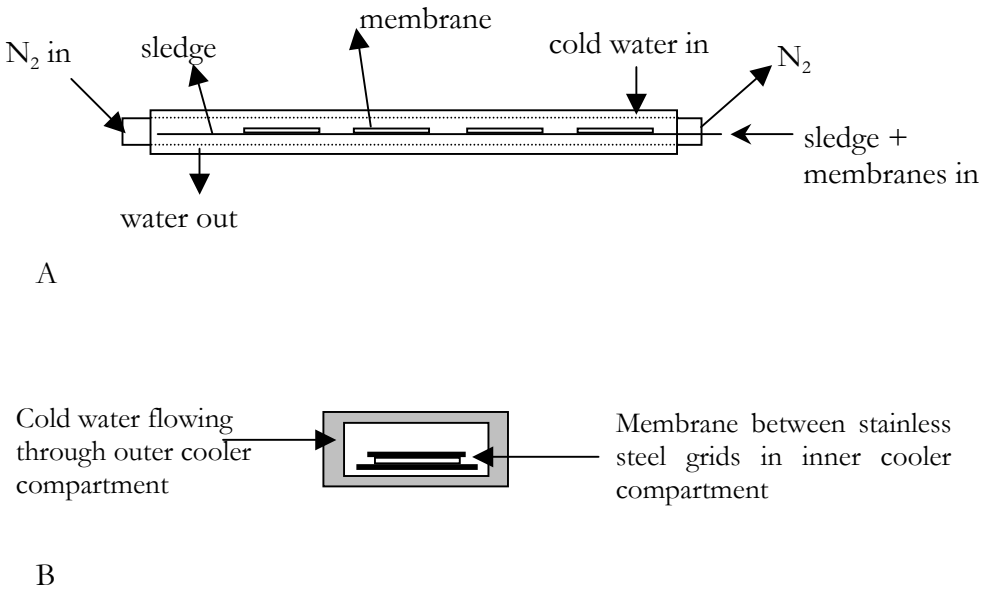

Fig. 6: Schematic representation of the cooler. A - Side view, B – Cross-section.

I.7 Pyrolysis procedure.

Heat treatment procedures allowed the temperature to rise from room temperature to 150°C with a heating rate of 50°C/min. Subsequently, this temperature was held for 15 min to remove any adsorbed water. From 150°C to 350°C the temperature was raised with by a rate of 5°C/min, thereafter the temperature increase was controlled at 1°C/min.
After reaching the end temperature, the membranes were quenched. In figure 7 this procedure is shown schematically.

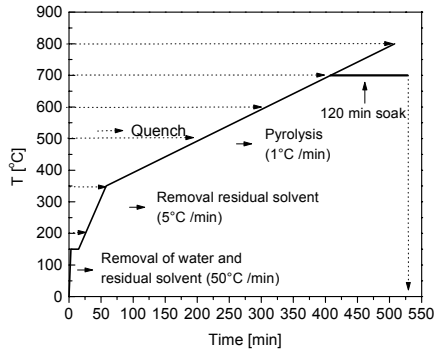

Fig. 7: A schematic overview of the pyrolysis trajectory and the temperatures at which the CMS membranes are quenched.

I.8 References.

[1] C. W. Jones, W. J. Koros, Carbon Molecular-Sieve Gas Separation Membranes .1. Preparation and Characterization Based on Polyimide Precursors, Carbon 32 (1994) p1419-1425.

[2] T. A. Centeno, A. B. Fuertes, Supported carbon molecular sieve membranes based on a phenolic resin, J. Membr. Sci. 160 (1999) p201-211.

[3] M. Ogawa, Y. Nakano, Gas permeation through carbonized hollow fiber membranes prepared by gel modification of polyamic acid, J. Membr. Sci. 162 (1999) p189-198.

[4] H. Kita, H. Maeda, K. Tanaka, K. Okamoto, Carbon molecular sieve membrane prepared from phenolic resin, Chem. Lett. (1997) p179-180.

[5] J. Hayashi, H. Mizuta, M. Yamamoto, K. Kusakabe, S. Morooka, Pore size control of carbonized BPDA-pp'ODA polyimide membrane by chemical vapor deposition of carbon, J. Membr. Sci. 124 (1997) p243-251.

[6] V. C. Geiszler, W. J. Koros, Effects of polyimide pyrolysis conditions on carbon molecular sieve membrane properties, Ind. Eng. Chem. Res. 35 (1996) p2999-3003.

[7] W. M. Rohsenow, H. Choi, Prentice-Hall series in engineering of physiscal sciences, Heat, mass, and momentum transfer, K. R.

Wadleigh , J. B. Reswick, Edition, Prentic-Hall, Inc., Englewood Cliffs, 1961.

[8] Heraeus Amersil, www.quartzglass.com/props/thermprop.html, 29/04/2003.

[9] L. P. B. M. Janssen, M. M. C. G. Warmoeskerken, Transport phenomena data compagnion, 2 Edition, Delftse U.M., Delft, 1991.

[10] Handbook of chemistry and physiscs in D. R. Lidle ed., CRC Press inc., New York, 1996.

Appendix I

Appendix II

Formation of carbon fibers by metal particle catalysis.

II.1 Introduction.

A side effect when preparing metal functionalized CMS membranes is the formation of carbon nano fibers on the surface of the membrane. These carbon fibers are formed during the pyrolysis and build from the evolving pyrolysis gases.

II.2 Preparation of carbon fibers.

One method for preparing carbon fibers is using a vapor growth technique [2]. These fibers can be prepared on several substrates, like carbon, silicon or quartz, and use CO or hydrocarbons as carbon source. The carbon source is decomposed in a H_2 atmosphere at temperatures between 500 and 2500 °C, resulting in a wide variety of carbon fiber structures.

II.3 Carbon fibers on Ag-and Pd-CMS membranes.

When preparing Ag containing membranes from a P84/AgSPEEK blend precursor an interesting effect is seen on the surface of the MAgS800-9.1 and MAgS800-16.7 samples, where thin pillars or fibers have appeared during pyrolysis, see figure 1.

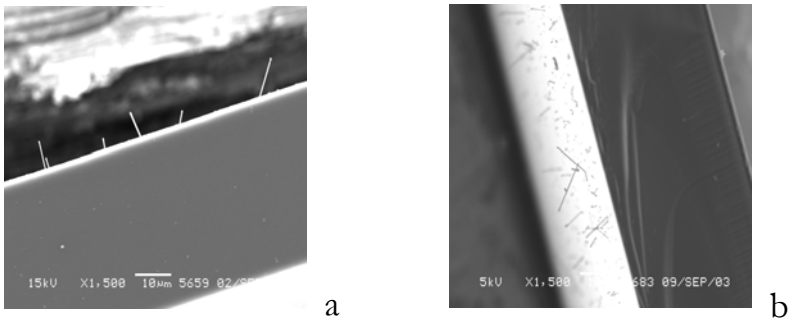

a b

Fig. 1: SEM micrograph of carbon fibers on the surface of (a) MAgS800-9.1 and MAgS800-16.6 (b) membranes.

The formation of fiber structures on the carbon surface was also observed when preparing carbon molecular sieves functionalized with Pd-nanoclusters (see Figure 2).

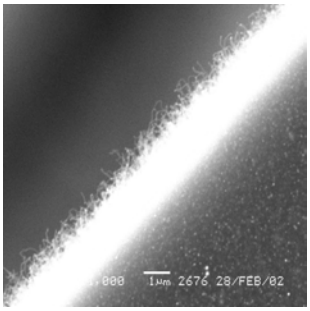

Fig. 2: SEM micrograph of carbon fibers of the surface of a MPd700 membrane. (Pd source: 6.8 wt% $PdAc_2$, T_{pyros}: 700 °C).

The fibers are carbon based and most likely originate from the evolving CO interacting with small metal particles [1, 2], a graphical example of this process is shown in Figure 12. In this example, CO is converted to C and CO_2, where the C migrates through the metal particle and is subsequently deposited below the particle and the CO_2 evolves. The metal particle remains at the end of the carbon fiber. This process takes place at relatively low temperatures, between 500 and 650 °C.

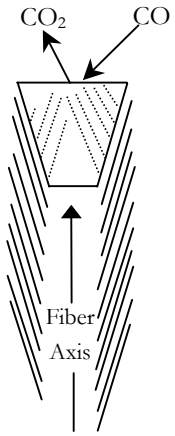

Fig. 12: Schematic representation of carbon fiber formation [2].

Contrary to the method described in section II.2, the atmosphere is N_2 and no additional carbon sources are added, but for those originating from the pyrolysis process.
This phenomenon is not seen when the lower (5 wt%) AgSPEEK content or the $AgNO_3$ based membranes are examined. An explanation can be that the formation of small individual metal clusters on the surface is necessary, in contrast to a continues surface structure.

II.4 References.

[1] P. J. F. Harris, Carbon nanotubes and related structures, 1st Edition, Cambridge University Press, Cambridge, 1999, p32.

[2] M. Endo, R. Saito, M. S. Dresselhaus, D. Dresselhaus, in Carbon nano tubes - Preparation and properties, T. W. Ebbesen ed., CRC Press Inc., New York, 1997, p59.

Levensloop

Op 20 juni 1972 ben ik geboren in Groningen. Na het succesvol doorlopen van het HAVO en het VWO aan het Ommelander College te Appingedam, ben ik in 1992 begonnen aan de studie Chemische Technologie aan de Universiteit Twente, waarbij ik het eerste jaar heb gevolgd aan de Vestiging Friesland van de UT in Leeuwarden. Tijdens mijn studie heb ik een stageopdracht volbracht bij NPBI te Emmer-Compacuum, met als onderwerp het karakteriseren van nonwoven filters voor de verwijdering van leukocyten uit donorbloed.
Ter afsluiting van mijn studie ben ik in 1998 begonnen aan een afstudeeropdracht bij de Membraan Technologie Groep waarbij ik keek naar de het effect van vormstabiliserende additieven in CO_2 geblazen polyethylene schuimen door middel van dielectrische spectroscopie.
In januari 2000 startte mijn promotieonderzoek binnen de Membraan Technologie Groep, met als onderwerp het vervaardigen van koolstofmembranen. De resultaten van het onderzoek staan beschreven in dit proefschrift.